ON THE SIMULATION OF THERMO-MECHANICAL FORMING PROCESSES

a mixed Eulerian-Lagrangian
finite element method

Han Huetink

Second Edition, August 1992.

ON THE SIMULATION OF THERMO-MECHANICAL FORMING PROCESSES

PROEFSCHRIFT

ter verkrijging van de graad
van doctor in de technische wetenschappen
aan de Technische Hogeschool Twente,
op gezag van de rector magnificus,
Prof.dr.ir. H.H. van den Kroonenberg
volgens besluit van het College van Dekanen
in het openbaar te verdedigen
op vrijdag 20 juni 1986 te 16.00 uur

door

Jantje Huetink

geboren op 9 juni 1947 te Borne

Dit proefschrift is goedgekeurd door de promotoren

prof.ir. A. Rijken

en

prof.dr.ir. J.F. Besseling

aan MARIJKE

aan KASPER

TIJMEN

FLORIS

Samenvatting.

Gebaseerd op algemene uitgangspunten van de continuum-mechanica en de thermodynamica, zijn constitutieve vergelijkingen geformuleerd voor elastisch-plastische vervormingen.
Energie-dissipatie en fase-transformaties zijn tevens in het wiskundig model verwerkt.
Aangetoond wordt dat kinematische versteviging bij grote vervormingen kan worden beschreven met een fractiemodel bestaande uit twee fracties.
Een gemengd Eulers-Lagrangiaanse eindige elementen methode is ontwikkeld waarin de lokatie van knooppunten kan worden aangepast onafhankelijk van de materiële verplaatsingen. Numerieke problemen als gevolg van grote element-vervormingen, zoals kunnen optreden bij de "Updated Lagrange" methode, kunnen worden vermeden. Bewegingen van (vrije) oppervlakken kunnen in rekening worden gebracht door de lokatie van knooppunten op een dergelijk oppervlak zodanig aan te passen dat deze op het oppervlak blijven.
Door introduktie van een lokale en een gewogen globale middelingsprocedure (smoothing) kunnen numerieke instabiliteiten voorkomen worden.
De methode is toegepast bij simulaties van een stuikproces, een draadtrek-proces en een hardingsproces van staal. De resultaten van de simulatie van een stuikproces zijn vergeleken met de resultaten van een in het laboratorium uitgevoerd experiment. Simulatie en experiment stemmen goed met elkaar overeen.

Summary.

A formulation for elastic-plastic constitutive equations is given based on principles of continuum thermo-mechanics and thermodynamics.
Energy dissipation and phase changes are included in the mathematical model. It is shown that kinematic hardening can be described properly for large deformations, by a two-fractions model.
A mixed Eulerian-Lagrangian finite element method has been developed by which nodal point locations may be adapted independently of the material displacement. Numerical problems, due to large distortions of elements, as may occur in the case of an Updated Lagrangian method, can be avoided, movement of (free) surfaces can be taken into account by adapting nodal surface point locations in a way that they remain on the moving surface. Local and weighed global smoothing are introduced in order to avoid numerical instabilities.
Applications are shown by simulations of an upsetting process, a wire drawing process and a steel quenching process. The results of the simulation of the upsetting process show satisfactory agreement with the results of an experiment carried out.

Contents

Appendices

LIST OF SYMBOLS

a, b, A_x, A_y, A_1, A_2 - parameters in velocity field and displacement field

$\underline{A}$ - transformation tensor of a line element from the reference state to the current state

$\underline{B}$ - transformation tensor from the current state to the natural reference state

$\underset{\sim}{\underline{B}}^N$ - third order tensor in the relation between strain rate and nodal point velocity

c, c^k, c^* - specific heat

C_b - bulk modulus

$\underline{C}$ - strain tensor $\underline{C} = \underline{B} \bullet \underline{B}^T$

C_1, C_2, C_3 - invariants of $\underline{C}$

$\underline{D}$ - rate of deformation tensor

$\underline{D}^P$ - rate of plastic deformation tensor

e, e^k - internal energy

$\underset{\sim}{e}_i$ - unit base vector

E - Young's modulus

$\underset{\sim}{f}$ - body force per unit mass

$\underset{\sim}{f}^N$ - nodal point generalized force

F - free energy

$\underline{g}$ - metric tensor of the natural reference state

$$\underline{g} = \underline{B}^T \bullet \underline{B}$$

g - determinant of $\underline{g}$

G - shear modulus

h, h_o - hardening modulus

H^k - hardening parameter

$\underline{\underline{H}}$ - fourth order identity tensor $\underline{\underline{H}} : \underline{\sigma} = \underline{\sigma}$ for any $\underline{\sigma}$

$\underline{I}$ - second order identity tensor $\underline{I} \bullet \underset{\sim}{v} = \underset{\sim}{v}$ for any $\underset{\sim}{v}$

J - Jacobian

J_2 - second invariant of the deviatoric stress tensor ($\underline{s}$)

$\underline{\underline{K}}$ - fourth order 'transposed identity' tensor $\underline{\underline{K}} : \underline{\sigma} = \underline{\sigma}^T$ for any $\underline{\sigma}$

$\underline{K}^{MN}$ - element sub-matrix representing the relation between nodal displacement rate and nodal force rate

$\underline{\underline{K}}_s^{MN}$ - element sub-matrix representing the rate of change of the outer surface of an element loaded by external surface traction

ℓ - length of a line element

$\underline{\underline{L}}$ - elasticity tensor for small elastic deformation

$\underline{\underline{L}}^*$ - elasticity tensor for large elastic deformation

$\underline{\underline{L}}^y$ - elasto-plasticity tensor

$\underline{L}^q$ - thermo-mechanical exertion tensor

$\underline{M}$ - second order tensor, as a factor of the yield tensor $\underline{\underline{Y}}$

n - unit normal vector of a surface

$\tilde{N}^y$ - factor in the yield tensor

p - isotropic stress, first invariant of the Cauchy stresstensor $\underline{\sigma}$

$\underline{P}$ - plasticity tensor

P^{MN} - components of an element sub-matrix related to the internal energy rate

Q^F - function of the temperature in the free energy

Q^{MN} - components of an element sub-matrix related to dissipation

$\delta\dot{Q}$ - virtual heat rate

$r,\ r^k$ - constants in the internal energy

$\underline{R}$ - material rotation tensor

R^{MN} - components of an element sub-matrix related to thermal expansion

R^M - nodal point reaction force vector

$\tilde{R}^F$ - unbalance ratio of prescribed nodal forces and nodal reaction forces

R^T - thermal unbalance ratio of external and internal nodal point energy flow

s - entropy

$\underline{s}$ - deviatoric stress tensor $\underline{s} = \underline{\sigma} - 1/3\ \underline{I}\ \mathrm{tr}\ \underline{\sigma}$

t - time

$\underline{t}$ - surface traction

$\tilde{T}$ - absolute temperature

T^N - nodal point temperature

$[T]$ - ordered collection of nodal point temperatures, regarded as components of a multi-dimensional vector

$\underset{\sim}{u}$ - material displacement vector

u_x, u_y - components of a material displacement vector

$\underline{U}$ - symmetric deformation tensor obtained from a polar decomposition of $\underline{B} = \underline{U} \bullet \underline{R}$

$[\dot{U}]$ - ordered collection of nodal point degrees of freedom (velocity and temperature rate)

$\underset{\sim}{v}$ - material velocity vector

$\underset{\sim}{v}^N$ - material velocity vector at a nodal point

v_x, v_y - components of a velocity vector

$[v]$ - ordered collection of nodal point velocities

V - volume of the current state

V_o - volume of the reference state

w_s - weight factor for global smoothing

δW - virtual power

$\underset{\sim}{x}$ - vector representing the current location of a material particle

$\underset{\sim}{X}$ - initial or reference location of a material particle

x, y - coordinates in the current state

X, Y - coordinates in the initial or reference state

$\underline{\underline{Y}}$ - yield tensor

$\underline{Y}^*$ - tensor related to thermal exertion of yielding

$\underline{\underline{Y}}^{**}$ - tensor related to density changes in elasto-plastic deformation

$\underline{\underline{Y}}^{***}$ - tensor related to recovery due to thermal effect

α, α^k, α^* - coefficient of thermal expansion

$\underline{\alpha}$ - internal backstress or orientation tensor representing anisotropic yielding and hardening

β - parameter in a formula for the weightfactor for global smoothing

γ - shear strain in simple shear
virtual power, etc.

Δ - prefix for an increment

$\underline{\varepsilon}$ - Euler-Almansi strain tensor

ε_x, ε_y, ε_{xy} - components of the Euler-Almansi strain tensor

ε, ε^k - equivalent plastic strain

ζ^k - mass fraction

λ - parameter in time dependent plasticity (creep)

$\underline{\lambda}$ - thermal conductivity tensor

λ^{MN} - components of an element sub-matrix related to thermal conductivity

μ - parameter in time independent plasticity

ν - Poisson's ratio

$\bar{\xi}$ - dissipation function related to time dependent plasticity (creep)

ρ, ρ^k - density

ρ_o - reference density

ρ_F, ρ_F^K - density in a stress-free state

$\underline{\sigma}$, $\underline{\sigma}^k$ - Cauchy stress tensor

$\underline{\sigma}'$ - Kirchhoff stress tensor

$\underline{\sigma}^{\nabla}$ - corotational Jaumann rate (of the stress tensor)

σ_v - yield stress

ϕ - yield surface

$\underset{\sim}{\phi}$ - heat flux vector

ϕ^e - rate of change of the internal energy due to irriversible phase transformations

ϕ^M - nodal point thermal energy flow

Φ^d - function of state variables related to dissipation

χ - yield-potential

ψ^k - volume fraction

Ψ^k - finite element interpolation function

$\underline{\Omega}$ - spintensor

$\underset{\sim}{\overrightarrow{\nabla}}$ - pre-gradient operator vector

$\underset{\sim}{\overleftarrow{\nabla}}$ - post-gradient operator vector

I. INTRODUCTION.

Many products of complex shape are made by forming processes. The designers of these processes demand mathematical models in order to obtain a better understanding of a process. The objectives are to obtain products which satisfy the required specifications and of course to lower the costs by improving the design and durability of tools.
Mathematical models of these processes are based on the principles of continuum thermo-mechanics. Equations derived from these principles are very complicated.
In general there are no exact solutions to these equations so one has to approximate. Formerly, these approximations usually had to do with properties of the material. For instance, elastic deformations are neglected (rigid-plastic solids), in many cases strain hardening effects are not taken into account (perfectly plastic solids), and the material is assumed to be isotropic. After these simplifications it is often not yet possible to find analytical solutions to the equations. Approximate solutions are found based on upper- and lowerbound criteria and slip-line theory.
Solutions given in handbooks concerning engineering plasticity are based on these approximations. Many processes are analysed in this way by Avizur [3], Mellor and Johnson [36], Rowe [43].

After computers became available, numerical solution procedures have been developed.
The evolution of these procedures occurs in two fields. The first one is based on the upper-bound criterion and hence rigid-plastic material properties are used. Much work in this field has been done for instance by Kobayashi [27].
The second field is based on extension of small strain elastic-plastic theories to large plastic deformations.
One of the first developments in this field was published by Hibbit, Marcal and Rice [15] in 1970. Improvements were made by Mc. Meeking and Rice [34] in 1975. They introduced the updated-Lagrange approach.

Approximations based on rigid-plastic material models are provided by rather simple equations as compared to those based on elastic-plastic

material models. Particularly when no strain-hardening is taken into account, the solution for the current state is independent from the history, similar to Newtonian viscous flow problems.
However, a disadvantage of the rigid-plastic approach is that an iteration procedure is required which will not converge unconditionally. Besides assumptions have to be made as to the area in which plastic deformations are concentrated in order to avoid numerical problems due to a vanishing rate of deformation in (rigid) parts of a workpiece.
Another disadvantage of the rigid-plastic approach is that residual stresses cannot be predicted and therefore no prediction can be given for elastic springback in a formed product.

Constitutive equations for large elastic-plastic deformations are rather complicated. Widely used are equations obtained from an extension of small strain small rotation theory by replacing the strain rate tensor by the rate of deformation tensor, and the stress rate tensor by the corotational Jaumann rate of the Cauchy stress tensor [14, 26, 38, 44, 49]. This extended theory results into equations which are valid as long as elastic strains are small.

Anisotropic strain hardening can be taken into account by the Prager/Ziegler kinematic hardening model [41, 50]. Extension of this small strain model to large deformations by replacing the increment of the shift tensor by the Jaumann rate, and the plastic strain increment by the rate of plastic deformation tensor, leads to unrealistic predictions. Nagtegaal and De Jong [39] showed that in a simple shear test, there is an oscillating shear stress response. They proposed a modified shift rule by introducing an anisotropic hardening modulus which vanishes for increasing deformation. However, it can be shown that oscillations are suppressed only if the hardening modulus vanishes within a sufficiently small strain range. Hence for (common) materials which obey a nonvanishing hardening modulus, the modified model of Nagtegaal and De Jong cannot be applied.

Besseling observed that a kinematic hardening model can be regarded as a composition of an elastic ideally plastic fraction and a purely elastic fraction [7].
In the case of large deformation the elastic fraction is subjected to

large elastic deformations. Besseling found this unrealistic and therefore he rejected the kinematic hardening mode. Nevertheless it is interesting to pay some more attention to the two-fractions model in relation to the kinematic hardening model.
In a shear test the ideally plastic fraction yields a constant shear stress, hence the hardening is obtained from the elastic fraction. If for the elastic fraction a linear relation is assumed between the Jaumann rate of the stress tensor and the rate of deformation tensor, then it can be shown that in a simple shear test, the stress response is determined by the same differential equations as those for the shift tensor given by Nagtegaal and De Jong (see section 3.1.).
The solution to these equations yields an oscillating shear stress response. At this stage it becomes interesting whether the assumed linear relation between the Jaumann stress rate and the rate of deformation tensor is valid for large elastic deformation. In section 3.1. it is shown that this relation results into a stress response dependent on the path of deformation and should therefore be rejected on the basis of thermodynamic principles.
In section 3.2. is shown that in a simple shear test no oscillations are predicted if the small elastic fraction satisfies a thermodynamically valid stress-strain relation. Consequently a modified shift rule for kinematic hardening can be derived from this adapted two fraction model which is given in section 3.2.

Besides hardening, heat conduction and heat production due to plastic deformation and friction, may largely affect a forming process. In processes at high temperature, also phase changes may occur.
In order to be able to simulate these kinds of nonisothermal processes, constitutive equations must be applied in which thermal effects are taken into account.
The natural reference state theory of Besseling [5] includes all these thermal effects. Constitutive equations used in this thesis are based on this theory summarized in section 3.3.
This theory has been adopted because it was proved by Van der Heyden and Besseling [18] that in the case of time independent plasticity, the results are identical to those in the theory developed by Lee [28]. The J_2- flow theory developed by Budiansky and Hutchinson [16] is included as

a special case.

Extensions are given with respect to materials which do not satisfy the normality rule and may show inelastic density changes such as apply to soil mechanics.
In section 3.4. constitutive equations for isotropic materials are derived which are not restricted to small elastic deformations.

A finite element formulation for numerical simulation of thermo-mechanical forming processes is given in section 4. An incremental procedure is used in which the element mesh and state variables are adapted after each increment. If these adaptations are carried out according to the updated Lagrange method [34, 38], numerical problems may arise due to large distorsion of elements. Besides, a simultaneous simulation of workpiece and tool cannot be carried out if slip occurs. This restriction also applies to the natural formulation presented by Argyris and Doltsinis [1, 2].
A simultaneous analysis of workpiece and tool is of particular interest in problems with considerable heat conduction and heat production, as well as in problems where deformations of the tool cannot be neglected (rolling of tin-plate). Therefore a procedure has been developed in which nodal point locations can be (incrementally) adapted independent of the material displacement increments. Conditions for free (or forced) surface movements can be satisfied. An updated Lagrange approach as well as an Eulerian approach can be regarded as special cases of the procedure.
Therefore it is called the mixed Eulerian-Lagrangian formulation.
The procedure was first presented by the author in 1982 [20]. In section 4.3. improvements are given by introducing weighed global smoothing. This improved procedure has been verified by a large number of numerical simulations of a strain propagation problem.

In section 5 a number of simulations of real forming processes are shown. The predictions for an upsetting process are verified by an experiment.

II. KINEMATICS, DYNAMICS AND ENERGY.

The mathematical description of finite deformations is based on the principles of continuum mechanics. In this section the basic equations of continuum thermo-mechanics will be summarized briefly. A more extensive description is given in [6, 9, 12, 33, 40, 52].

The material of a body is supposed to consist of a continuous distribution of particles (or volume elements).
The motions of these particles are described as a transition from a reference state (or reference geometry) to the current state. Say that the position of a particle in the reference state is given by a vector $\underset{\sim}{X}$ and the current position by a vector $\underset{\sim}{x}$. We can express the current position as a function of the reference position and the time t

$$\underset{\sim}{x} = \underset{\sim}{x}\,(\underset{\sim}{X},\ t) \tag{2.1.1}$$

This function has for any time t a uniquely defined inverse

$$\underset{\sim}{X} = \underset{\sim}{X}\,(\underset{\sim}{x}\ ,\ t) \tag{2.1.2}$$

The velocity of a particle is defined by

$$\underset{\sim}{v} = \dot{\underset{\sim}{x}} = \frac{d\underset{\sim}{x}}{dt} = \left(\frac{\partial \underset{\sim}{x}}{\partial t}\right)_{\underset{\sim}{X}} \tag{2.1.3}$$

The transition of a line element from the reference state to the current state, is defined by

$$d\underset{\sim}{x} = \underline{A} \bullet d\underset{\sim}{X} \tag{2.1.4}$$

where $\underline{A}$ is a second order tensor given by

$$\underline{A} = \left(\frac{\partial \underset{\sim}{x}}{\partial \underset{\sim}{X}}\right)_{t} \tag{2.1.5}$$

The length dl of a line element $d\underset{\sim}{x}$ is found from

$$(dl)^2 = d\underset{\sim}{x} \bullet d\underset{\sim}{x} = d\underset{\sim}{X} \bullet \underline{A}^T \bullet \underline{A} \bullet d\underset{\sim}{X} \tag{2.1.6}$$

The tensor $\underline{A}^T \bullet \underline{A}$ is known as the Green's strain tensor.

The rate of change of the line element $d\underset{\sim}{x}$ follows from

$$(d\underset{\sim}{x})^{\bullet} = \frac{\partial \underline{A}}{\partial t} \bullet d\underset{\sim}{X} \qquad (2.1.7)$$

where

$$\frac{\partial \underline{A}}{\partial t} = \frac{\partial}{\partial t}\left(\frac{\partial \underset{\sim}{x}}{\partial \underset{\sim}{X}}\right) = \frac{\partial}{\partial \underset{\sim}{X}}\left(\frac{\partial \underset{\sim}{x}}{\partial t}\right) = \frac{\partial \underset{\sim}{v}}{\partial \underset{\sim}{x}} \bullet \frac{\partial \underset{\sim}{x}}{\partial \underset{\sim}{X}} = \frac{\partial \underset{\sim}{v}}{\partial \underset{\sim}{x}} \bullet \underline{A} \qquad (2.1.8)$$

Substitution of (2.1.8) and (2.1.4) into (2.1.7) yields

$$(d\underset{\sim}{x})^{\bullet} = d\dot{\underset{\sim}{x}} = \frac{\partial \underset{\sim}{v}}{\partial \underset{\sim}{x}} \bullet d\underset{\sim}{x} \qquad (2.1.9)$$

The partial derivative with respect to $\underset{\sim}{x}$ is known as the gradient and can be denoted as a dyadic product.

$$\frac{\partial \underset{\sim}{v}}{\partial \underset{\sim}{x}} = \underset{\sim}{v}\overleftarrow{\underset{\sim}{\nabla}} \qquad (2.1.10)$$

This gradient can be subdivided into a symmetric part and a antisymmetric part

$$\underline{D} = \frac{1}{2}\left(\underset{\sim}{v}\,\overleftarrow{\underset{\sim}{\nabla}} + \overrightarrow{\underset{\sim}{\nabla}}\,\underset{\sim}{v}\right) \qquad (2.1.11)$$

and

$$\underline{\Omega} = \frac{1}{2}\left(\underset{\sim}{v}\,\overleftarrow{\underset{\sim}{\nabla}} - \overrightarrow{\underset{\sim}{\nabla}}\,\underset{\sim}{v}\right) \qquad (2.1.12)$$

The tensors $\underline{D}$ and $\underline{\Omega}$ are known as the rate of deformation tensor and the spintensor respectively.
The determinant of the transition tensor $\underline{A}$ is called the Jacobian

$$J = \det \underline{A}$$

The rate of change of J can be expressed, by applying eqn. (A 53) of appendix A, as

$$\dot{J} = J\,\underline{A}^{-T} : \dot{\underline{A}} = J\,\underline{A}^{-T} : (\underset{\sim}{v}\,\overleftarrow{\underset{\sim}{\nabla}} \bullet \underline{A}) = J\,\mathrm{tr}\,(\underset{\sim}{v}\,\overleftarrow{\underset{\sim}{\nabla}})$$

or

$$\frac{\dot{J}}{J} = \mathrm{tr}\,\underline{D} = \underset{\sim}{v} \bullet \overleftarrow{\underset{\sim}{\nabla}} \qquad (2.1.14)$$

The material rate of change of an arbitrary field variable Φ can be written as

$$\dot{\Phi} = \frac{d\Phi}{dt} = \left(\frac{\partial \Phi}{\partial t}\right)_{\underset{\sim}{X}} = \frac{\partial \Phi}{\partial t} + \frac{\partial \Phi}{\partial \underset{\sim}{x}} \cdot \frac{d\underset{\sim}{x}}{dt}$$

or

$$\dot{\Phi} = \frac{\partial \Phi}{\partial t} + \underset{\sim}{v} \cdot \overset{\rightarrow}{\underset{\sim}{\nabla}} \Phi \qquad (2.1.15)$$

The material rate of change of a volume integral or functional, which depends on Φ, can be written as

$$\frac{d}{dt} \int_V \Phi \, dV = \int_{V_o} (\dot{\Phi} J + \Phi \dot{J}) \, dV_o = \int_V (\dot{\Phi} + \Phi \, \mathrm{tr} \, \underline{D}) \, dV \qquad (2.1.16)$$

With the kinematic relations and definitions of the preceding we can formulate the basic equations of continuum thermomechanics as follows. Conservation of mass is expressed by

$$\frac{\dot{\rho}}{\rho} = -\frac{\dot{J}}{J} = -\mathrm{tr} \, \underline{D} = -\overset{\rightarrow}{\underset{\sim}{\nabla}} \cdot \underset{\sim}{v} \qquad (2.1.17)$$

where ρ is the mass density.

Balance of momentum can be written as

$$\underline{\sigma} \cdot \overset{\leftarrow}{\underset{\sim}{\nabla}} + \rho \, \underset{\sim}{f} = \rho \, \dot{\underset{\sim}{v}} \qquad (2.1.18)$$

where $\underline{\sigma}$ is the symmetrical Cauchy stress tensor, and $\underset{\sim}{f}$ a body force per unit of mass.

Conservation of energy (first law of thermodynamics) is expressed by

$$\underline{\sigma} : \underline{D} - \rho \, \dot{e} = \overset{\rightarrow}{\underset{\sim}{\nabla}} \cdot \underset{\sim}{\phi} \qquad (2.1.19)$$

where e is the internal energy per unit mass and $\underset{\sim}{\phi}$ is the heat flux due to conduction.
The entropy production (second law of thermodynamics) must satisfy the condition

$$\rho \, \dot{s} + \overset{\rightarrow}{\underset{\sim}{\nabla}} \cdot \left(\frac{\underset{\sim}{\phi}}{T}\right) \geqslant 0 \qquad (2.1.20)$$

where T is the absolute temperature and s the entropy per unit mass.
The law of heat conduction is written as

$$\underset{\sim}{\phi} = -\underline{\lambda} \cdot \overset{\rightarrow}{\underset{\sim}{\nabla}} T \qquad (2.1.21)$$

where $\underline{\lambda}$ is a positive definite second order conductivity tensor.

Note: Local heat production other than due to mechanical energy dissipation will not be taken into account.

Combination of (2.1.19), (2.1.20) and (2.1.21) yields the inequality

$$\underline{\sigma} : \underline{D} - \rho (\dot{e} - T\dot{s}) + \frac{1}{T} \tilde{\nabla} T \bullet \underline{\lambda} \bullet \tilde{\nabla} T \geqslant o \qquad (2.1.22)$$

For forming processes that will be regarded, the internal energy can sufficiëntly accurate be approximated as a function of the temperature, provided that no phase changes occur. This function can be determined from (2.1.19) considering the case that the first term vanishes (no mechanical work). The rate of change of the internal energy is then

$$\dot{e} = c(T)\, \dot{T} \qquad (2.1.23)$$

where c(T) is the specific heat which may be dependent of the temperature. Hence the internal energy can be denoted as

$$e = e(T) = \int_{T_o}^{T} c(t)\, dt + r \qquad (2.1.24)$$

For solids and liquids the specific heat is determined by evaluating (2.1.19) in a stress-free state. For gases a stress free state does not exist and hence the specific heat is determined while suppressing expansion ($c_v = c$).

II. CONSTITUTIVE EQUATIONS.

3.1. Thermodynamic constraints with respect to extension of small strain theory to large deformations.

A hypothesis that is commonly accepted in large plastic deformation theories is that, under isothermal conditions, the rate of deformation tensor can be subdivided into an elastic and a plastic part

$$\underline{D} = \underline{D}^{e} + \underline{D}^{p} \qquad (3.1.1)$$

The relation between the stress and the rate of deformation is generally assumed to be of the form [14, 26, 34, 38, 39, 44, 49].

$$\overset{\bullet}{\underline{\sigma}}' - \underline{\Omega} \bullet \underline{\sigma}' + \underline{\sigma}' \bullet \underline{\Omega} = \underline{\underline{L}} : \underline{D}^{e} \qquad (3.1.2)$$

where $\underline{\sigma}'$ is the Kirchhoff stress tensor [16], which is related to the Cauchy stress tensor $\underline{\sigma}$ by

$$\underline{\sigma}' = \frac{\rho_o}{\rho} \, \underline{\sigma} \qquad (3.1.3)$$

The factor $\frac{\rho_o}{\rho}$ is the ratio of the reference density and the current density respectively and is introduced in order to satisfy the symmetry requirements formulated by Hill [17] in 1958.
For metals the difference between $\underline{\sigma}'$ and $\underline{\sigma}$ is generally neglected because density changes are very small.

The left hand side of (3.1.2) is known as the corotational Jaumann rate:

$$\underline{\sigma}^{\nabla} = \overset{\bullet}{\underline{\sigma}} - \underline{\Omega} \bullet \underline{\sigma} + \underline{\sigma} \bullet \underline{\Omega} \qquad (3.1.4)$$

The fourth order tensor $\underline{\underline{L}}$ depends on material parameters. For isotropic material $\underline{\underline{L}}$ is commonly chosen equal to the linear elasticity tensor according to the law of Hooke.

$$\underline{\underline{L}} = 2 G \, \underline{\underline{H}} + (C_b - \frac{2}{3} G) \, \underline{I} \, \underline{I} \qquad (3.1.5)$$

where G and C_b are the shear modulus and the bulk modulus respectively, which can also be expressed in Young's modulus E and Poisson's ratio ν

$$G = \frac{E}{2\,(1+\nu)}\,, \qquad C_b = \frac{E}{3\,(1-2\nu)} \tag{3.1.6}$$

Purely elastic deformation ($\underline{D}^p = \underline{o}$) will be considered as a reversible process and (3.1.2) will therefore result into a deformation path independent stress-strain relation.
However, with $\underline{\underline{L}}$ according to (3.1.5), this condition is <u>not</u> satisfied as shown by the following example.

Consider a two dimensional deformation problem of combined compressing and shearing. The displacements are referred to a Cartesian coordinate system. The displacement components are expressed as linear functions from the (X,Y) coordinates of the undeformed state

$$u_x = A_x(t)\,Y \qquad , \qquad u_y = A_y(t)\,Y \tag{3.1.7}$$

The coordinates of the undeformed state can be expressed in the current state (x,y)

$$X = x - \frac{A_x}{1 + A_y}\,y \qquad , \qquad Y = \frac{y}{1+A_y} \tag{3.1.8}$$

The components of the velocity v are

$$v_x = \frac{\dot{A}_x}{1+A_y}\,y \qquad , \qquad v_y = \frac{\dot{A}_y}{1+A_y}\,y \tag{3.1.9}$$

The components of the rate of deformation tensor and the spintensor are

$$\begin{aligned} D_{xx} &= \frac{\partial v_x}{\partial x} = 0 \qquad , \qquad D_{yy} = \frac{\partial v_y}{\partial y} = \frac{\dot{A}_y}{1+A_y} \qquad , \\ D_{xy} &= \tfrac{1}{2}\,\frac{\partial v_x}{\partial y} = \frac{\tfrac{1}{2}\,\dot{A}_x}{1+A_y} \qquad , \qquad \Omega = \Omega_{xy} = \frac{\tfrac{1}{2}\,\dot{A}_x}{1+A_y} \end{aligned} \tag{3.1.10}$$

For the sake of convenience we assume that ν (Poisson's ratio) vanishes in this case. The stress-strain relation (3.1.2) then reduces to

$$\overset{\nabla}{\underline{\sigma}}' = 2\,G\,\underline{D} \tag{3.1.11}$$

With (3.1.10) we find that the components of σ' satisfy the relations

$$\dot{\sigma}_x = \tau\, a$$

$$\dot{\sigma}_y = -\tau\, a + 2\, G\, b \qquad (3.1.12)$$

$$\dot{\tau} = [G + \tfrac{1}{2}\,(\sigma_y + \sigma_x)]\, a$$

where $a = \dfrac{\dot{A}_x}{1+A_y}$ and $b = \dfrac{\dot{A}_y}{1+A_y}$ (3.1.13)

In the case of pure compression, a vanishes. The only non vanishing stress rate component is

$$\dot{\sigma}_y = 2\, G\, b \qquad (3.1.14)$$

This equation can directly be integrated by using (3.1.13)

$$\sigma_y = 2\, G \log (1+A_y) + \sigma_{yo} \qquad (3.1.15)$$

In the case of pure shear b vanishes. Besides we assume that a is constant during shearing.
The solution of (3.1.12) in the case of pure shear, and $\sigma_x = \tau = 0$ at time $t = t_o$ is

$$\sigma_x = -\, G\, [\cos (a(t - t_o)) - 1]$$

$$\sigma_y = G\, [\cos (a(t - t_o)) - 1] + \sigma_{yo} \qquad (3.1.16)$$

$$\tau = G \sin (a(t - t_o))$$

We now define two different deformation paths. The first path is given by shearing followed by compression (1a, 1b in fig. 3.1.1)

$$0 < t < 1 \quad : \quad A_x = A_1 t \quad , \quad A_y = 0$$

$$1 < t < 2 \quad : \quad A_x = A_1 \quad , \quad A_y = A_2\,(t-1) \qquad (3.1.17)$$

The second path consist of compression followed by shearing (2a, 2b in fig. 3.1.1).

$$0 < t < 1 \quad : \quad A_x = 0 \quad , \quad A_y = A_2\, t$$

$$1 < t < 2 \quad : \quad A_x = A_1\,(t-1) \quad , \quad A_y = A_2 \qquad (3.1.18)$$

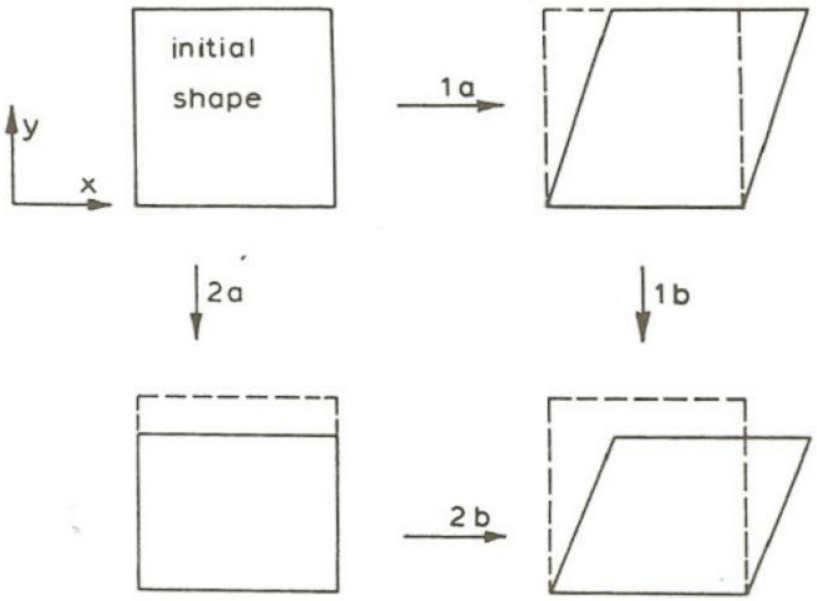

Fig. 3.1.1 Subsequent shearing and compression (1a-1b), or subsequent compression and shearing (2a-2b).

Following the first path we find after shearing ($a = \dot{A}_x = A_1$, according (3.1.13)).

$$\sigma_x = -G\,(\cos A_1 - 1)$$
$$\sigma_y = G\,(\cos A_1 - 1) \qquad (3.1.19)$$
$$\tau = G \sin A_1$$

During subsequent compression only σ_y changes according to (3.1.14) and (3.1.15). Hence the final state after path 1a - 1b is

$$\sigma_x = -G\,(\cos A_1 - 1)$$
$$\sigma_y = G\,(\cos A_1 - 1) + 2\,G \log (1 + A_2) \qquad (3.1.20)$$
$$\tau = G \sin A_1$$

If we follow the second path we find after compression

$$\sigma_x = 0$$
$$\sigma_y = 2\,G \log (1 + A_2) \qquad (3.1.21)$$
$$\tau = 0$$

During subsequent shearing we find from (3.1.13) and (3.1.18) that

$$a = \frac{A_1}{1+A_2} \qquad (3.1.22)$$

Hence the final state after path 2a - 2b is

$$\sigma_x = -G \left(\cos \frac{A_1}{1+A_2} - 1\right)$$
$$\sigma_y = G \left(\cos \frac{A_1}{1+A_2} - 1\right) + 2\,G \log (1+A_2) \qquad (3.1.23)$$
$$\tau = G \sin \frac{A_1}{1+A_2}$$

Comparing (3.1.20) to (3.1.23) shows that the stress state after path (1a - 1b) is different from that after path (2a - 2b) in fig. (3.1.1). Hence constitutive equations based on (3.1.2) and (3.1.5) cannot represent finite elastic deformations.

The elastic stress response should be path-independent from a thermodynamical viewpoint. Equations (3.1.2) and (3.1.5) involve an extension of the small strain theory to finite rotations, but the elastic strains are restricted to infinitesimal deformations.

In the case of elastic-plastic deformations the elastic part of the deformations should be small, the plastic part may be finite.

3.2 Kinematic hardening.

The kinematic hardening model is introduced by Prager [41] and Ziegler [50]. In their theory, which is restricted to small deformations and rotations, it is assumed that during plastic deformation the yield surface moves in translation in stress-space. If the initial yield surface is given by

$$\phi\ (\underline{\sigma}) = 0 \tag{3.2.1}$$

then after a certain amount of plastic deformation the yield surface satisfies the relation

$$\phi\ (\underline{\sigma} - \underline{\alpha}) = 0 \tag{3.2.2}$$

The tensor $\underline{\alpha}$ represents the total translation and may be regarded as an internal stress tensor.
Prager assumed that the rate of $\underline{\alpha}$ is in the direction of the normal on ϕ• Ziegler modified the model by assuming that the rate of $\underline{\alpha}$ is in the direction of $\underline{s} - \underline{\alpha}$ (where $\underline{s}$ is the deviatoric stress).
If the initial yield surface satisfies the Von Mises criterion, then Prager's and Ziegler's rules coincide. In this section the theory will be restricted to that case. After a certain amount of plastic deformation the yield surface is given by

$$\phi = \frac{\rho_o}{\rho}\,\sigma^1 - \sigma_v \tag{3.2.3}$$

where $$\sigma^1 = \left[\frac{3}{2}\,(\underline{s} - \underline{\alpha}) : (\underline{s} - \underline{\alpha})\right]^{1/2} \tag{3.2.4}$$

The shift tensor $\underline{\alpha}$ satisfies the condition tr $\underline{\alpha} = 0$.

For small deformation the rate of change of $\underline{\alpha}$ is given by

$$\dot{\underline{\alpha}} = \frac{2}{3}\,\frac{h\|\underline{D}^p\|}{\sigma_v}\,(\underline{s} - \underline{\alpha}) = h\,\underline{D}^p \tag{3.2.5}$$

in which h is the hardening modulus, related to the slope of an uniaxial stress-strain curve. Usually h is assumed to be constant, but it may be a function of the deformation history and the stress state.

For large deformation and rotation equation (3.2.5) cannot be applied because $\dot{\underline{\alpha}}$ is not materially objective. If $\dot{\underline{\alpha}}$ is replaced by the Jaumann rate, then the objectivity requirements are satisfied:

$$\overset{\nabla}{\underline{\alpha}} = \frac{2}{3} \frac{h\|\underline{D}^p\|}{\sigma_v} (\underline{s} - \underline{\alpha}) = h \underline{D}^p \qquad (3.2.6)$$

However, Nagtegaal and De Jong [39, 26] observed that in the case of simple finite shear, equation (3.2.6) results into an alternating shear stress prediction. This was considered highly unrealistic. They proposed a modified translation rule, which can be written as

$$\overset{\nabla}{\underline{\alpha}} = \frac{2}{3} \frac{h_o\|\underline{D}^p\|}{\sigma_v} (\underline{s} - \underline{\alpha} - \frac{h_o - h}{h_o \alpha} \underline{\alpha}) \qquad (3.2.7)$$

in which $\alpha = (\frac{3}{2} \underline{\alpha} : \underline{\alpha})^{1/2} = (\frac{3}{2})^{1/2} \|\underline{\alpha}\|$ (3.2.8)

and h is regarded as a function of α, which is vanishing for large values of α , $h_o = h(\alpha = o)$•

Simulation of large plastic shear with the modified shift rule showed, that the oscillating shear stress disappeared [39, 26]. However, that result can be attributed to the rapidly decreasing parameter h. If h would not vanish very rapidly, it is obvious that the shear stress will still show oscillations as in the limiting case of h being constant and equal to h_o, eqn. (3.2.7) reduces to (3.2.6).Hence it can be expected that for materials which show a non vanishing hardening modulus, the modified shift rule will not result into satisfactory stress predictions.
With respect to the kinematic hardening model Besseling [7] noticed, that it can be regarded as a fraction model consisting of one isotropic elastic ideally plastic fraction, parallel to a (small) purely elastic isotropic fraction, a Kelvin like model.
In the case of simple shear, the ideally plastic fraction shows a constant shear stress contribution. Hence the hardening is obtained from the elastic fraction. Indeed, the differential equations derived by Nagtegaal and De Jong [39, 26] for the shift tensor of the kinematic hardening model in the case of simple shear, are identical to equations (3.1.12) for 'elastic' material (with b = o). The solution (3.1.16) superimposed on a constant shear stress of the ideal-plastic fraction shows the same

oscillations as found in [39, 26]. However, in section 3.1 is shown that (3.1.12) and (3.1.16) are only valid for infinitesimal elastic deformations. Hence it can be concluded that an improved shift rule can be derived from a two-fraction (Kelvin) model, provided that the description for the elastic fraction is thermodynamically valid for finite deformations.
A simple relation to satisfy this condition is a linear relation between the Cauchy stress tensor and the Euler-Almansi strain tensor $\underline{\varepsilon}$

$$\underline{\sigma} = 2\,G\,\underline{\varepsilon} \tag{3.2.9}$$

$d\underset{\sim}{y} \bullet d\underset{\sim}{x}$ in the deformed state and the scalar product of these line elements $d\underset{\sim}{Y} \bullet d\underset{\sim}{X}$ in the undeformed state by

$$d\underset{\sim}{y} \bullet d\underset{\sim}{x} - d\underset{\sim}{Y} \bullet d\underset{\sim}{X} = 2\, d\underset{\sim}{y} \bullet \underline{\varepsilon} \bullet d\underset{\sim}{x} \tag{3.2.10}$$

With (2.1.4) and (2.1.6) it follows that

$$\underline{\varepsilon} = \tfrac{1}{2}\,(\underline{I} - \underline{A}^{-T} \bullet \underline{A}^{-1}) \tag{3.2.11}$$

In the constitutive equation of the assembly of two fractions, equation (3.2.9) must be transformed to a relation between the stress rate and the rate of deformation tensor $\underline{D}$• Hence a relation between $\underline{\varepsilon}$ and $\underline{D}$ must be established by taking the rate of change of (3.2.10). Using (2.1.9) we find

$$\begin{aligned} &d\underset{\sim}{y} \bullet \overset{\rightarrow}{\nabla}\underset{\sim}{v} \bullet d\underset{\sim}{x} + d\underset{\sim}{y} \bullet \underset{\sim}{v}\overset{\leftarrow}{\nabla} \bullet d\underset{\sim}{x} = \\ &2\, d\underset{\sim}{y} \bullet \dot{\underline{\varepsilon}} \bullet d\underset{\sim}{x} + 2\, d\underset{\sim}{y} \bullet \overset{\rightarrow}{\nabla}\underset{\sim}{v} \bullet \underline{\varepsilon} \bullet d\underset{\sim}{x} + 2\, d\underset{\sim}{y} \bullet \underline{\varepsilon} \bullet \underset{\sim}{v}\overset{\leftarrow}{\nabla} \bullet d\underset{\sim}{x} \end{aligned} \tag{3.2.12}$$

This relation is valid for any value of $d\underset{\sim}{y}$ and $d\underset{\sim}{x}$, hence

$$\tfrac{1}{2}\,(\overset{\rightarrow}{\nabla}\underset{\sim}{v} + \underset{\sim}{v}\overset{\leftarrow}{\nabla}) = \dot{\underline{\varepsilon}} + \overset{\rightarrow}{\nabla}\underset{\sim}{v} \bullet \underline{\varepsilon} + \underline{\varepsilon} \bullet \underset{\sim}{v}\overset{\leftarrow}{\nabla} \tag{3.2.13}$$

The right hand side of (3.2.13) is known as the covariant convective rate (or lower convective rate) [9].
The rate of change of the stress can now be written, using (2.1.11), (2.1.12), (3.1.4), (3.2.9) and (3.2.13) as

$$\overset{\nabla}{\underline{\sigma}} = 2\,G\,\underline{D} - \underline{D}\bullet\underline{\sigma} - \underline{\sigma}\bullet\underline{D} \tag{3.2.14}$$

The Jaumann rate of the deviatoric stress is then

$$\overset{\nabla}{\underline{s}} = (\underline{\sigma} - 1/3 \text{ tr } \underline{\sigma}\ \underline{I})^{\nabla} =$$

$$2\ G\ (\underline{D} - 1/3 \text{ tr } \underline{D}\ \underline{I}) - \underline{D}\bullet\underline{\sigma} - \underline{\sigma}\bullet\underline{D} + 2\ \underline{D} : \underline{\sigma}\ \underline{I} \qquad (3.2.15)$$

In the case of small deformations the shift tensor $\underline{\alpha}$ coincides with the difference of deviatoric stresses of the two fractions. For large deformations the shift tensor will slightly deviate from this relation because the rate of change of the stresses in the fractions are not equal during elastic unloading and reloading.

Based on equation (3.2.14) we can define a shift rule for $\underline{\alpha}$ by

$$\overset{\nabla}{\underline{\alpha}} = h\ [2\ G\ \underline{D}^{p} - \underline{D}^{p}\bullet\underline{\alpha} - \underline{\alpha}\bullet\underline{D}^{p} + 2\underline{\alpha} : \underline{D}^{p}\ \underline{I}] \qquad (3.2.16)$$

where it has been assumed that tr $\underline{D}^{p}$ vanishes.
A kinematic hardening model with this shift rule yields approximately the same stress response as a two fraction (Kelvin) model if the elastic strain limit of the elastic-plastic fraction is small. In the limiting case that the elastic-plastic fraction degenerates to a rigid plastic fraction, both models are identical.

We will now return to the simple shear test. The displacement components are given by (3.1.7) with $A_y = 0$

$$u_x = A_x(t)y = \gamma\ y \qquad , \qquad u_y = 0 \qquad (3.2.17)$$

The components of the Euler-Almansi strain tensor are

$$\varepsilon_x = \frac{\partial u_x}{\partial x} - \frac{1}{2}\left(\frac{\partial u_x}{\partial x}\right)^2 - \frac{1}{2}\left(\frac{\partial u_y}{\partial x}\right)^2 = 0$$

$$\varepsilon_y = \frac{\partial u_y}{\partial y} - \frac{1}{2}\left(\frac{\partial u_x}{\partial y}\right)^2 - \frac{1}{2}\left(\frac{\partial u_y}{\partial y}\right)^2 = -\frac{1}{2}\gamma^2 \qquad (3.2.18)$$

$$\varepsilon_{xy} = \frac{1}{2}\left(\frac{\partial u_x}{\partial y} + \frac{\partial u_y}{\partial x}\right) - \frac{1}{2}\frac{\partial u_x}{\partial y}\frac{\partial u_x}{\partial x} - \frac{1}{2}\frac{\partial u_y}{\partial y}\frac{\partial u_y}{\partial x} = \frac{1}{2}\gamma$$

The stress response of the two fraction model with elastic fraction ψ_1 and elastic-plastic fraction $(1-\psi_1)$ in the plastic range is then found by

$$\sigma = 0 \qquad , \qquad \sigma = -\psi\ G\ \gamma^2$$
$$\tau = \tau_y + \psi_1\ G\ \gamma \qquad (3.2.19)$$

This result is shown by figure 3.2.2., the elastic strain limit is assumed to be very small. This figure also shows the result of a kinematic harde ning model with a shift rule according to equation (3.2.5).
It can be concluded that the modified shift rule (3.2.16) does not show the unrealistic stress oscillations. Moreover, a purely bi-linear shear stress - shear strain curve is found. However, the magnitude of the stress component normal to the direction of the displacement, increases rapidly. This effect can be attributed to the simple linear stress-strain relation (3.2.9) for the elastic fraction. The model can be improved by replacing this relation by a more sophisticated one, which involves a hardening modulus h, which is not constant. Of course, also a non-isotropic hardening modulus introduces by Nagtegaal and De Jong, represented by the additional term in (3.2.7), may be taken into account to obtain a better prediction as regards the Bausschinger effect. Development of more sophisticated models is beyond the scope of the current research programme. The objective of this section is, to make reasonable that extension of the kinematic hardening model to large deformations and rotations can be obtained by replacing the material rate of change of the shift tensor by the covariant convective rate instead of the Jaumann rate. If the Jaumann rate is applied, an extension to large rotation is obtained, but the model is still restricted to small deformations.
Another modification of the shift rule is proposed by Lee [30]. In his rule the spintensor is replaced by a modified spintensor, depending on the total rotation.
This modification is based on the assumption that the gliding mechanism of the atoms is not continuously rotating according to the spintensor, but is more or less related to the total rotation tensor (obtained from the polar decomposition of the deformation tensor $\underline{A}$ of equation (2.1.5)).
In the simple shear test, the rotation angle has an upperbound of $\pi/2$ whereas the time integral of the spintensor increases continuously. By the modified spintensor this upperbound is taken into account and therefore no oscillations are predicted.
At this stage there is no reason to decide as to which rule should be preferred, the rule by Lee or the present rule based on the covariant convective rate.

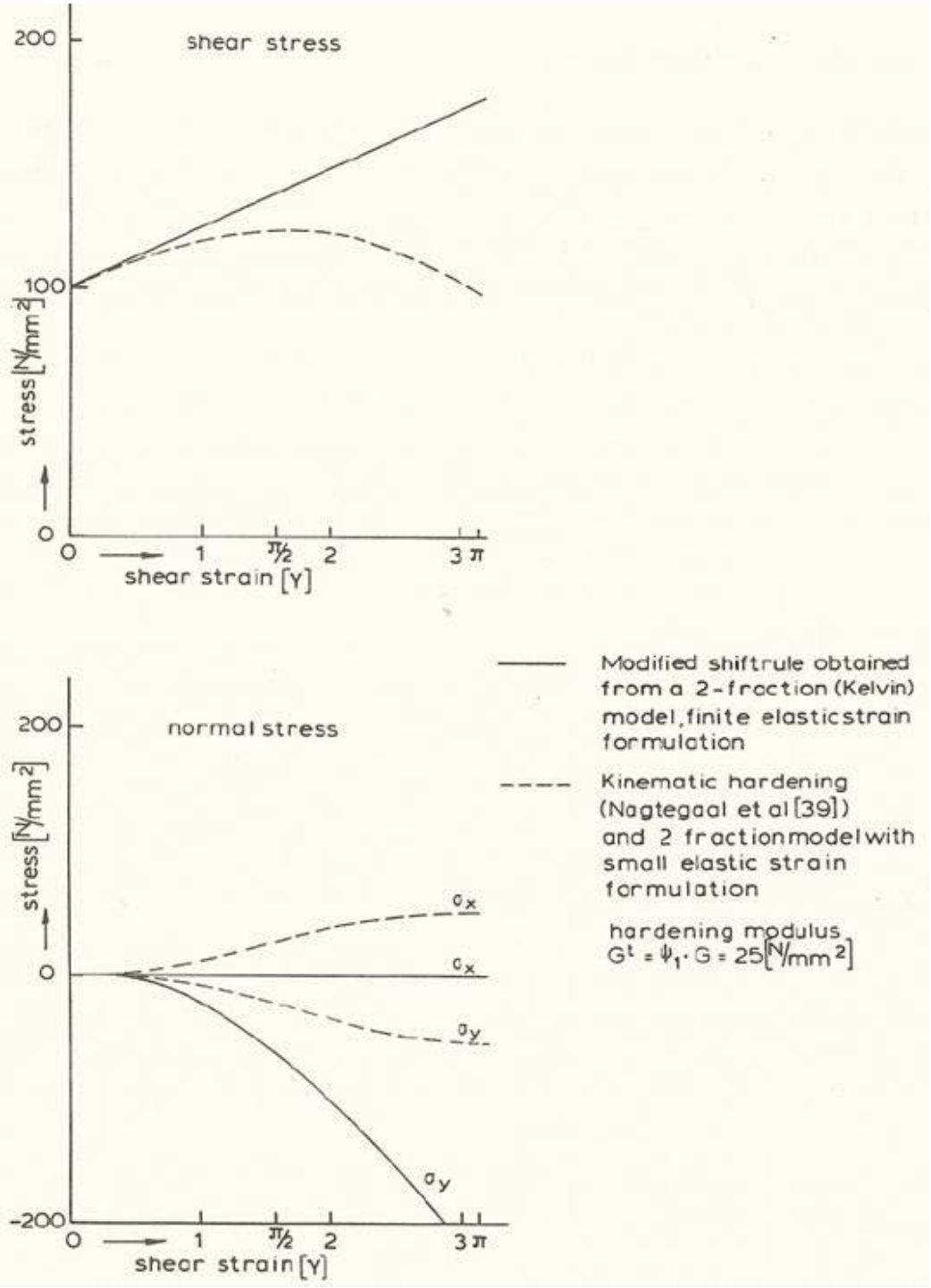

Fig. 3.2.2 Stress prediction of kinematic hardening models in simple shear deformation.

3.3. Natural reference state theory.

In the foregoing sections isothermal conditions were (implicitly) assumed. However, in many processes the temperature changes are considerable and even phase changes may occur in forming processes at increased temperature. In numerical simulations these non-isothermal condition must be taken into account because material properties change when the temperature changes.
A theory in which these non-isothermal effects are taken into account is the natural reference state theory developed by Besseling [5].

The theory is based on the principle of conservation of mass, the first and second law of thermodynamics, the concept of a local thermodynamic state and of a local geometric natural reference state.
As special cases Besseling [5] considered gases, elastic materials, simple solids, and liquids.
In this theory stress is thermodynamically defined. The theory has been further worked out for large elastic-plastic deformations [18,7]. However, a restriction has finally been introduced for small elastic strains.
In this section the theory will be briefly summarized. Besides it will be shown that rather simple constitutive equations can be obtained without making restrictions to small elastic strains, hence kinematic hardening can be taken into account in a way as presented in the previous section.

The natural reference state is related to the current state by a transition of a line element $d\underset{\sim}{x}$ in the current state to it's local natural reference state $d\underset{\sim}{a}$

$$d\underset{\sim}{a} = \underline{B} \bullet d\underset{\sim}{x} \qquad (3.3.1)$$

This transition is invertible. By the polar decomposition theorem, $\underline{B}$ can be written as

$$\underline{B} = \underline{U} \bullet \underline{R} \qquad (3.3.2)$$

The tensor $\underline{U}$ defines a deformation and is symmetric ($\underline{U}^T = \underline{U}$)• The tensor $\underline{R}$ defines a rotation and is orthonormal ($\underline{R}^T = \underline{R}^{-1}$)•
The length dl_o of a line element in the natural reference state is defined by

$$(dl_o)^2 = d\underset{\sim}{a} \cdot d\underset{\sim}{a} = d\underset{\sim}{x} \cdot \underline{B}^T \cdot \underline{B} \cdot d\underset{\sim}{x} \qquad (3.3.3)$$

The tensor $\underline{g} = \underline{B}^T \cdot \underline{B}$ is the metric tensor that defines the generally non-Euclidian metric of the natural reference state.
The metric tensor $\underline{g}$ is not invariant under rigid rotations and therefore not a proper geometrical state variable. The tensor

$$\underline{C} = \underline{B} \cdot \underline{B}^T \qquad (3.3.4)$$

is invariant under rigid rotations and therefore a proper state variable. The tensor $\underline{U}$ is also a proper state variable. From (3.3.2) and (3.3.4) follows that

$$\underline{C} = \underline{U} \cdot \underline{U} \qquad (3.3.5)$$

or

$$\underline{U} = \underline{C}^{1/2} \qquad (3.3.6)$$

The metric tensor g is obtained by rigid rotation of C

$$\underline{g} = \underline{R}^T \cdot \underline{C} \cdot \underline{R} \qquad (3.3.7)$$

According to Besseling the internal energy e is assumed to be a function of $\underline{C}$ and the entropy s per unit mass

$$e = e(\underline{C}, s) \qquad (3.3.8)$$

The rate of change of the natural reference state, characterized by $(d\underset{\sim}{a})^{\bullet}$ is due to a local plasticity and creep process and can be expressed in the rate of change of B and the velocity gradient,

$$(d\underset{\sim}{a})^{\bullet} = \underline{P} \cdot d\underset{\sim}{x} = (\dot{\underline{B}} + \underline{B} \cdot \underset{\sim\sim}{v\nabla}) \cdot d\underset{\sim}{x} \qquad (3.3.9)$$

or

$$\dot{\underline{B}} = \underline{P} - \underline{B} \cdot \underset{\sim\sim}{v\nabla} \qquad (3.3.10)$$

The rate of change of $\underline{C}$ can be expressed as

$$\dot{\underline{C}} = \underline{P} \cdot \underline{B}^T + \underline{B} \cdot \underline{P}^T - 2\, \underline{B} \cdot \underline{D} \cdot \underline{B}^T \qquad (3.3.11)$$

By introducing the fourth order identity tensor $\underline{\underline{H}}$ (see appendix A eqn. (A 31) etc) we can write (using property (A 34) of appendix A)

$$\dot{\underline{C}} = (\underline{B} \bullet \underline{\underline{H}} \bullet \underline{B}) : (\underline{B}^{-1} \bullet \underline{P} + \underline{P}^{T} \bullet \underline{B}^{-T} - 2\,\underline{D}) \qquad (3.3.12)$$

The material behaviour of a material particle in a homogeneous deformation process is assumed to be equal to the behaviour in a non-homogeneous process. Hence it follows with (2.1.22) that the existence of a temperature gradient is irrelevant with respect to the local material behaviour, we may regard the homogeneous case in which the inequality

$$\underline{\sigma} : \underline{D} - \rho\,(\dot{e} - T\dot{s}) \geqslant o \qquad (3.3.13)$$

must be satisfied.

Note: The last term in the left hand side of (2.1.22) is positive definite, hence (2.1.22) is satisfied if (3.3.13) is satisfied.

The material rate of change of the internal energy can be expressed as

$$\dot{e} = \frac{\partial e}{\partial \underline{C}} : \dot{\underline{C}} + \frac{\partial e}{\partial s}\,\dot{s} \qquad (3.3.14)$$

Substitution of (3.3.12) and using formula (A 35) of appendix A yields

$$\dot{e} = (\underline{B}^{T} \bullet \frac{\partial e}{\partial \underline{C}} \bullet \underline{B}) : (\underline{B}^{-1} \bullet \underline{P} + \underline{P}^{T} \bullet \underline{B}^{-T} - 2\underline{D}) + \frac{\partial e}{\partial s}\,\dot{s} \qquad (3.3.15)$$

Substitution of (3.3.15) into (3.3.13) yields

$$\begin{aligned}(\underline{\sigma} + 2\rho\,\underline{B}^{T} \bullet \frac{\partial e}{\partial \underline{C}} \bullet \underline{B}) : \underline{D} + \rho\,(T - \frac{\partial e}{\partial s})\,\dot{s} + \\ - (\rho\,\underline{B}^{T} \bullet \frac{\partial e}{\partial \underline{C}} \bullet \underline{B}) : (\underline{B}^{-1} \bullet \underline{P} + \underline{P}^{T} \bullet \underline{B}^{-T}) \;\geqslant\; 0\end{aligned} \qquad (3.3.16)$$

The equal sign corresponds to the case that only elastic deformations occur currently. Condition (3.3.16) can only be satisfied if

$$\underline{\sigma} = -\,2\rho\,\underline{B}^{T} \bullet \frac{\partial e}{\partial \underline{C}} \bullet \underline{B} \qquad (3.3.17)$$

and

$$T = \frac{\partial e}{\partial s} \qquad (3.3.18)$$

The energy dissipation due to inelastic deformation must satisfy the condition

$$\frac{1}{2}\,\underline{\sigma} : (\underline{B}^{-1} \bullet \underline{P} + \underline{P}^{T} \bullet \underline{B}^{-T}) \geqslant 0 \qquad (3.3.19)$$

Because of the symmetry of $\underline{\sigma}$ this can be written as

$$\underline{\sigma} : (\underline{B}^{-1} \bullet \underline{P}) \geqslant 0 \qquad (3.3.20)$$

Equation (3.3.17) defines the stress tensor as a function of the deformation and entropy differences in the current state and the natural reference state respectively. If this formula is applied, material parameters must be given as a function of the entropy. However, material handbooks usually offer material data as functions of the temperature. Therefore it is more convenient to express the stress as a function of the free energy F [8, 42] where the free energy is a function of the tensor $\underline{C}$ and the absolute temperature

$$F = F(\underline{C}, T) = e - Ts \qquad (3.3.21)$$

It can be shown (see appendix B) that

$$\left(\frac{\partial e}{\partial \underline{C}} \right)_s = \left(\frac{\partial F}{\partial \underline{C}} \right)_T \qquad (3.3.22)$$

and

$$s = \left(- \frac{\partial F}{\partial T} \right)_{\underline{C}} \qquad (3.3.23)$$

Equation (3.3.17) can with (3.3.22) be replaced by

$$\underline{\sigma} = -2\rho \, \underline{B}^T \bullet \frac{\partial F}{\partial \underline{C}} \bullet \underline{B} \qquad (3.3.24)$$

The tensor $\underline{B}^{-1} \bullet \underline{P}$, which appears in the energy dissipation (3.3.20) is denoted by the rate of plastic deformation tensor $\underline{D}^P$

$$\underline{D}^P = \underline{B}^{-1} \bullet \underline{P} \qquad (3.3.25)$$

Motivated by a principle of determinism, Besseling concludes that $\underline{D}^P$ is symmetric. This is not strictly necessary because a nonvanishing anti-symmetric part supplies no contribution to the energy dissipation. At this stage there is no physical evidence to assume that $\underline{D}^P$ is not symmetric. The rate of change of the transition tensor $\underline{B}$ can, with (3.3.10) and (3.3.25) be expressed as

$$\dot{\underline{B}} = \underline{B} \bullet (\underline{D}^P - \underline{D}) - \underline{B} \bullet \underline{\Omega} \qquad (3.3.26)$$

The rate of change of the stress tensor can be written as a function

of the rate of deformation and the temperature rate:
From (3.3.17) we find

$$\dot{\underline{\sigma}} = \frac{\dot{\rho}}{\rho}\,\underline{\sigma} - 2\rho\,\{\dot{\underline{B}}^T \bullet \frac{\partial F}{\partial \underline{C}} \bullet \underline{B} + \underline{B}^T \bullet \frac{\partial F}{\partial \underline{C}} \bullet \dot{\underline{B}} + \underline{B}^T \bullet (\frac{\partial^2 F}{\partial \underline{\underline{C}}^2} : \dot{\underline{C}}) \bullet \underline{B} + \\ + \underline{B}^T \bullet \frac{\partial^2 F}{\partial \underline{C}\partial T} \bullet \underline{B}\,\} \qquad (3.3.27)$$

where $\frac{\partial^2 F}{\partial \underline{\underline{C}}^2}$ is a fourth order tensor, $\qquad \frac{\partial^2 F}{\partial \underline{\underline{C}}^2} = \frac{\partial}{\partial \underline{C}}\,(\frac{\partial F}{\partial \underline{C}}) \qquad (3.3.28)$

Substitution of (3.3.10), (3.3.12) and (3.3.26), while using the formula's (A 34) and (A 35) of appendix A, we find

$$\underline{\sigma}^{\nabla} = \dot{\underline{\sigma}} - \underline{\underline{\Omega}} \bullet \underline{\sigma} + \underline{\sigma} \bullet \underline{\underline{\Omega}} = \\ \frac{\dot{\rho}}{\rho}\,\underline{\sigma} - (\underline{D} - \underline{D}^P) \bullet \underline{\sigma} - \underline{\sigma} \bullet (\underline{D} - \underline{D}^P) + \qquad (3.3.29) \\ + \underline{\underline{L}} : (\underline{D} - \underline{D}^P) - 2\rho\,\underline{B}^T \bullet \frac{\partial^2 F}{\partial \underline{C}\partial T} \bullet \underline{B}\,\dot{T}$$

where the fourth order tensor $\underline{\underline{L}}$ is given by

$$\underline{\underline{L}} = 4\rho\,(\underline{B}^T \bullet \underline{\underline{H}} \bullet \underline{B}^T) : \frac{\partial^2 F}{\partial \underline{\underline{C}}^2} : (\underline{B} \bullet \underline{\underline{H}} \bullet \underline{B}) \qquad (3.3.30)$$

Hitherto section 3.3 has dealt with a continuum theory that is applicable to gases, liquids and solids. In the next part the theory will be focussed on solids, including elasticity, plasticity and creep.
An energy dissipation function ξ is introduced for creep

$$\underline{\sigma} : \underline{D}^P = \xi\,(\underline{\sigma}\,,\ \underline{\alpha}\,,\ \rho\,,\ T) \geqslant 0 \qquad (3.3.31)$$

The second order tensor $\underline{\alpha}$ is associated with anisotropy and is materially objective. This tensor may change due to inelastic deformation (strain hardening).

Time independent plastic deformation will occur when the stress tensor reaches the yield surface. This yield surface is defined by

$$\phi = \phi\,(\underline{\sigma}\,,\ \underline{\alpha}\,,\ \rho\,,\ T) = 0 \qquad (3.3.32)$$

In metal plasticity the natural reference state is characterized by a constant mass density. In that case only the deviatoric components of the stress tensor contribute to the energy dissipation, therefore the rate of plastic deformation tensor is dual to the deviatoric stress [7]. In soil mechanics however, the density in the natural reference state is not constant. Hence dissipation due to density changes must be taken into account in addition to dissipation as regards distortion. The rate of plastic deformation can in that case be associated with the gradient of a potential function in stress space [46]. This (yield) potential χ depends on the same variables as the yield surface

$$\chi = \chi \ (\underline{\sigma} \ , \ \underline{\alpha} \ , \ \rho \ , \ T) \tag{3.3.33}$$

When both creep and time-independent plasticity occur, the rate of plastic deformation must satisfy equation

$$\underline{D}^{P} = \lambda \frac{\partial \xi}{\partial \underline{\sigma}} + \mu \frac{\partial \chi}{\partial \underline{\sigma}} \tag{3.3.34}$$

where $\mu \geqslant 0$ if $\phi = 0$ and $\dot{\phi} \geqslant 0$

$\mu = 0$ if $\phi < 0$ or $\phi = o$, $\dot{\phi} < 0$

In the case of metal plasticity we may assume that

$$\frac{\partial \phi}{\partial \underline{\sigma}} = \frac{\partial \chi}{\partial \underline{\sigma}} \tag{3.3.35}$$

The factor λ is completely determined by the dissipation function ξ•

$$\lambda \ \underline{\sigma} : \frac{\partial \xi}{\partial \underline{\sigma}} = \xi \quad \rightarrow \quad \lambda = (\underline{\sigma} : \frac{\partial \xi}{\partial \underline{\sigma}})^{-1} \xi \tag{3.3.36}$$

The scalar factor μ can be calculated from (3.3.34) on condition that the stress tensor must satisfy the yield condition (3.3.32); hence

$$\dot{\phi} = \frac{\partial \phi}{\partial \underline{\sigma}} : \dot{\underline{\sigma}} + \frac{\partial \phi}{\partial \underline{\alpha}} : \dot{\underline{\alpha}} + \frac{\partial \phi}{\partial \rho} \dot{\rho} + \frac{\partial \phi}{\partial T} \dot{T} = 0 \tag{3.3.37}$$

or by introducing the Jaumann rate of $\underline{\sigma}$ and $\underline{\alpha}$

$$\dot{\phi} = \frac{\partial \phi}{\partial \underline{\sigma}} : \overset{\nabla}{\underline{\sigma}} + \frac{\partial \phi}{\partial \underline{\alpha}} : \overset{\nabla}{\underline{\alpha}} + \frac{\partial \phi}{\partial \rho} \dot{\rho} + \frac{\partial \phi}{\partial T} \dot{T} + \tag{3.3.38}$$

$$+ \left[\frac{\partial \phi}{\partial \underline{\sigma}} \bullet \underline{\sigma}^{T} + \left(\frac{\partial \phi}{\partial \underline{\sigma}}\right)^{T} \bullet \underline{\sigma} + \frac{\partial \phi}{\partial \underline{\alpha}} \bullet \underline{\alpha}^{T} + \left(\frac{\partial \phi}{\partial \underline{\alpha}}\right)^{T} \bullet \underline{\alpha}\right] : \underline{\Omega} = 0$$

The yield function ϕ must be invariant under rigid rotation, hence the last term in (3.3.38) must vanish identically. This condition is satisfied if the term between the compound brackets in (3.3.38) yields a symmetric second order tensor. Because of the symmetry of $\underline{\sigma}$ this condition is

$$\begin{aligned} &2 \frac{\partial \phi}{\partial \underline{\sigma}} \bullet \underline{\sigma} + \frac{\partial \phi}{\partial \underline{\alpha}} \bullet \underline{\alpha}^{T} + \left(\frac{\partial \phi}{\partial \underline{\alpha}}\right)^{T} \bullet \underline{\alpha} + \\ &-2\, \underline{\sigma} \bullet \frac{\partial \phi}{\partial \underline{\sigma}} - \underline{\alpha} \bullet \left(\frac{\partial \phi}{\partial \underline{\alpha}}\right)^{T} - \underline{\alpha}^{T} \bullet \frac{\partial \phi}{\partial \underline{\alpha}} = \underline{0} \end{aligned} \qquad (3.3.39)$$

Note: The kinematic hardening model satisfies this condition. The orientation tensor $\underline{\alpha}$ is symmetric in that case.

With (3.3.39) we can reduce (3.3.38) to

$$\dot{\phi} = \frac{\partial \phi}{\partial \underline{\sigma}} : \overset{\nabla}{\underline{\sigma}} + \frac{\partial \phi}{\partial \underline{\alpha}} : \overset{\nabla}{\underline{\alpha}} + \frac{\partial \phi}{\partial \rho} \dot{\rho} + \frac{\partial \phi}{\partial T} \dot{T} = 0 \qquad (3.3.40)$$

We assume that the rate of change of the hardening tensor $\underline{\alpha}$ may be subdivided into a part that is proportional to the rate of plastic deformation and a part that is independent of plastic deformation (for instance softening due to recristallizing or phase changes). So we can write

$$\frac{\partial \phi}{\partial \underline{\alpha}} : \overset{\nabla}{\underline{\alpha}} = \phi_1 \mu + \phi_2 \qquad (3.3.41)$$

By substitution of (3.3.29) and (3.3.41) in (3.3.40) we can derive that

$$\begin{aligned} \mu = &\left\{\frac{\partial \phi}{\partial \underline{\sigma}} : \underline{\underline{L}}^{*} : \left(\underline{D} - \lambda \frac{\partial \xi}{\partial \underline{\sigma}}\right) + \left[\frac{\partial \phi}{\partial T} - \frac{\partial \phi}{\partial \underline{\sigma}} : \left(2\rho B^{T} \bullet \frac{\partial^{2} F}{\partial \underline{C} \partial T} \bullet B\right)\right] \dot{T} + \right. \\ &\left. + \left(\frac{\partial \phi}{\partial \underline{\sigma}} : \underline{\sigma} + \frac{\partial \phi}{\partial \rho} \rho\right) \frac{\dot{\rho}}{\rho} + \phi_2 \right\} \left(\frac{\partial \phi}{\partial \underline{\sigma}} : \underline{\underline{L}}^{*} : \frac{\partial X}{\partial \underline{\sigma}} - \phi_1\right)^{-1} \end{aligned} \qquad (3.3.42)$$

where

$$\underline{\underline{L}}^{*} = \underline{\underline{L}} - \underline{\underline{H}} \bullet \underline{\sigma} - \underline{\sigma} \bullet \underline{\underline{H}} \qquad (3.3.43)$$

Substitution of (3.3.34) with μ according to (3.3.42) into (3.3.29) yields

$$\overset{\nabla}{\underline{\sigma}} = \frac{\dot{\rho}}{\rho} \underline{\sigma} + \left(\underline{\underline{L}}^{*} - (1-h)\, \underline{\underline{Y}}\right) : \left(\underline{D} - \lambda \frac{\partial \xi}{\partial \underline{\sigma}}\right) +$$

$$- (1-h)\ \underline{Y}^{*}\ \dot{T} + (1-h)\ \underline{\underline{Y}}^{**} : \underline{D} - (1-h)\ \underline{Y}^{***} + \tag{3.3.44}$$

$$-2\ \rho\ \underline{B}^{T} \cdot \frac{\partial^2 F}{\partial \underline{C} \partial T} \cdot \underline{B}\ \dot{T}$$

where

$$\underline{Y} = \frac{\underline{\underline{L}}^{*} : \frac{\partial \chi}{\partial \underline{\sigma}}\ \frac{\partial \phi}{\partial \underline{\sigma}} : \underline{\underline{L}}^{*}}{N^{y}} \tag{3.3.45}$$

$$h = \frac{\phi_1}{\phi_1 - N^{y}} \tag{3.3.46}$$

$$\underline{Y}^{*} = \frac{\underline{\underline{L}}^{*} : \frac{\partial \chi}{\partial \underline{\sigma}}\ [\frac{\partial \phi}{\partial T} - \frac{\partial \phi}{\partial \underline{\sigma}} : (2\rho\ \underline{B}^{T} \cdot \frac{\partial^2 F}{\partial \underline{C} \partial T} \cdot \underline{B})]}{N^{y}} \tag{3.3.47}$$

$$\underline{\underline{Y}}^{**} = \frac{\underline{\underline{L}}^{*} : \frac{\partial \chi}{\partial \underline{\sigma}}\ (\frac{\partial \phi}{\partial \underline{\sigma}} : \underline{\sigma} + \frac{\partial \phi}{\partial \rho}\ \rho)\ \underline{I}}{N^{y}} \tag{3.3.48}$$

$$\underline{Y}^{***} = \frac{\underline{\underline{L}}^{*} : \frac{\partial \chi}{\partial \underline{\sigma}}\ \phi_2}{N^{y}} \tag{3.3.49}$$

with

$$N^{y} = \frac{\partial \phi}{\partial \underline{\sigma}} : \underline{\underline{L}}^{*} : \frac{\partial \chi}{\partial \underline{\sigma}} \tag{3.3.50}$$

The tensor $\underline{Y}^{**}$ has been determined by using the relation (2.1.17). In metal plasticity $\underline{Y}^{**}$ must vanish in order to satisfy the desired symmetry conditions [18].

The constitutive equation represented by (3.3.44) through (3.3.50) may be applied for materials showing anisotropic strain hardening and time dependent plastic deformation (viscous creep flow). However the description is restricted to fixed directions of elastic anisotropic properties. If these directions change during the process, as will happen in flow of polymers due to molecular orientation, the free energy function should be dependent on an orientation tensor similar to the dissipation function and yield surface.

3.4. Isotropic materials.

For isotropic materials the free energy, the dissipation and the yield criterion are functions of the invariants of $\underline{C}$. The invariants of $\underline{C}$ are equal to the invariants of the metric tensor g and are given by

$$\begin{aligned} C_1 &= \operatorname{tr} \underline{C} = \operatorname{tr} \underline{g} \\ C_2 &= \operatorname{tr} \underline{C} \cdot \underline{C} = \operatorname{tr} (\underline{C}^2) = \underline{C} : \underline{C} = \underline{g} : \underline{g} \\ C_3 &= \det \underline{C} = \det \underline{g} = g \end{aligned} \tag{3.4.1}$$

The free energy can now be expressed as

$$F = F(C_1, C_2, C_3, T) \tag{3.4.2}$$

$$\text{or} \quad F = F(\operatorname{tr} \underline{C}, \operatorname{tr}(\underline{C} \cdot \underline{C}), g, T) \tag{3.4.3}$$

In order to establish the constitutive equation we have to determine the derivatives of the invariants. With equation (A 40) of appendix A we find

$$\frac{\partial C_1}{\partial \underline{C}} = \frac{\partial \operatorname{tr} \underline{C}}{\partial \underline{C}} = \underline{I} \tag{3.4.4}$$

With equation (A 52) and (A 42)

$$\frac{\partial C_2}{\partial \underline{C}} = \frac{\partial \underline{C} : \underline{C}}{\partial \underline{C}} = 2\, \underline{C} \tag{3.4.5}$$

With equation (A 53)

$$\frac{\partial C_3}{\partial \underline{C}} = \frac{\partial \det \underline{C}}{\partial \underline{C}} = g\, \underline{C}^{-1} \tag{3.4.6}$$

The second order derivatives of the invariants are

$$\frac{\partial^2 C_1}{\partial \underline{\underline{C}}^2} = \underline{\underline{0}} \tag{3.4.7}$$

$$\frac{\partial^2 C_2}{\partial \underline{\underline{C}}^2} = 2\, \underline{\underline{H}} \tag{3.4.8}$$

and with (A 56)

$$\frac{\partial^2 C_3}{\partial \underline{\underline{C}}^2} = g\, \underline{C}^{-1}\, \underline{C}^{-1} - g\, \underline{C}^{-1} \bullet \underline{\underline{H}} \bullet \underline{C}^{-1} \qquad (3.4.9)$$

In order to establish expressions for the stress according to (3.3.24) and the fourth order tensor $\underline{\underline{L}}$ according to (3.3.30), we must first work out expressions containing the derivatives of the invariants.

$$\underline{B}^T \bullet \frac{\partial C_1}{\partial \underline{C}} \bullet \underline{B} = \underline{B}^T \bullet \underline{B} = \underline{g} \qquad (3.4.10)$$

$$\underline{B}^T \bullet \frac{\partial C_2}{\partial \underline{C}} \bullet \underline{B} = 2\, \underline{B}^T \bullet \underline{C} \bullet \underline{B} = 2\, \underline{g} \bullet \underline{g} \qquad (3.4.11)$$

$$\underline{B}^T \bullet \frac{\partial C_3}{\partial \underline{C}} \bullet \underline{B} = g\, \underline{B}^T \bullet \underline{C}^{-1} \bullet \underline{B} = g\, \underline{B}^T \bullet \underline{B}^{-T} \bullet \underline{B}^{-1} \bullet \underline{B} = g\, \underline{I} \qquad (3.4.12)$$

With these expressions we can write for the stress tensor (3.3.24)

$$\underline{\sigma} = -2\rho \left[\frac{\partial F}{\partial C_1}\, \underline{g} + 2\frac{\partial F}{\partial C_2}\, \underline{g} \bullet \underline{g} + \frac{\partial F}{\partial C_3}\, g\, \underline{I}\right] \qquad (3.4.13)$$

It is obvious that a rather simple relation between $\underline{g}$ and $\underline{\sigma}$ is obtained if the free energy is independent of the second invariant.
We shall consider this simple material. Besides it is a condition that the stress tensor vanishes if $\underline{C} = \underline{I}$ and $T = T_o$ and that the stress rate is isotropic and proportional to the temperature rate if $\underline{C} = \underline{I}$ and $T \neq T_o$. A free energy function which satisfies these conditions is given by

$$F = \frac{G}{2\rho_o} (\mathrm{tr}\, \underline{C} - 3g^{1/3}) + \frac{3C_b}{2\rho_o} (6\, g^{1/6} - (\frac{\rho_F}{\rho_o})^{1/3} \log g) + Q^F(T) \qquad (3.4.14)$$

In this formula is ρ_o the density in a stress-free state at $T = T_o$, and ρ_F is a function of the temperature, representing the density in a stress-free state at arbitrary temperature. The relation between ρ_F and the coefficient of thermal expansion α is

$$\frac{\partial}{\partial T} (\frac{\rho_F}{\rho_o})^{1/3} = -\alpha(T) \qquad (3.4.15)$$

The third invariant g is related to the current density $\rho\mu$ by

$$g = \left(\frac{\rho}{\rho_o}\right)^2 \tag{3.4.16}$$

The derivatives of F with respect to the invariants are

$$\begin{aligned}
\frac{\partial F}{\partial C_1} &= \frac{\partial F}{\partial \mathrm{tr}\underline{C}} = \frac{G}{2\rho_o} \\
\frac{\partial F}{\partial C_2} &= o \\
\frac{\partial F}{\partial C_3} &= \frac{\partial F}{\partial g} = \frac{-G}{2\rho_o}\, g^{-2/3} + \frac{3C_b}{2\rho_o}\left(g^{-5/6} - \left(\frac{\rho_F}{\rho_o}\right)^{1/3} g^{-1}\right)
\end{aligned} \tag{3.4.17}$$

substitution of (3.4.17) in (3.4.13) yields

$$\underline{\sigma} = -2\rho\left[\frac{G}{2\rho_o}\left(\underline{g} - g^{1/3}\,\underline{I}\right) + \frac{3C_b}{2\rho_o}\left(g^{1/6} - \left(\frac{\rho_F}{\rho_o}\right)^{1/3}\right)\underline{I}\right] \tag{3.4.18}$$

The tensor $\underline{\varepsilon}' = \frac{1}{2}(g^{1/3}\underline{I} - \underline{g})$ (3.4.19)

vanishes in the case of isotropic deformation and is therefore a measure for the distortion of a volume element.
In order to establish the constitutive rate equation from the general form (3.3.44) we must first calculate the second order derivatives of F by using (3.4.4) to (3.4.9) inclusive, (3.4.14) and (3.4.17).

$$\begin{aligned}
\frac{\partial^2 F}{\partial \underline{\underline{C}}^2} &= \left(-1/3\,\frac{G}{2\rho_o}\, g^{1/3} + \frac{C_b}{4\rho_o}\, g^{1/6}\right)\underline{C}^{-1}\,\underline{C}^{-1} + \\
&+ \left[\frac{G}{2\rho_o}\, g^{1/3} - \frac{3C_b}{2\rho_o}\left(g^{1/6} - \left(\frac{\rho F}{\rho_o}\right)^{1/3}\right)\right]\underline{C}^{-1} \bullet \underline{\underline{H}} \bullet \underline{C}^{-1}
\end{aligned} \tag{3.4.21}$$

Substitution of (3.4.21) in (3.3.30) yields (see appendix C)

$$\begin{aligned}
\underline{\underline{L}} &= \frac{2\rho}{\rho_o}\left(-1/3\, g^{1/3} G + \tfrac{1}{2}\, C_b\, g^{1/6}\right)\underline{I}\,\underline{I} + \\
&+ \frac{2\rho}{\rho_o}\left[g^{1/3} G - 3\, C_b\left(g^{1/6} - \left(\frac{\rho F}{\rho_o}\right)^{1/3}\right]\right.\underline{\underline{H}}
\end{aligned} \tag{3.4.22}$$

If the volume changes are very small ($g^{1/2} = \frac{\rho}{\rho_o} \simeq \frac{\rho_F}{\rho_o} = 1$), expression (3.4.22) reduces to expression (3.1.5) obtained from linear elastic material. The mixed derivative of the free energy with respect to $\underline{C}$ and T is of particular interest in non-isothermal processes. With (3.4.14) and

(3.1.6) we find

$$\frac{\partial^2 F}{\partial \underline{C} \partial T} = \frac{1}{G} \frac{dG}{dT} \frac{\partial F}{\partial \underline{C}} + \left[\frac{3C_b}{2\rho_o} \alpha + \frac{3G}{\rho_o (1-2\nu)^2} \frac{d\nu}{dT} \left(g^{1/6} - \left(\frac{\rho_F}{\rho_o}\right)^{1/3}\right)\right] \underline{C}^{-1} \qquad (3.4.23)$$

The variation of Poisson's ratio with respect to the temperature plays a minor role in large elastic plastic deformation processes, and will be neglected. With this approximation we can write

$$-2\rho \, \underline{B}^T \cdot \frac{\partial^2 F}{\partial \underline{C} \partial T} \cdot \underline{B} = \frac{1}{G} \frac{dG}{dT} \underline{\sigma} - \frac{3\rho}{\rho_o} C_b \alpha \underline{I} \qquad (3.4.24)$$

With respect to plastic deformation we shall consider a yield criterion and dissipation function which are widely used in metal plasticity and generally referred to as the J_2-flow theory [16]. The energy dissipation function can be written as

$$\xi = \xi \left(\frac{\rho_o}{\rho} \sigma, \; T\right) \qquad (3.4.25)$$

where σ is the equivalent (deviatoric) stress

$$\sigma = \left(\frac{3}{2} \underline{s} : \underline{s}\right)^{1/2} \qquad (3.4.26)$$

with

$$\underline{s} = \underline{\sigma} - \frac{1}{3} \operatorname{tr} \underline{\sigma} \, \underline{I} \qquad (3.4.27)$$

The tensor $\underline{s}$ is the deviatoric stress tensor.

The yield surface and yield potential are assumed to be equal and satisfy the Von Mises yield criterion

$$\phi = \chi = \frac{\rho_o}{\rho} \sigma - \sigma_v \; (T, \; \varepsilon) \qquad (3.4.28)$$

The factor $\frac{\rho_o}{\rho}$ is introduced by V.d. Heijden and Besseling [18] in order to obtain the desired symmetry in the plasticity relation based on normality conditions, (the tensor $\underline{\underline{Y}}^{**}$ in (3.3.44) and (3.3.48) vanishes in that case).

Noting that $$\frac{\partial \sigma}{\partial \underline{\sigma}} = \frac{3}{2\sigma} \underline{s} \qquad (3.4.29)$$

we can write, according to (3.3.36)

$$\lambda \frac{\partial \xi}{\partial \underline{\sigma}} = \left(\frac{\partial \xi}{\partial \sigma}\, \sigma\right)^{-1} \xi \frac{\partial \xi}{\partial \sigma} \frac{3}{2\sigma} \underline{s} = \frac{3\xi}{2\sigma 2} \underline{s} \qquad (3.4.30)$$

Comparing the general form of the yield surface (3.3.32) to (3.4.28) we can formally write

$$\underline{\alpha} = \varepsilon \underline{I} \qquad (3.4.31)$$

and

$$\frac{\partial \phi}{\partial \underline{\alpha}} : \overset{\nabla}{\underline{\alpha}} = - \frac{\partial \sigma_v}{\partial \varepsilon} \dot{\varepsilon} \qquad (3.4.32)$$

We assume that the hardening parameter ε will only change due to time independent plastic deformation, (ϕ_2 in (3.3.41) vanishes) and satisfies the relation

$$\dot{\varepsilon} = \mu \left(\frac{2}{3} \frac{\partial \phi}{\partial \underline{\sigma}} : \frac{\partial \phi}{\partial \underline{\sigma}}\right)^{1/2} = \mu \frac{\rho_o}{\rho} \qquad (3.4.33)$$

In this relation, ε will coincide with the logarithmic (natural) plastic strain in a uniaxial tensile test, hence it is denoted as the equivalent plastic strain. With (3.3.41) we find that

$$\phi_1 = - \frac{\rho_o}{\rho} \frac{\partial \sigma_v}{\partial \varepsilon} \qquad (3.4.34)$$

The yield tensor (3.3.45) up to (3.3.50) inclusive can for this isotropic material be written as

$$\underline{\underline{Y}} = \frac{\underline{M}\,\underline{M}}{N^Y}$$

$$h = \frac{\frac{\rho_o}{\rho} \frac{\partial \sigma_v}{\partial \varepsilon}}{N^Y + \frac{\rho_o}{\rho} \frac{\partial \sigma_v}{\partial \varepsilon}} \qquad (3.4.35)$$

$$\underline{Y}^* = \frac{\underline{M} \left[\frac{\rho_o}{\rho} \frac{\sigma}{G} \frac{\partial G}{\partial T} - \frac{\partial \sigma_v}{\partial T} \right]}{N^Y}$$

where $\underline{M} = \frac{\rho}{\rho_o}\,\underline{\underline{L}}^{*} : \frac{\partial \phi}{\partial \underline{\sigma}} = \frac{\rho}{\rho_o}\,\underline{\underline{L}}^{*} : \left(\frac{\rho_o}{\rho}\,\frac{3\underline{s}}{2\sigma}\right)$

or $\underline{M} = \frac{1}{\sigma}\,[(3\,G^{1} - \mathrm{tr}\,\underline{\sigma})\,\underline{I} - 3\,\underline{s}] \bullet \underline{s}$

, $N^{Y} = \left(\frac{\rho}{\rho_o}\right)^{2} \frac{\partial \phi}{\partial \underline{\sigma}} : \underline{\underline{L}}^{*} : \frac{\partial \phi}{\partial \underline{\sigma}} = 3\,G^{*} - \mathrm{tr}\,\underline{\sigma} - \frac{g}{2\sigma^{2}}\,\mathrm{tr}\,(\underline{s}\bullet\underline{s}\bullet\underline{s})$ (3.4.36)

, $G^{*} = \frac{\rho}{\rho_o}\,[g^{1/3}\,G + 3\,C_b\,(g^{1/6} - \frac{\rho_F}{\rho_o})^{1/3})]$

Note that Y^{**} as well as Y^{***} vanishes.

In the case that the elastic part of the deformations is small, expressions (3.4.36) reduce to

$$\underline{M} = \frac{3\,G\,\underline{s}}{\sigma}$$
$$N^{Y} = 3\,G \qquad (3.4.37)$$

The constitutive rate equation (3.3.44) reduces for this isotropic material to

$$\underline{\sigma}^{\nabla} = -\underline{\sigma}\,\mathrm{tr}\,\underline{D} + (\underline{\underline{L}}^{*} - (1-h)\underline{\underline{Y}}) : (\underline{D} - \frac{3\xi}{2\sigma^{2}}\,\underline{s}) +$$
$$+ (-(1-h)\,\underline{Y}^{*} + \frac{1}{G}\frac{dG}{dT}\,\underline{\sigma} - \frac{3\rho}{\rho_o}\,C_b\,\alpha\,\underline{I})\,\dot{T} \qquad (3.4.38)$$

3.5. Fraction (or overlay) model.

In the fraction model each volume element is thought to be subdivided in a finite number of subelements or fractions. The fractions have mutually different properties but are isotropic. The fractions are all subjected to equal macroscopic deformations.
The fraction model introduced by Besseling [4], was at that time formulated for small deformations and rotations. The theory has been extended to large inelastic deformations and rotations, but restricted to small elastic strains within each fraction in [7, 18].
As has been shown in section 3.2, it is necessary to take into account at least one fraction which is subjected to large elastic deformations, in order to obtain a proper prediction of kinematic hardening. Therefore in the present formulation no restrictions are assumed as regards the elastic strains.

In the fraction model the stress tensor is obtained from a weighed sum of the fraction stress tensors

$$\underline{\sigma} = \sum_{k=1}^{N} \psi^k \, \underline{\sigma}^k \tag{3.5.1}$$

where N is the number of fractions and ψ^k the weight factors or volume fractions.

$$\sum_{k=1}^{N} \psi^k = 1 \tag{3.5.2}$$

The constitutive rate equation is accordingly given by

$$\overset{\nabla}{\underline{\sigma}} = \sum_{k=1}^{N} \psi^k \, \overset{\nabla}{\underline{\sigma}}{}^k \tag{3.5.3}$$

where the Jaumann rate $\overset{\nabla}{\underline{\sigma}}{}^k$ of each fraction satisfies the (isotropic) equation (3.4.38)

$$\overset{\nabla}{\underline{\sigma}}{}^{k} = -\underline{\sigma}^{k}\ \mathrm{tr}\ \underline{D} + [\underline{\underline{L}}^{*k} - (1-h^{k})\ \underline{\underline{Y}}^{k}] : (\underline{D} - \frac{3\xi^{k}}{2\ (\sigma^{k})^{2}}\ \underline{s}^{k}) +$$

$$+ [-\ (1-h)\ \underline{Y}^{*\,k} + \frac{1}{G}\ \frac{dG}{dT}\ \underline{\sigma}^{k}\ 1\ \frac{3\rho}{\rho o}\ C_{b}\ \alpha\ \underline{I}]\ \dot{T} \qquad (3.5.4)$$

The elastic properties, represented by G and G_b and the mass density are assumed to be equal for all fractions, and hence the elastic tensor $\underline{\underline{L}}$ (3.4.22) is the same for each fraction. However, the tensor $\underline{\underline{L}}^{*}$ will be different for each fraction because equation (3.3.43) must be evaluated at fraction level, hence fraction stresses must be substituted.
For small elastic strains the difference between $\underline{\underline{L}}$ and $\underline{\underline{L}}^{*}$ may be neglected.

The main advantage of the fraction model is that it describes anisotropic strain hardening such as the Bausschinger effect, primary and secondary creep and creep recovery, whereas the formulation is based on rather simple isotropic material properties on fraction level.

The fraction model has been verified by biaxial plastic deformation tests on tubular specimens, reported in [25].

3.6. Phase changes.

When phase changes occur, the material can be thought to be subdivided into a number of mass fractions (ζ^k), which values change due to phase transformations. For each single phase the internal energy is assumed to be a function of the temperature according to (2.1.24).

$$e^k = e^k(T) = \int_{T_o}^{T} c^k(\tau)\, d(\tau) + r^k \qquad (3.6.1)$$

The total internal energy is the weighed sum of the fractions

$$e = \sum_{k=1}^{N} e^k\,(T)\, \zeta^k \qquad (3.6.2)$$

The volume fraction ψ^k of each phase is related to the mass fraction by

$$\psi^k = \frac{\rho}{\rho^k}\, \zeta^k \qquad (3.6.3)$$

where ρ^k is the density referred to, when the material exists in phase k only ($\rho = \rho^k$ if $\psi^k = 1$ and $\zeta^k = 1$). Both ψ^k and ζ^k satisfy the condition

$$\sum_{k=1}^{N} \psi^k = 1$$

$$\sum_{k=1}^{N} \zeta^k = 1 \qquad (3.6.4)$$

The mass density can be expressed as a weighed sum using (3.6.3) and (3.6.4)

$$\rho = \sum_{k=1}^{N} \psi^k\, \rho^k \qquad (3.6.5)$$

In a reversible process, the mass fractions can be expressed as a function of state variables. In liquid-gas transformations the mass fractions are usually regarded as a function of the temperature and the entropy.

If transformations occur within a temperature range in solids, the mass

fractions can be expressed as a function of the temperature. These functions can be determined from a transformation test in a stress-free state. Consequently the internal energy is also a function of the temperature only. Phase changes are then implicitly taken into account by (a modification of) the specific heat. In the limited case that transformations occur at a constant temperature the mass fraction should be expressed as a function of the entropy. In numerical procedures however it is advantageous to approximate the latter case by a small temperature range in which the transformations occur with a large (finite) specific heat.

With these approximations, reversible phase changes can be taken into account within the formulation given in the previous sections. Phase dependent mechanical properties must be taken into account by appropriate temperature-dependent values.

When phase changes occur irreversibly, the mass fraction can not be expressed as a function of state variables. Irreversible phase changes occur in fast cooling processes, like quenching of steel. In this kind of processes, a phase that in an equilibrium state only exists beyond a particular temperature, remains present at a lower temperature. This phenomenon can mathematically be taken into account by introducing an upperbound for the rate of change of phase transformations

$$\dot{\xi}^k = \frac{d\xi_e^k}{dT}\dot{T} \quad \text{if} \quad \| \frac{d\xi_e^k}{dT}\dot{T} \| \leq \| \dot{\xi}^k_{crit} \| ,$$

$$\dot{\xi}^k = \dot{\xi}^k_{crit} \quad \text{if} \quad \| \frac{d\xi_e^k}{dT}\dot{T} \| > \| \dot{\xi}^k_{crit} \| \qquad (3.6.6)$$

or if T is out of the equilibrium range,

where $\xi_e^k = \xi_e^k(T)$ is the mass fractions in an equilibrium state at temperature T. The critical rates of phase changes $\dot{\xi}^k_{crit}$ are assumed to be a function of the state variables [23, 45, 47].
The rate of change of the internal energy can be expressed, using (3.6.1), (3.6.2) and (3.6.6) as

$$\dot{e} = \sum_{k=1}^{N} \dot{e}^k(T)\,\zeta^k + \sum_{k=1}^{N} e^k(T)\,\dot{\zeta}^k$$

or

$$\dot{e} = c^*\,\dot{T} + \sum_{k=1}^{N} \left[\int_{T_o}^{T} c^k(\tau)\,d\tau + r^k\right]\dot{\zeta}^k \qquad (3.6.7)$$

where

$$c^* = \sum_{k=1}^{N} c^k(T)\,\zeta^k \qquad (3.6.8)$$

The density changes due to phase transformation may, in a non-homogeneous process, result into internal stresses and inelastic deformations. (In a steel quenching process the density of the martensite phase is about 3% lower than the density of the austenite phase).
Residual stresses that remain in a product after the transformation may lead to damage (internal micro cracks) which in turn results in reduction of life time of the product or even disapproval. Hence density changes are of considerable interest. In the mathematical model we can take this into account by an extension of the description of thermal expansion by considering the density in a stress-free state ρ_F similar to the description given in section (3.4).According (3.6.5) we find for the stress-free state

$$\rho_F = \sum_{k=1}^{N} \psi^k\,\rho_F^k(T) \qquad (3.6.9)$$

The rate of change of the density is then

$$\frac{d}{dt}\left(\frac{\rho_F}{\rho_o}\right) = \sum_{k=1}^{N} \psi^k\,\frac{\partial}{\partial T}\left(\frac{\rho_F^k}{\rho_o}\right)\dot{T} + \sum_{k=1}^{N} \frac{\rho_F^k}{\rho_o}\,\dot{\psi}^k \qquad (3.6.10)$$

The first term in the right hand side of (3.6.10) represents thermal expansion and the second term expansion due to phase changes. According (3.4.15) we can write

$$\frac{\partial}{\partial T}\left(\frac{\rho_F^k}{\rho_o}\right) = -3\left(\frac{\rho_F^k}{\rho_o}\right)^{2/3}\alpha^k \qquad (3.6.11)$$

The rate of change of the volume fraction can be expressed in the rate of

change of the mass fractions using (3.6.3) for the stress-free case

$$\psi^k = \frac{\rho_F}{\rho_F^k}\,\zeta^k \qquad (3.6.12)$$

Hence

$$\dot{\psi}^k = \left(\frac{\rho_F}{\rho_F^k}\right)\dot{\xi}^k + \left(\frac{\rho_F}{\rho_F^k}\right)^{\bullet}\zeta^k \qquad (3.6.13)$$

In the second term of the right hand side of (3.6.13) the factor with the quotient of ρ_F and ρ_F^k should be eliminated using (3.6.10) and (3.6.11). In solids and liquids however, this quotient can be assumed to be approximately equal to 1 and consequently the second term in the right hand side of (3.6.13) can be neglected. Hence

$$\dot{\psi}^k \simeq \dot{\xi}^k \qquad (3.6.14)$$

(In an analysis of the steel quenching process, the difference between $\dot{\psi}^k$ and $\dot{\xi}^k$ has a maximum of 3%).
In the case of a full transformation from one single phase to another, ψ^k and ζ^k coincide at the start as well as at the end of the transformation, hence the accumulated error due to the approximation (3.6.14) is smaller then the relative difference between the density of phases respectively.

In the case of an isotropic material model, the density changes due to phase changes can be taken into account by replacing the factor $\alpha\,\dot{T}$ in (3.4.38) by

$$-\frac{d}{dt}\left\{\left(\frac{\rho_F}{\rho_o}\right)^{1/3}\right\} = -\,1/3\,\left(\frac{\rho_F}{\rho_o}\right)^{-2/3}\left(\frac{\rho_F}{\rho_o}\right)^{\bullet} \qquad (3.6.15)$$

or with (3.6.10)

$$-\frac{d}{dt}\left\{\left(\frac{\rho_F}{\rho_o}\right)^{1/3}\right\} = \alpha^*\,\dot{T} - 1/3\,\left(\frac{\rho_F}{\rho_o}\right)^{-2/3}\sum_{k=1}^{N}\frac{\rho_F^k}{\rho_o}\,\dot{\psi}^k \qquad (3.6.16)$$

where $\alpha^* = \sum_{k=1}^{N}\zeta^k\,\alpha^k$

Not only the density is dependent on the (change of the) phases, also the

mechanical properties change due to transformations. This means that material parameters, yield surface and dissipation must be regarded as functions of the fractions. However, an average yield stress as a weighed sum of the yield stresses of the fractions is expected to be unrealistic, yielding will occur if the yield stress of the weakest fraction is reached whereas the other fractions are not yet yielding. Hence it is to be expected that a description based on (an extension of) the fraction model may result into reasonable predictions for the material behaviour. In this extended model, the fractions are directly coupled with the volume fractions of the phases. This extension involves that all phases are assumed to be subjected to equal deformations, which may be a rather crude assumption.

The stress tensor in this extended model is given by the weighed sum of the fractional stresses (3.5.1) whereas the rate equation (3.5.3) must be extended to

$$\overset{\nabla}{\underline{\sigma}} = \sum_{k=1}^{N} \psi^k \overset{\nabla}{\underline{\sigma}}^k + \sum_{k=1}^{N} \underline{\sigma}^k \dot{\psi}^k \qquad (3.6.17)$$

The Jaumann rate of the fractional stresses satisfy equation (3.5.4) except that the thermal expansion term $\alpha\dot{T}$ is replaced by (3.6.16).

In the description of the hardening it should be taken into account that softening occurs due to transformations, because hardening in one phase will vanish after it is transformed. We can take this effect into account by a hardening parameter H^k for each phase. This parameter increases due to plastic deformation and decreases if a phase is growing.

$$\dot{H}^k = \dot{\varepsilon}^k - \frac{1}{\psi^k} \dot{\psi}^k H^k \qquad \text{if} \quad \dot{\psi}^k > 0 \ \text{and} \ \psi^k > 0 \qquad (3.6.18)$$

$$\dot{H}^k = \dot{\varepsilon}^k \qquad \text{if} \quad \dot{\psi}^k \leqslant 0$$

The yield surface for each fraction according to (3.4.28) is:

$$\phi = \frac{\rho_o}{\rho} \sigma^k - \sigma_v^k \ (T, H^k) \qquad (3.6.19)$$

Equation (3.6.17) implies that the parameter ϕ_2 in (3.3.41) does not vanish

$$\phi_2 = -\frac{\partial \sigma_v}{\partial H}\,\frac{H^k}{\psi^k}\,\dot{\psi}^k \quad \text{if} \quad \dot{\psi}^k > 0 \quad \text{and} \quad \psi^k > 0 \tag{3.6.20}$$

and in the constitutive equation also the tensor $\underline{Y}^{***}$ (3.3.49) must be taken into account.

The extended fraction model was applied for the purpose of making an analysis of a steel quenching process of a cylindrical bar. The results are discussed in chapter 5.

IV Finite element formulation.

4.1. Virtual power and virtual heat.

The finite element method can be regarded as a numerical method for solving differential equations approximately.
The basic (differential) equations describing a thermo-mechanical deformation process are given in chapters 2 and 3. A number of unknown field variables (rate of deformation, spin, heat flux) can easily be expressed in other field variables (velocity, temperature) and therefore be eliminated in the solution procedure. This implies that the equations by which field variables are eliminated, are satisfied exactly, whereas the remaining equations are only satisfied approximately.
A commonly applied procedure in finite element analysis of mechanical problems is solving the equilibrium equations approximately, whereas constitutive equations and compatibility equations are exactly satisfied. This procedure will be adapted here too with respect to both, mechanical and thermal equilibrium equations, (2.1.18) and (2.1.19) respectively.

Firstly we shall consider mechanical equilibrium (or conservation of momentum). The mechanical equilibrium equation can be written in the weak formulation

$$\delta W = \int_V \delta \underset{\sim}{v} \bullet (\underline{\sigma} \bullet \overset{\leftarrow}{\nabla} + \rho \underset{\sim}{f}) \, dV = o \quad \text{for any } \delta \underset{\sim}{v} \qquad (4.1.1)$$

Where V is the current volume of the body. The inertia terms are not explicitly taken into account in (4.1.1) but may be regarded as a part of the body force $\underset{\sim}{f}$.

By applying the divergence theorem, we can write

$$\delta W = \int_V (\overset{\rightarrow}{\nabla} \delta \underset{\sim}{v} : \underline{\sigma} - \delta \underset{\sim}{v} \bullet \rho \underset{\sim}{f}) \, dV - \int_V \delta \underset{\sim}{v} \bullet \underset{\sim}{t} \, ds = o \quad \text{for any } \delta \underset{\sim}{v} \qquad (4.1.2)$$

Equation (4.1.2) is known as the virtual power equation. The introduced independent field vector $\delta \underset{\sim}{v}$ is denoted as the virtual velocity. The vector $\underset{\sim}{t}$ represents the surface traction per unit outer surface and is related to the stress tensor and the unit normal vector $\underset{\sim}{n}$ by

$$\underset{\sim}{t} = \underline{\sigma} \cdot \underset{\sim}{n} \qquad (4.1.3)$$

The stress tensor cannot directly be eliminated from (4.1.2) (as against a linear elastic problem) because the constitutive equations (3.3.44) and (3.4.38) yield an explicit expression for the stress rate, not for the total stress.

We can obtain a weak formulation of the equilibrium equation containing the stress rate by considering the material rate of change of (4.1.2) and require that the resulting expression vanishes for any (time dependent) virtual velocity field. By applying formula (2.1.16) we find

$$\delta\dot{W} = \int_V [(\overset{\rightarrow}{\nabla}\, \delta\underset{\sim}{v})^{\bullet} : \underline{\sigma} + \overset{\rightarrow}{\nabla}\, d\underset{\sim}{v} : \dot{\underline{\sigma}} - \delta\dot{\underset{\sim}{v}} \cdot \rho\underline{f} - \delta\underset{\sim}{v} \cdot (\rho\underline{f})^{\bullet} +$$

$$+ (\overset{\rightarrow}{\nabla}\, \delta\underset{\sim}{v} : \underline{\sigma} - \delta\underset{\sim}{v} \cdot \rho\underline{f})\, \overset{\rightarrow}{\nabla} \cdot \underset{\sim}{v}]\, dV + \qquad (4.1.4)$$

$$- \int_S [\delta\dot{\underset{\sim}{v}} \cdot \underset{\sim}{t} + \delta\underset{\sim}{v} \cdot \dot{\underset{\sim}{t}} + (\delta\underset{\sim}{v} \cdot \underset{\sim}{t})\, \overset{\rightarrow}{\nabla}_{\sim s} \cdot \underset{\sim s}{v}]\, dS = o \quad \text{for any } \delta\underset{\sim}{v}$$

The term $\overset{\rightarrow}{\nabla}_{\sim s} \cdot \underset{\sim s}{v}$ is the divergence of the surface component of the velocity in the two-dimensional (curved) subspace s and denotes the rate of change of a unit surface area. The material rate of change of the gradient of the virtual velocity can be written as

$$(\overset{\rightarrow}{\nabla}\, \delta\underset{\sim}{v})^{\bullet} = \frac{\partial}{\partial t}\, \overset{\rightarrow}{\nabla}\, \delta\underset{\sim}{v} + \underset{\sim}{v} \cdot \overset{\rightarrow}{\nabla}\, (\overset{\rightarrow}{\nabla}\, \delta\underset{\sim}{v}) = \overset{\rightarrow}{\nabla}\, (\frac{\partial \delta\underset{\sim}{v}}{\partial t} + \underset{\sim}{v} \cdot \overset{\rightarrow}{\nabla}\, \delta\underset{\sim}{v}) - (\overset{\rightarrow}{\nabla}\, \underset{\sim}{v}) \cdot (\overset{\rightarrow}{\nabla}\, \delta\underset{\sim}{v})$$

$$\text{or} \qquad (\overset{\rightarrow}{\nabla}\, \delta\underset{\sim}{v})^{\bullet} = \overset{\rightarrow}{\nabla}\, \delta\dot{\underset{\sim}{v}} - \overset{\rightarrow}{\nabla}\, \underset{\sim}{v} \cdot \overset{\rightarrow}{\nabla}\, \delta\underset{\sim}{v} \qquad (4.1.5)$$

By substitution of (4.1.5) into (4.1.4) and separating the terms containing $\delta\underset{\sim}{v}$ and $\delta\dot{\underset{\sim}{v}}$ respectively, we find

$$\delta\dot{W} = \int_V [\overset{\rightarrow}{\nabla}\, \delta\underset{\sim}{v} : \dot{\underline{\sigma}} - (\overset{\rightarrow}{\nabla}\underset{\sim}{v} \cdot \overset{\rightarrow}{\nabla}\delta\underset{\sim}{v}) : \underline{\sigma} + \overset{\rightarrow}{\nabla}\delta\underset{\sim}{v} : \underline{\sigma}\, \overset{\rightarrow}{\nabla} \cdot \underset{\sim}{v}]\, dV +$$

$$- \int_V [\delta\underset{\sim}{v} \cdot (\rho\underline{f})^{\bullet} + \delta\underset{\sim}{v} \cdot \rho\underline{f}\, \overset{\rightarrow}{\nabla} \cdot \underset{\sim}{v}]\, dV +$$

$$- \int_S (\delta\underset{\sim}{v} \cdot \dot{\underset{\sim}{t}} + \delta\underset{\sim}{v} \cdot \underset{\sim}{t}\, \overset{\rightarrow}{\nabla}_{\sim s} \cdot \underset{\sim s}{v})\, dS +$$

$$+ \int_V (\overset{\rightarrow}{\nabla}\delta\dot{\underset{\sim}{v}} : \underline{\sigma} - \delta\dot{\underset{\sim}{v}} \cdot \rho\underline{f})\, dV - \int_S \delta\dot{\underset{\sim}{v}} \cdot \underset{\sim}{t}\, dS = o \quad \text{for any } \delta\underset{\sim}{v} \qquad (4.1.6)$$

Because of equation (4.1.2) all terms containing $\delta\dot{\underset{\sim}{v}}$ (the last two

integrals) vanish.

The stress rate can now be eliminated by means of the constitutive equation. We can formally write the constitutive equations as

$$\overset{\nabla}{\sigma} = \frac{\dot{\rho}}{\rho}\,\underline{\sigma} + \underline{\underline{L}}^{Y} : \underline{D} + \underline{L}^{q}\,\dot{T} - \underline{\Phi}^{d} \qquad (4.1.7)$$

The tensors $\underline{\underline{L}}^{Y}$ and $\underline{L}^{q}$ are found by substituting the appropriate terms of either (3.3.44), (3.4.38), (3.5.3), (3.5.4) or (3.6.17) depending on the type of the analysis. The tensor $\underline{\Phi}^{d}$ represents dissipation due to creep and terms related to irreversible phase transformation depending on the state variables.
Substitution of (4.1.7) in (4.1.6) using (3.1.4), we find

$$\dot{\delta W} = \int_V [\overset{\rightarrow}{\nabla}\,\delta\underset{\sim}{v} : \underline{\sigma}\,\frac{\dot{\rho}}{\rho} + \overset{\rightarrow}{\nabla}\,\delta\underset{\sim}{v} : \underline{\underline{L}}^{Y} : \underline{D} + \overset{\rightarrow}{\nabla}\,\delta\underset{\sim}{v} : (\underline{\Omega}\cdot\underline{\sigma} - \underline{\sigma}\cdot\underline{\Omega}) +$$
$$+ \overset{\rightarrow}{\nabla}\,\delta\underset{\sim}{v} : \underline{\underline{L}}^{q}\dot{T} - \overset{\rightarrow}{\nabla}\,\delta\underset{\sim}{v} : \underline{\Phi}^{d} - (\overset{\rightarrow}{\nabla}\underset{\sim}{v} \cdot \overset{\rightarrow}{\nabla}\,\delta\underset{\sim}{v}) : \underline{\sigma} + \overset{\rightarrow}{\nabla}\,\delta\underset{\sim}{v} : \underline{\sigma}\,\overset{\rightarrow}{\nabla}\cdot\underset{\sim}{v}]\,dV + \qquad (4.1.8)$$
$$- \int_V (\delta\underset{\sim}{v} \cdot \rho\dot{\underset{\sim}{f}})dV - \int_S (\delta\underset{\sim}{v} \cdot \dot{\underset{\sim}{t}} + \delta\underset{\sim}{v} \cdot \underset{\sim}{t}\,\overset{\rightarrow}{\nabla}_{\underset{\sim}{s}} \cdot \underset{\sim}{v}_{\underset{\sim}{s}})dS = o \qquad \text{for any } \delta\underset{\sim}{v}$$

The first and last term in the first integral cancel due to equation (2.1.17). The third and sixth term can be combined

$$\overset{\rightarrow}{\nabla}\,\delta\underset{\sim}{v} : (\underline{\Omega}\cdot\underline{\sigma} - \underline{\sigma}\cdot\underline{\Omega}) - \overset{\rightarrow}{\nabla}\underset{\sim}{v} \cdot \overset{\rightarrow}{\nabla}\,\delta\underset{\sim}{v} : \underline{\sigma} =$$
$$= \mathrm{tr}\,[\tfrac{1}{2}\,\delta\underset{\sim}{v}\,\overset{\leftarrow}{\nabla} \cdot \underset{\sim}{v}\overset{\leftarrow}{\nabla} \cdot \underline{\sigma} - \tfrac{1}{2}\,\delta\underset{\sim}{v}\,\overset{\leftarrow}{\nabla} \cdot \overset{\rightarrow}{\nabla}\,\underset{\sim}{v} \cdot \underline{\sigma} +$$
$$- \tfrac{1}{2}\,\overset{\rightarrow}{\nabla}\,\delta\underset{\sim}{v} \cdot \overset{\rightarrow}{\nabla}\underset{\sim}{v} \cdot \underline{\sigma} + \tfrac{1}{2}\,\overset{\rightarrow}{\nabla}\,\delta\underset{\sim}{v} \cdot \underset{\sim}{v}\overset{\leftarrow}{\nabla} \cdot \sigma - \delta\,\underset{\sim}{v}\overset{\leftarrow}{\nabla} \cdot \underset{\sim}{v}\overset{\leftarrow}{\nabla} \cdot \underline{\sigma}]$$
$$= \mathrm{tr}\,[-\tfrac{1}{2}\,(\delta\underset{\sim}{v}\,\overset{\leftarrow}{\nabla} + \overset{\rightarrow}{\nabla}\,\delta\underset{\sim}{v}) \cdot (\underset{\sim}{v}\overset{\leftarrow}{\nabla} + \overset{\rightarrow}{\nabla}\underset{\sim}{v}) \cdot \underline{\sigma} + \overset{\rightarrow}{\nabla}\,\delta\underset{\sim}{v} \cdot \underset{\sim}{v}\overset{\leftarrow}{\nabla} \cdot \underline{\sigma}]$$
$$= -2\,(\delta\,\underline{D} \cdot \underline{D}) : \underline{\sigma} + (\overset{\rightarrow}{\nabla}\,\delta\underset{\sim}{v} \cdot \underset{\sim}{v}\overset{\leftarrow}{\nabla}) : \underline{\sigma} \qquad (4.1.9)$$

Here $\delta\underline{D}$ is the virtual rate of deformation tensor

$$\delta\underline{D} = \tfrac{1}{2}\,(\delta\underset{\sim}{v}\,\overset{\leftarrow}{\nabla} + \overset{\rightarrow}{\nabla}\,\delta\underset{\sim}{v}) \qquad (4.1.10)$$

With (4.1.9) we can write (4.1.8) as

$$\delta\dot{W} = \int_V [\delta\underline{D} : \underline{\underline{L}}^{Y} : \underline{D} - 2(\delta\underline{D} \bullet \underline{D}) : \underline{\sigma} + (\overset{\rightarrow}{\underset{\sim}{\nabla}}\, \delta\underset{\sim}{v} \bullet \underset{\sim}{v}\overset{\leftarrow}{\underset{\sim}{\nabla}}) : \underline{\sigma}]\, dV +$$

$$+ \int_V (\delta\underline{D} : \underline{L}^{q}\dot{T})dV - \int_V (\delta\underline{D} : \underline{\Phi}^{d})dV - \int_V (\rho\, \delta\underset{\sim}{v} \bullet \dot{\underset{\sim}{f}})\, dV + \qquad (4.1.11)$$

$$- \int_S (\delta\underset{\sim}{v} \bullet \dot{\underset{\sim}{t}} + \delta\underset{\sim}{v} \bullet \underset{\sim}{t}\, \overset{\rightarrow}{\underset{\sim}{\nabla}}_{s} \bullet \underset{\sim}{v}_{s})\, dS = o \quad \text{for any } \delta\underset{\sim}{v}$$

Note that the first integral is symmetric with respect to $\delta\underset{\sim}{v}$ and $\underset{\sim}{v}$ providing that $\underline{\underline{L}}^{Y}$ obeys an associated flow rule. Hence it will yield a symmetrical finite element matrix. However, the surface tractions may lead to a non symmetric contribution if the surface part with non vanishing tractions changes considerably (second term in the last integral of 4.1.11).

In order to calculate the temperature changes, the thermal equilibrium equation (2.1.19), (conservation of energy) is also written in a weak formulation

$$\delta\dot{Q} = \int_V [\delta\dot{T}\, (-\underline{\sigma} : \underline{D} + \rho\dot{e} - \overset{\rightarrow}{\underset{\sim}{\nabla}} \bullet (\underline{\lambda} \bullet \overset{\rightarrow}{\underset{\sim}{\nabla}} T)]\, dV = o \quad \text{for any } \delta\dot{T} \qquad (4.1.12)$$

By the divergence theorem, we can write

$$\delta\dot{Q} = \int_V [\delta\dot{T}\, (-\underline{\sigma} : \underline{D} + \rho\dot{e}) + \overset{\rightarrow}{\underset{\sim}{\nabla}}\, \delta\dot{T} \bullet \underline{\lambda} \bullet \overset{\rightarrow}{\underset{\sim}{\nabla}} T]\, dV +$$

$$+ \int_S \delta\dot{T}\, \underset{\sim}{\phi} \bullet \underset{\sim}{n}\, dS = o \quad \text{for any } \delta\dot{T} \qquad (4.1.13)$$

The rate of change of the internal energy can, according to (3.6.7), formally be written as

$$\dot{e} = c\dot{T} + \phi^{e} \qquad (4.1.14)$$

where ϕ^{e} represents the second term in (3.6.7) and vanishes if no phase changes occur.
Particularly in cold forming processes, temperature changes are mainly due to plastic deformation work and friction. Hence the thermal problem cannot be solved independently from the mechanical problem. They have to be solved simultaneously. We can combine (4.1.11) and 4.1.13) in one functional that must vanish for all (kinematically admissible) virtual velocity fields and virtual rate of temperature fields

$$\delta\dot{P} = \delta\dot{W} + \delta\dot{Q} = 0 \qquad \text{for any } \delta\underset{\sim}{v},\ \delta\dot{T} \qquad (4.1.15)$$

4.2. Finite element discretization.

If we assume that at a particular time t all state variables are known, then we can calculate (approximately) the velocity and temperature rate at that time from (4.1.15). We will use the commonly applied (isoparametric) finite element discretization [51].

In each element the velocity and temperature are approximated by interpolation between (unknown) nodal point values.

$$\begin{aligned} \underset{\sim}{v} &= \sum_N \Psi^N \, \underset{\sim}{v}^N \\ T &= \sum_N \Psi^N \, T^N \\ \delta\underset{\sim}{v} &= \sum_N \Psi^N \, \delta\underset{\sim}{v}^N \\ \delta\dot{T} &= \sum_N \Psi^N \, \delta\dot{T}^N \end{aligned} \qquad (4.2.1)$$

Isoparametric elements are used. The interpolation functions Ψ^N depend on local natural coordinates and are therefore time independent. The temperature rate can then be expressed in the nodal point temperature rates

$$\dot{T} = \sum_N \Psi^N \, \dot{T}^N \qquad (4.2.2)$$

The gradients of the velocity and temperature are respectively

$$\begin{aligned} \overset{\rightarrow}{\nabla}\underset{\sim}{v}\,\underset{\sim}{v} &= \sum_N \overset{\rightarrow}{\nabla}\underset{\sim}{\Psi}^N \, \underset{\sim}{v}^N \\ \overset{\rightarrow}{\nabla}\underset{\sim}{T} &= \sum_N \overset{\rightarrow}{\nabla}\underset{\sim}{\Psi}^N \, T^N \end{aligned} \qquad (4.2.3)$$

The rate of deformation tensor can be expressed as

$$\underline{D} = \sum_N \underline{\underline{B}}^N \bullet \underset{\sim}{v}^N \qquad (4.2.4)$$

where $\underline{\underline{B}}^N$ is a third order tensor depending on $\overset{\rightarrow}{\nabla}\underset{\sim}{\Psi}^N$

$$\underline{\underline{B}}^N = \tfrac{1}{2}\,[\overset{\rightarrow}{\nabla}\underset{\sim}{\Psi}^N \, \underline{I} + \underline{\underline{K}} : (\overset{\rightarrow}{\nabla}\underset{\sim}{\Psi}^N \, \underline{I})] \qquad (4.2.5)$$

Note: The Cartesian components of $\underline{\underline{B}}^N$ are

$$B_{ijk}^{N} = \frac{1}{2} \left[\delta_{jk} \frac{\partial \Psi^{N}}{\partial x_i} + \delta_{ik} \frac{\partial \Psi^{N}}{\partial x_j} \right] \qquad (4.2.6)$$

For the virtual velocity and virtual temperature rate, relations similar to (4.2.3) and (4.2.4) hold

$$\begin{aligned} \overset{\rightarrow}{\nabla}_{\sim} \delta \underset{\sim}{v} &= \sum_{N} \overset{\rightarrow}{\nabla}_{\sim} \Psi^{N} \delta \underset{\sim}{v}^{N} \\ \overset{\rightarrow}{\nabla}_{\sim} \delta \dot{T} &= \sum_{N} \overset{\rightarrow}{\nabla}_{\sim} \Psi^{N} \delta \dot{T} \end{aligned} \qquad (4.2.7)$$

$$\delta \underline{D} = \sum_{N} \underset{\approx}{B}^{N} \bullet \delta \underset{\sim}{v}^{N} = \sum_{N} \delta \underset{\sim}{v}^{N} \bullet \underset{\approx}{B}^{*N} \qquad (4.2.8)$$

where $$\underset{\approx}{B}^{*N} = \frac{1}{2} \left[\underline{I} \, \Psi^{N} \overset{\leftarrow}{\nabla}_{\sim} + (\underline{I} \, \Psi^{N} \overset{\leftarrow}{\nabla}_{\sim}) : \underline{\underline{K}} \right] \qquad (4.2.9)$$

Substitution of (4.2.1) up to (4.2.8) inclusive in the expression for $\delta \dot{W}$ (4.1.11) yields

$$\begin{aligned} \delta W = & \sum_{M,N} \{ \delta \underset{\sim}{v}^{M} \bullet [\underline{K}^{MN} + \underline{K}_{s}^{MN}] \bullet \underset{\sim}{v}^{N} \} + \\ & + \sum_{M,N} (\delta \underset{\sim}{v}^{M} \bullet \underset{\sim}{R}^{MN} \dot{T}^{N}) - \sum_{M} \delta \underset{\sim}{v}^{M} + \dot{\underset{\sim}{f}}^{M} \end{aligned} \qquad (4.2.10)$$

where

$$\begin{aligned} \underline{K}^{MN} = & \int_{V} [\underset{\approx}{B}^{*M} : (\underline{\underline{L}}^{Y} - \underline{\underline{H}} \bullet \underline{\sigma} - \underline{\sigma} \bullet \underline{\underline{H}}) : \underset{\approx}{B}^{N}] \, dV + \\ & + \int_{V} [\underline{I} \, (\overset{\rightarrow}{\nabla}_{\sim} \Psi^{M} \bullet \underline{\sigma} \bullet \overset{\rightarrow}{\nabla}_{\sim} \Psi^{N})] \, dV \end{aligned} \qquad (4.2.11)$$

$$\underline{K}_{s}^{MN} = - \int_{S} \Psi^{M} \underset{\sim}{t} \overset{\rightarrow}{\nabla}_{\sim s} \Psi^{N} \, dS \qquad (4.2.12)$$

$$\underset{\sim}{R}^{MN} = \int_{V} \underset{\approx}{B}^{*M} : \underline{L}^{q} \Psi^{N} \, dV \qquad (4.2.13)$$

and

$$\dot{\underset{\sim}{f}}^{M} = \int_{V} [\underset{\approx}{B}^{*M} : \underline{\Phi}^{d} + \Psi^{M} \rho \dot{\underset{\sim}{f}}] \, dV + \int_{S} \Psi^{M} \dot{\underset{\sim}{t}} \, dS \qquad (4.2.14)$$

For $\delta \dot{Q}$ (4.1.13) we find

$$\delta\dot{Q} = \sum_{M,N} (-\delta\dot{T}^M \underset{\sim}{Q}^{MN} \bullet \underset{\sim}{v}^N + \delta\dot{T}^M P^{MN} \dot{T}^N) +$$

$$+ \sum_{M,N} (\delta\dot{T}^M \lambda^{MN} T^N) + \sum_{M} (\delta\dot{T}^M \phi^M) \qquad (4.2.15)$$

where

$$\underset{\sim}{Q}^{MN} = \int_V \Phi^M \underline{\sigma} : \underline{\underline{B}}^N \, dV \qquad (4.2.16)$$

$$P^{MN} = \int_V \Psi^M \rho \, c \, \Psi^N \, dV \qquad (4.2.17)$$

$$\lambda^{MN} = \int_V \overset{\rightarrow}{\nabla}_{\sim} \Psi^M \bullet \underline{\lambda} \bullet \overset{\rightarrow}{\nabla}_{\sim} \Psi^N \, dV \qquad (4.2.18)$$

$$\phi^M = \int_S \Psi^M \underset{\sim}{\phi} \bullet \underset{\sim}{n} \, dS + \int_V \Psi^M \phi^e \, dV \qquad (4.2.19)$$

We now require that both $\delta\dot{W}$ and $\delta\dot{Q}$ vanish for all nodal virtual velocities and virtual temperature rates that are 'kinematically admissible'. In a matrix form this can be written as

$$\sum_{M,N} \left[\delta\underset{\sim}{v}^M, \; \delta\dot{T}^M \right] \begin{bmatrix} \underline{K}^{*MN} & \underset{\sim}{R}^{MN} \\ -\underset{\sim}{Q}^{MN} & P^{MN} \end{bmatrix} \begin{bmatrix} \dot{\underset{\sim}{v}}^N \\ \dot{T}^N \end{bmatrix} +$$

$$\left[\delta\underset{\sim}{v}^M, \; \delta\dot{T}^M\right] \begin{bmatrix} \underline{o} & \underset{\sim}{o} \\ \underset{\sim}{o} & \lambda^{MN} \end{bmatrix} \begin{bmatrix} \underset{\sim}{o} \\ T^N \end{bmatrix} + \qquad (4.2.20)$$

$$\left[\delta\underset{\sim}{v}^M, \; \delta\dot{T}^M\right] \begin{bmatrix} -\underset{\sim}{f}^M \\ \phi^M \end{bmatrix} = o \qquad \text{for any } \delta\underset{\sim}{v}^M, \; \delta\dot{T}^M$$

We can regard all nodal degrees of freedom as an ordered collection representing a multidimensional vector $[\dot{U}]$. This vector contains four components per node, three velocity components and the temperature rate. The subvector with all velocity components will be denoted as $[v]$ and the subvector with all temperature rates as $[\dot{T}]$

$$[\dot{U}]^T = [\, [v]^T, \; [\dot{T}]^T \,] = [\, \{v_i^N\}, \; \{\dot{T}^N\}] \qquad (4.2.21)$$

The requirement that (4.2.20) vanishes for all values of $\delta\underset{\sim}{v}^M$ and $\delta\dot{T}^M$

results in a set of linear algebraic equations for the components of $[\dot{U}]$ which is formally written as

$$\begin{bmatrix} [K] & [R] \\ [-Q] & [P] \end{bmatrix} \begin{bmatrix} [v] \\ [\dot{T}] \end{bmatrix} = \begin{bmatrix} [\dot{f}] \\ -[\lambda][T] - [\phi] \end{bmatrix} \qquad (4.2.22)$$

It is obvious that the matrix is nonsymmetric. By using the Crout factorization the matrix can be written as the product of an upper triangular matrix with unit diagonal and a lower triangular matrix. The triangular decomposition allows the set of equations to be solved in two steps, the "forward elimination" and the "back substitution" [48].
The nonsymmetric matrix has a symmetric structure. Therefore it is possible to reduce the required storage and computational effort by storing only the components of the matrix within a local bandwidth. This was noted for symmetrical matrices by Zienkiewicz [51] and Bathe and Wilson [10]. The local bandwidth remains unchanged after factorization.

4.3. Incremental formulation.

4.3.1. Solution procedure for an increment.

The nodal point velocities and temperature rates can be solved from (4.2.22). We are however not only interested in the current velocity but in the (history of the) process. Therefore an incremental procedure will be used.

During a time increment Δt the velocity and temperature rate are approximated as being constant. The displacement increment and temperature increment are then given by respectively

$$\begin{aligned} \Delta \underset{\sim}{u} &= \hat{\underset{\sim}{v}}\, \Delta t \\ \Delta T &= \hat{\dot{T}} \Delta t \end{aligned} \qquad (4.3.1)$$

where $\hat{\underset{\sim}{v}}$ and $\hat{\dot{T}}$ are the average velocity and temperature rate during the time increment.
The equations from which the increments have to be solved are, according to (4.2.22), given by

$$\begin{bmatrix} [\hat{K}] & [\hat{R}] \\ [-\hat{Q}] & [\hat{P}] \end{bmatrix} \begin{bmatrix} [\Delta u] \\ [\Delta T] \end{bmatrix} = \begin{bmatrix} [\Delta f] \\ -[\hat{\lambda} \Delta t] \; [\hat{T}] - [\hat{\phi}\, \Delta t] \end{bmatrix} \qquad (4.3.2)$$

The circumflex indicates that average values are taken during the time increment. These average values are not known yet. A first approximation is found by the known state at the start of an increment. The increments of displacement and temperature are predicted by the solution of

$$\begin{bmatrix} [K^o] & [R^o] \\ [-Q^o] & [P^o] + \frac{1}{2}[\lambda^o \Delta t] \end{bmatrix} \begin{bmatrix} [\Delta u^1] \\ [\Delta T^1] \end{bmatrix} = \begin{bmatrix} [\Delta f] \\ -[\lambda^o \Delta t] \; [T^o] - [\phi^o \Delta t] \end{bmatrix} \qquad (4.3.3)$$

From the solved nodal increments the average deformation and temperature rates in the integration points are calculated using (4.2.2) and (4.2.4)

$$\hat{\underline{D}} = \left(\sum_N \underline{\underline{\underset{\sim}{B}}}^N \bullet \Delta \underset{\sim}{u}^N\right) \frac{1}{\Delta t} \qquad \text{and} \qquad \hat{\dot{T}} \cong \left(\sum_N \Psi^N \, \Delta \, T^N\right) \frac{1}{\Delta t} \qquad (4.3.4)$$

The stresses are calculated by numerical integration of the constitutive equation (4.1.7) while assuming that during the increment the rate of deformation and temperature rate are constant and equal to the average values given by (4.3.4)

$$\underline{\sigma}^1 = \underline{\sigma}^o - \left(\int_t^{t+\Delta t} \underline{\sigma}\, dt\right) \underline{I} : \hat{\underline{D}} + \left(\int_t^{t+\Delta t} \underline{\underline{L}}^Y dt\right): \hat{\underline{D}} + \left(\int_t^{t+\Delta t} \underline{L}^q dt\right) \hat{\dot{T}} +$$

$$- \int_t^{t+\Delta t} \underline{\Phi}^d dt + \hat{\underline{\Omega}} \bullet \left(\int_t^{t+\Delta t} \underline{\sigma}\, dt\right) - \left(\int_t^{t+\Delta t} \underline{\sigma}\, dt\right) \bullet \hat{\underline{\Omega}} \qquad (4.3.5)$$

In the case of simple constitutive equations based on J_2-flow-theory (3.4.38) and without either time depend deformation or phase changes, the "mean normal" method [53, 38, 26] has been applied as numerical integration procedure of (4.3.5). In the mean normal method a fictive elastic mid-increment (deviatoric) stress is used, defined by

$$\hat{\underline{s}}^1 = \underline{s}^o + 2\,G\,(\hat{\underline{D}} - 1/3\ \mathrm{tr}\ \hat{\underline{D}}\ \underline{I})\ \Delta t \qquad (4.3.6)$$

This stress is used in the calculation of the yield tensors (3.4.35) up to inclusive (3.4.37). The stress after the time increment is approximated by

$$\underline{\sigma}^* = \underline{\sigma}^o - \underline{\sigma}^o\ \mathrm{tr}\ \hat{\underline{D}}\ \Delta t + \hat{\underline{\underline{L}}}^{Y1} : \hat{\underline{D}}\Delta t + \hat{\underline{L}}^{q1}\ \hat{\dot{T}}\ \Delta t \qquad (4.3.7)$$

Note that $\underline{\sigma}^*$ is the new stress which is implicitly referred to a rotated frame. The stress tensor referred to a fixed global frame is found by "back rotating" according to the Jaumann rate

$$\underline{\sigma}^1 = \underline{\sigma}^* + (\hat{\underline{\Omega}} \bullet \underline{\sigma}^* - \underline{\sigma}^* \bullet \hat{\underline{\Omega}})\ \Delta t \qquad (4.3.8)$$

This equation can be regarded as a linearised transformation according to the Mohr circles. A subincremental technique is applied for other (smooth) yield surfaces or when time dependent effects are to be taken into account. The strain and temperature increments are subdivided into a number of subincrements. The corresponding stress subincrements are calculated while the stress and temperature are updated after each subincrement. Equation (4.3.5) is applied for each subincrement whereas the integrals are approximated by the (updated) value of the integrand multiplied by the subtime increment.
Due to the approximations in the incremental stress calculation, the final

stress at the end of the time increment will generally not satisfy the yield condition ($\phi \neq o$) exactly. Therefore the final (deviatoric) stress components are proportionally scaled down in a way that the yield condition is satisfied afterward.

From the stresses in the integration points the nodal point (reaction) forces can be calculated by

$$\underset{\sim}{R}^M = \int_V \underline{\underline{B}}^{*M} : \underline{\sigma} \, dV \qquad (4.3.9)$$

These nodal point forces are generally not in equilibrium with the prescribed nodal point forces $\underset{\sim}{f}^M$. The residue is denoted as the mechanical unbalance ratio,

$$R^F = \frac{\| \underset{\sim}{f}^M - \underset{\sim}{R}^M \|}{\| \underset{\sim}{R}^M \|} \qquad (4.3.10)$$

Beside the unbalance R^F a discrepancy may arise between the prescribed accumulated nodal heat flow, the internal energy and the mechanical work of the nodal point forces. This energy unbalance can be calculated as follows.

The accumulated nodal heat flow is, according to (4.2.19) given by

$$\phi_S^M = \int_S \left(\int_{t_o}^{t} \Psi^M \underset{\sim}{\phi} \bullet \underset{\sim}{n} \, dt \right) dS \qquad (4.3.11)$$

The principle of conservation of energy requires that this, according to (4.1.13) and (4.2.15), is equal to

$$\phi_V^M = - \int_V \left(\Psi^M \int_{t_o}^{t} \underline{\sigma} : \underline{D} \, dt \right) dV + \int_V \Psi^M \rho \, e \, dV + \int_V \left(\underset{\sim}{\nabla} \Psi^M \int_{t_o}^{t} \bullet \underline{\lambda} \bullet \underset{\sim}{\nabla} T \, dt \right) dV \qquad (4.3.12)$$

There will generally be a discrepancy between ϕ^M and ϕ_V^M due to the incremental procedure . The dimensionless energy residue is denoted as the thermal unbalance ratio

$$R^T = \frac{\| \phi_S^M - \phi_V^M \|}{\| \phi_V^M \|} \qquad (4.3.13)$$

The mechanical and thermal unbalance ratio are a measure for the accuracy of the calculated increment. If they are not sufficiently small, then the recalculated in an iteration process. The increments after the n^{th} iteration can be written as

$$\begin{aligned} \Delta \underset{\sim}{u}^n &= \Delta \underset{\sim}{u}^{n-1} + \Delta\Delta \underset{\sim}{u}^n \\ \Delta T^n &= \Delta T^{n-1} + \Delta\Delta T^n \end{aligned} \qquad (4.3.14)$$

where $\Delta\Delta u^n$ and $\Delta\Delta T^n$ are found by solving

$$\begin{bmatrix} [K] & [R] \\ [-Q] & [P] \end{bmatrix} \begin{bmatrix} [\Delta\Delta u^n] \\ [\Delta\Delta T^n] \end{bmatrix} = \begin{bmatrix} [f] - [R^{n-1}] \\ [\phi_S] - [\phi_V{}^{n-1}] \end{bmatrix} \qquad (4.3.15)$$

The stresses, mechanical work, dissipation and nodal reaction are recalculated with the new increments $\Delta\underset{\sim}{u}^n$ and ΔT^n.
The iteration process stops if the unbalance ratio's are "sufficiently small". The acceptable unbalance ratio depends on the type of the analysed problem. The remaining unbalance after stopping the iterations, is taken into account in the next increment as an additional "load" increment (load correction). Hence a relatively large unbalance after an intermediate increment does not necessarily result into inaccurate predictions in the final increments. However, a large unbalance ratio may result into a nonconverging iteration process in the next increment.

4.3.2. Incremental adaptation of the finite element state, the mixed Eulerian-Lagrangian formulation.

In the foregoing section the calculation of the new state in a material point after an increment has been discussed. This new state is only calculated for a finite number of grid points of the mesh: the nodal points (for displacement and temperature) and the integration points (for stresses, strains, internal energy and dissipation). These grid points correspond to material points; hence the location of these points (coordinates) change implicitly during an increment. Therefore the nodal point coordinates must be adapted before the next increment is started. This procedure of incremental adaptation of the nodal point coordinates after each step according to the material displacement of the nodal points is known as the updated Lagrange method. This method is introduced by Mc. Meeking and Rice [34].

The updated Lagrange method has some disadvantages. Particularly if very large local deformations occur, the method becomes impracticable because of numerical problems: elements are too much distorted or even turned inside out.
In order to be able to continue a simulation, rezoning techniques have been developed [13]; the simulation is stopped and restarted with a new mesh.

The problems with respect to the element distortion can be avoided if the material displacement increments are uncoupled from the grid point displacement increments. This means that material flows through the elements. The nodal point displacement increments can be chosen more or less freely. They are restricted by the condition that nodal points at free surfaces or at a contact surface of different materials, must remain on that surface, but not necessarily at the same material particle.

Uncoupling of material and grid point displacement implies that in addition to the incremental calculation of the previous section, convection must be taken into account in order to be able to update the state at the grid points. A method to calculate this convection has been presented by the author in 1982 [20].
The basic principle of this method is the introduction of additional continuous stress and strain fields by interpolation of nodal point

stresses and strains. These nodal point stresses and strains are determined as average values from all elements that are connected with a nodal point. The convective terms are calculated as a product of gradients of these additional continuous fields and the displacement increments. After this work has been published it appeared that, particularly when displacement increments are large relative to the element size, the stress and strain prediction shows oscillations. These oscillations are increasing with the number of increments until an upperbound of the amplitude is reached. Investigations have been carried out to avoid these oscillations and to improve the method. The improved method and the effects of the improvements will now be discussed.

The value of a material associated quantity σ in a grid point with location $\underset{\sim}{x} + \Delta\underset{\sim}{x}$ at the end of an increment and location $\underset{\sim}{x}$ at the start of an increment can be written as

$$\sigma\ (\underset{\sim}{x} + \Delta\underset{\sim}{x},\ t + \Delta t) = \sigma\ (\underset{\sim}{x}, t) + \hat{\dot{\sigma}}\ \Delta t + (\Delta\underset{\sim}{x} - \hat{\underset{\sim}{v}}\ \Delta t) \bullet \overset{\rightarrow}{\nabla}\sigma \qquad (4.3.16)$$

or alternatively

$$\sigma\ (\underset{\sim}{x} + \Delta\underset{\sim}{x},\ t + \Delta t) = \sigma\ (\underset{\sim}{x} + \Delta\underset{\sim}{x} - \hat{\underset{\sim}{v}}\ \Delta t,\ t) + \hat{\dot{\sigma}}\ \Delta t \qquad (4.3.17)$$

From formula (4.3.17) we see that the new state at grid point $\underset{\sim}{x} + \Delta\underset{\sim}{x}$ can be calculated by the same procedure as in the updated Lagrange method, provided that the state at grid point $\underset{\sim}{x} + \Delta\underset{\sim}{x} - \hat{\underset{\sim}{v}}\ \Delta t$ is known at time t. The calculation of the state in this point can be carried out after the velocity (or displacement increment) is known, hence after the iteration process of the preceding section.

Subtraction of (4.3.17) from (4.3.16) yields

$$\sigma\ (\underset{\sim}{x} + \Delta\underset{\sim}{x} - \Delta\underset{\sim}{u},\ t) = \sigma\ (\underset{\sim}{x}, t) + (\Delta\underset{\sim}{x} - \Delta\underset{\sim}{u}) \bullet \overset{\rightarrow}{\nabla}\sigma \qquad (4.3.18)$$

From this equation we find that, in addition to the updated Lagrange method, the gradient of the stress has to be determined. This complicates the solution procedure considerably. If for instance simple 3 node triangular elements are used then the stress and strain are constant within an element and the gradients vanish. This implies that convection of stresses and strains cannot directly be taken into account at element level. Stresses (or stress rates) are related to the gradient of the displacement increment, hence the gradient of the stress depends on the

second order derivatives of the displacement increment.
This may lead to the conclusion that elements with C_1 continuity of hybrid elements with continuous stresses are required. However, it will be shown that C_o continuity is sufficient if the convective terms are calculated from the differences between the values in adjacent elements of each material associated quantity respectively.

Several procedures have been devised and investigated by means of numerical experiments. All procedures have in common that nodal stresses and strains are calculated as mean values of all elements that are connected with a particular nodal point. By interpolation between these nodal point values we find additional stress and strain fields, these fields will be denoted as σ^* and obey C_o continuity.
From these additional fields the convective terms in equation (4.3.18) can be determined. Equation (4.3.18) will be replaced by

$$\sigma\ (\underset{\sim}{x} + \Delta\underset{\sim}{x} - \Delta\underset{\sim}{u},\ t) = \sigma\ (\underset{\sim}{x}, t) + (\Delta\underset{\sim}{x} - \Delta\underset{\sim}{u}) \bullet \overset{\rightarrow}{\underset{\sim}{\nabla}}\sigma^* \qquad (4.3.19)$$

It is however also reasonable to calculate the values in the grid points (i.e. integration points) with coordinates $\underset{\sim}{x} + \Delta\underset{\sim}{x} - \Delta\underset{\sim}{u}$ directly by substituting these coordinates directly in the interpolation functions;

$$\sigma\ (\underset{\sim}{x} + \Delta\underset{\sim}{x} - \Delta\underset{\sim}{u},\ t) = \sigma^*\ (\underset{\sim}{x} + \Delta\underset{\sim}{x} - \Delta\underset{\sim}{u},\ t) =$$
$$= \sum_N \sigma^{*N}\ (t)\ \Psi^N\ (\underset{\sim}{x} + \Delta\underset{\sim}{x} - \Delta\underset{\sim}{u}) \qquad (4.3.20)$$

Both procedures will yield different results. If for instance $\Delta\underset{\sim}{x} = \Delta\underset{\sim}{u}$ (updated Lagrange), the grid point values remain unchanged when (4.3.19) is used. The corresponding stress field is discontinuous at element boundaries.
If (4.3.20) is applied, then grid point values may change even if $\Delta\underset{\sim}{x} = \Delta\underset{\sim}{u}$. The new field is continuous (and generally rather smooth, depending on the element type). However, this field will generally not satisfy nodal point equilibrium exactly.

4.3.2.1. Local and global smoothing.

In order to investigate the description of convection, a numerical experiment has been devised in which the convection problem is reduced to a one-dimensional case of material flow through a number of spatial fixed elements. We started with 20 isoparametric axial-symmetric elements with 4 nodes as shown in fig. 4.1.

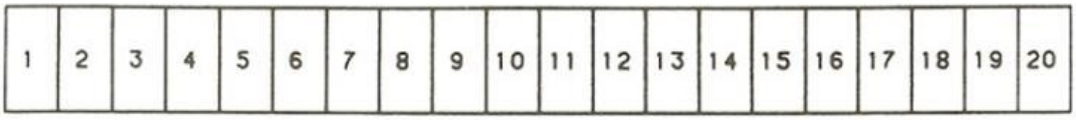

Fig. 4.1 Element mesh for convection tests.

In the numerical experiment the element mesh is non-homogeneously prestrained and after that the material is translated without additional straining. During the translation the elements are spatially fixed. At the left hand side material enters in the mesh and at the right hand side material leaves the mesh.
The prestraining has been performed in two steps. In the first step all longitudinal nodal point displacement components are non-homogeneously prescribed. Points within a cross-section (equal coordinates y) are subjected to equal displacements. The longitudinal distribution of the prescribed displacement component is shown in fig. 4.2 and the distorted element mesh is shown in fig. 4.3. A large scale-factor has been applied in order to visualize the distortion.
The distribution of the axial strain component is shown in fig. 4.4 a. After determining average nodal point strains, a continuous approximation is found shown by the dotted line in this figure.
In order to obtain inelastic deformations, the yield stress has been chosen very low. Isotropic properties have been assumed, material properties are given in table 4.1.
The resulting equivalent plastic strain field based on average nodal point values is given in fig. 4.4 b.

Note: No iterations have been performed, hence the deformations are calculated on the basis of an initially elastic state. Because of the elastic volumetric deformation the deviatoric strain level, and consequently the equivalent plastic strain, is lower than the axial strain component.

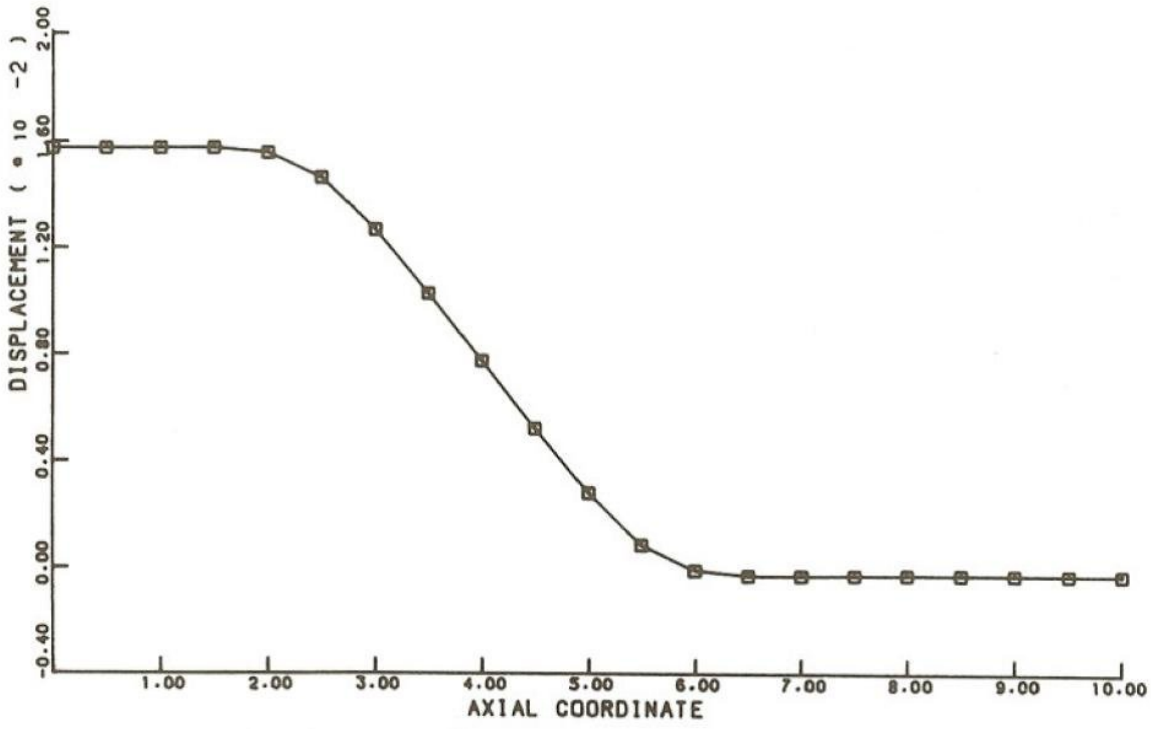

Fig. 4.2 Prescribed longitudinal displacement field for prestraining of convection tests.

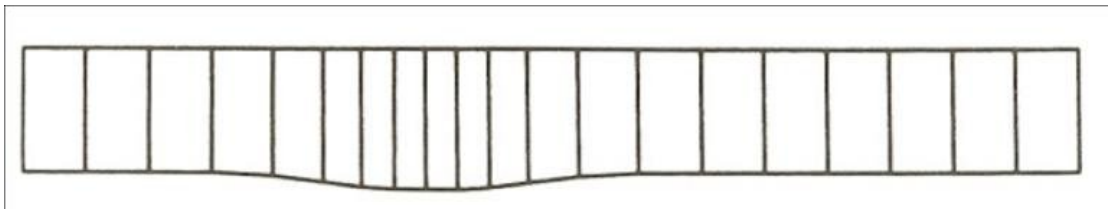

Fig. 4.3 Deformed mesh after prestraining (displacement scale factor is 100).

Youngs modulus	100000 N/mm^2
Poisson's ratio	.3
Yield stress (no hardening)	10 N/mm^2

Table 4.1 Material properties for convection simulations.

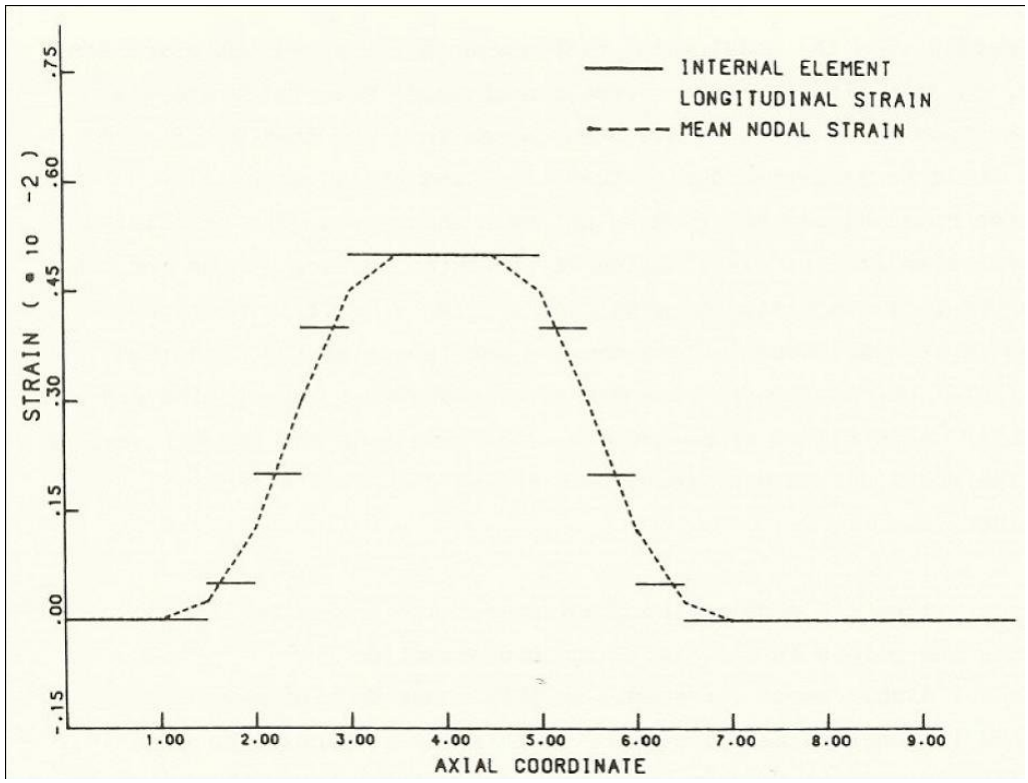

Fig. 4.4a Longitudinal strain distribution after prestraining.

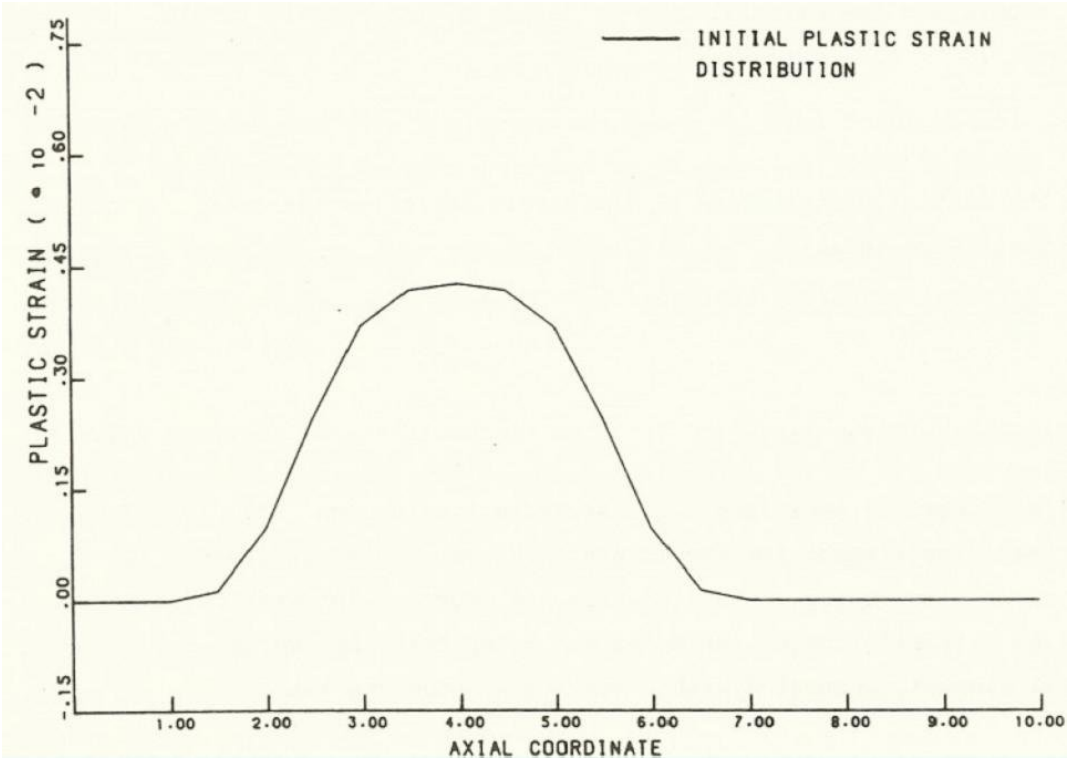

Fig. 4.4b Equivalent plastic strain distribution after prestraining.

In the second step the nodal point displacements are freed. Stresses are relaxed, but the plastic strains remain unchanged. Material properties and prescribed displacements have been chosen in a way that geometrical changes could be neglected during these load and unload steps. The transverse nodal displacements have not been suppressed. The calculated transverse displacement distribution at the outer surface of the rod can be observed from the distorted mesh plot of fig. 4.3. It is obvious that the transverse displacement field has the same shape as the (smoothed) strain field. Due to the free transverse displacements the strains are not exactly uniform in a cross-section. The deviations are however very small. The shown strain distribution of fig. 4.4 is that at the centerline.

In the next steps all nodal point displacement increments are free, except for the points in the right hand cross-section.
The material displacement increments in this cross-section have been prescribed in longitudinal direction. In this way a translation without any additional deformation is prescribed. The nodal point coordinates are spatially fixed ($\Delta \underset{\sim}{x} = \underset{\sim}{o}$), the material moves through the elements. During this translation the material rate of change of the plastic strain vanishes

$$\frac{d\varepsilon}{dt} = o \qquad (4.3.21)$$

Hence the spatial distribution of the strain satisfies the one-dimensional wave equation

$$\frac{\partial \varepsilon}{\partial t} + v \frac{\partial \varepsilon}{\partial x} = o \qquad (4.3.22)$$

or

$$\varepsilon\,(x,\ t + \Delta t) = \varepsilon\,(x - \Delta u,\ t) \qquad (4.3.23)$$

The first numerical experiment was carried out using eqn. (4.3.19). The prescribed displacement increments are 0.125 mm. Within an element the nodal point strains are calculated from the Gaussian integration point values by extrapolation to the nodes and after that the average value from all elements connected with a particular node are taken.

Fig. 4.5 shows the predicted strain distribution after 12 steps and after 24 steps. The results show rather large deviations from the initial distribution.

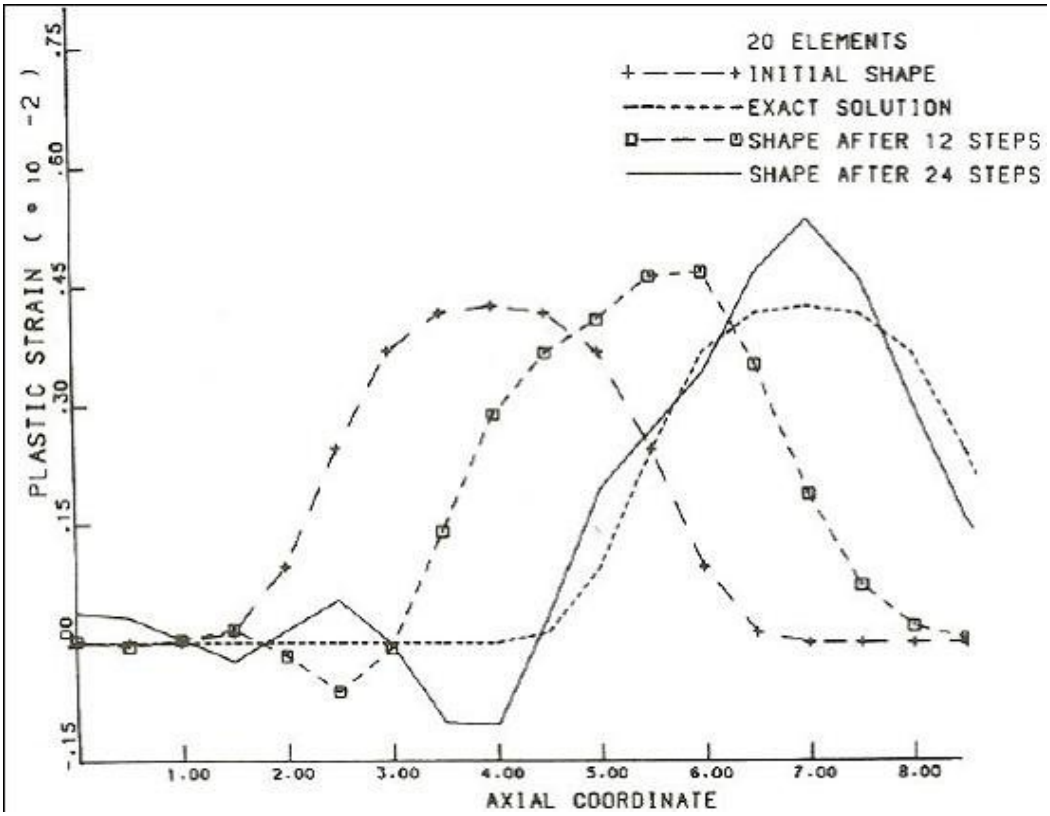

Fig. 4.5 Predicted strain propagation based on nodal point values calculated by extrapolation of integration point values.

Increasing oscillations are observed in that part of the rod where the strains should vanish (down stream). The algorithm obviously leads to instable predictions.

The next experiment was carried out by first calculating a mean (constant) strain within each element. After that nodal point values are calculated as an average value of all elements connected to a node. The procedure based on mean element values will be denoted as 'local smoothing'. Fig. 4.6.a. shows the results of this second numerical experiment. The predicted strain propagation deviates less from the exact solution than in the first experiment, but is not yet very accurate. Less overshoot and smaller oscillations can be observed.

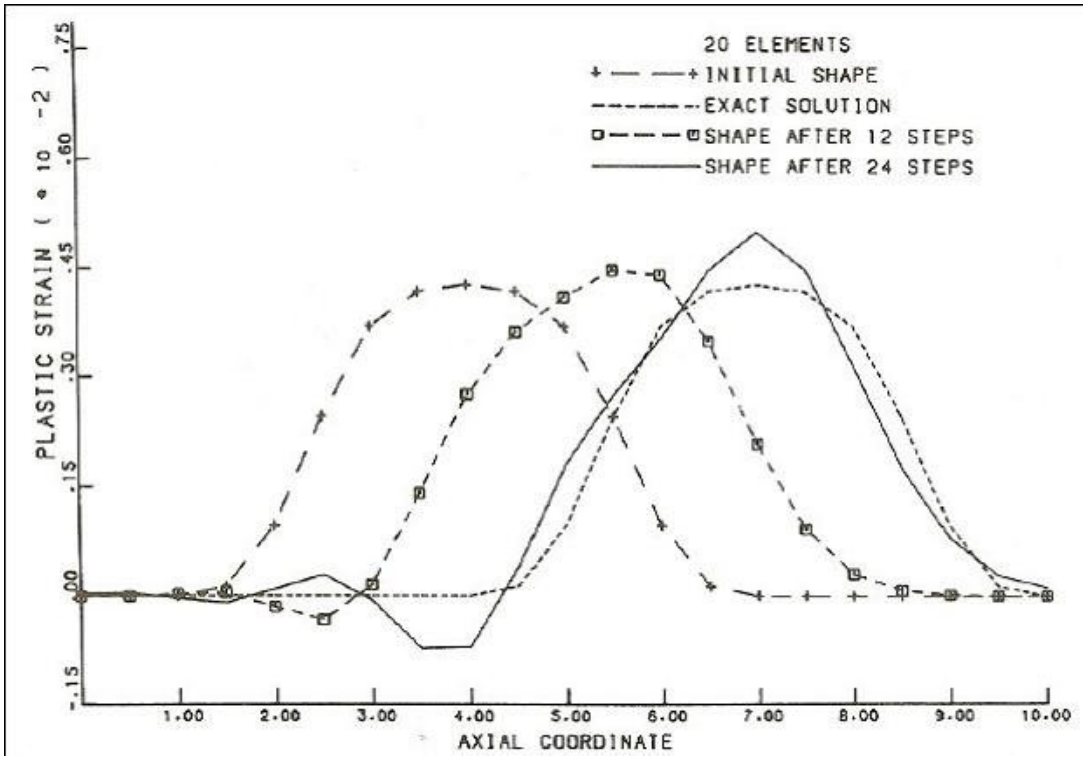

Fig. 4.6a Predicted strain propagation based on nodal point values calculated from mean element values (local smoothing)

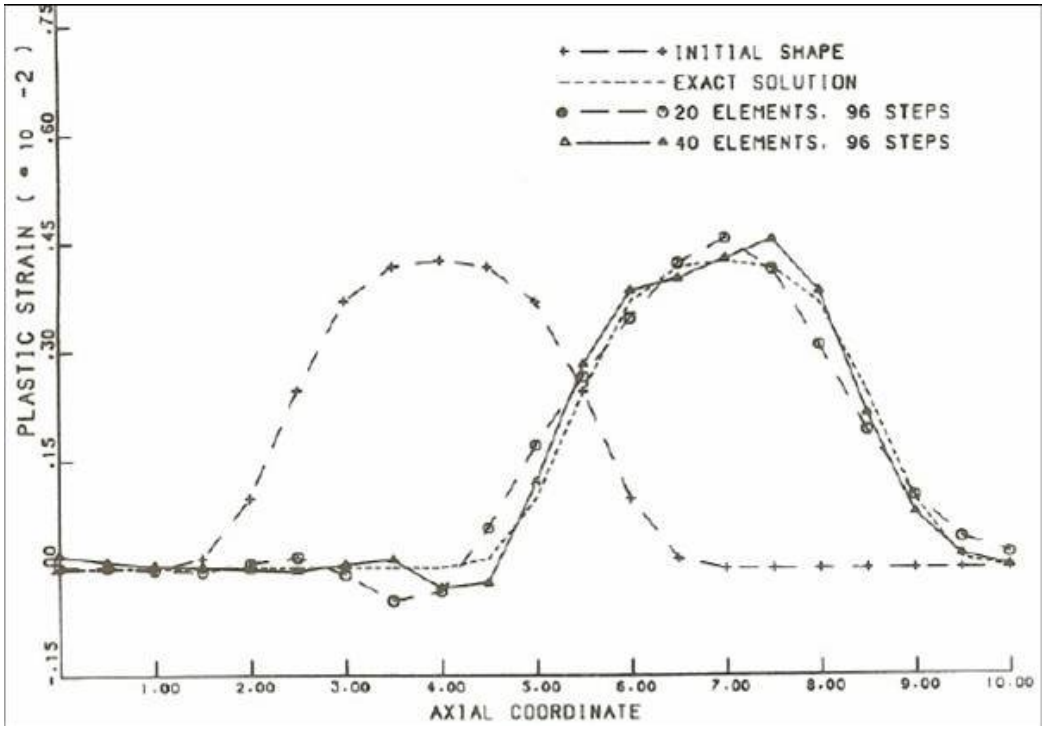

Fig. 4.6b Predicted strain propagation based on local smoothing with reduced increment size and mesh refinement.

Calculations based on local smoothing were repeated with decreasing prescribed displacement increments and also with a larger number of elements. Results are shown in fig. 4.6.b. It can be observed that overshoot and oscillations very slowly decrease with decreasing displacement increments (and increasing number of increments).

The next two experiments were carried out using equation (4.3.20). We will denote the procedure based on this equation as 'global smoothing'. In one experiment, extrapolation at element level was applied and in the other local smoothing. By the combination of extrapolation and global smoothing, nearly the same results were predicted as in the case without smoothing (shown in fig. 4.5), and are therefore not shown again.
The prediction based on simultaneous local and global smoothing are shown in fig. 4.7. Neither overshoot nor oscillations are predicted, but apparent diffusion of strain occurs. This apparent diffusion is obviously a numerical effect of a combination of local and global smoothing. We will denote this effect as 'numerical diffusion'.

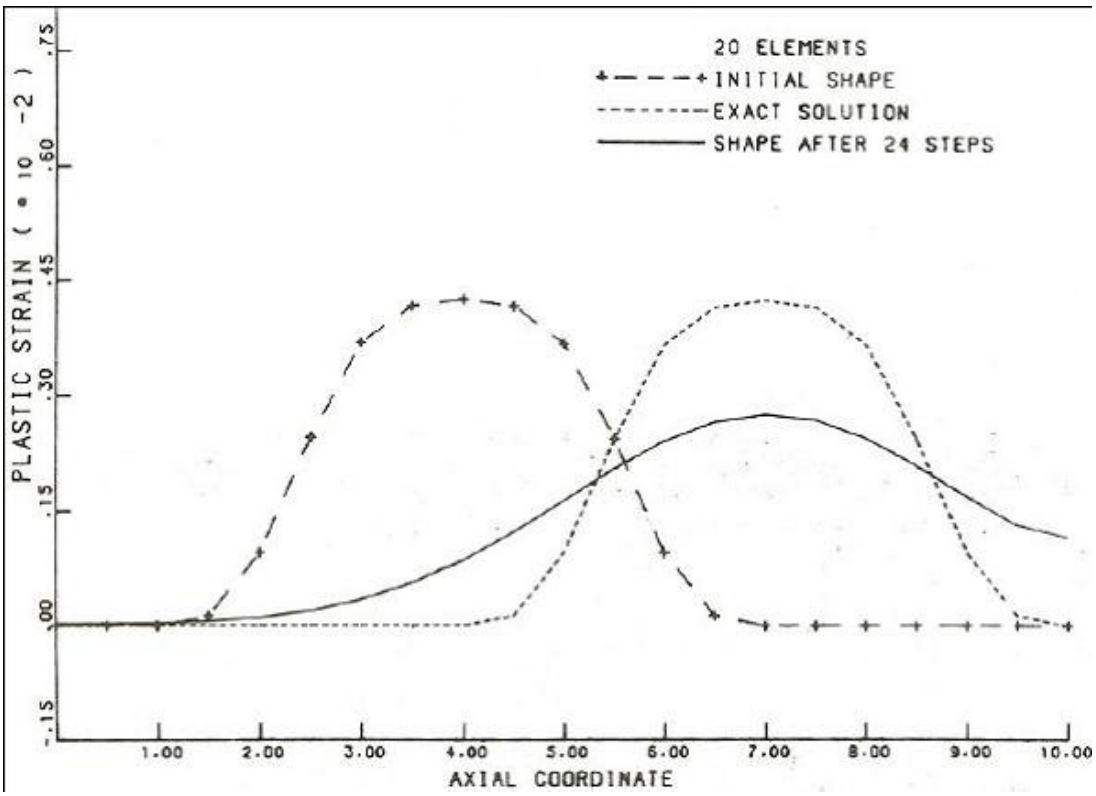

Fig. 4.7 Predicted strain propagation based on both local smoothing and global smoothing of integration point values.

Additional computations with various number of elements were carried out in order to investigate the effect of the finite element discretization on the phenomenon of numerical diffusion. Results are given by fig. 4.8 for 10 elements, 20 elements, 40 elements and 60 elements respectively.

It is shown that the amount of diffusion decreases rapidly, when increasing the number of elements. It appears that the amount of diffusion is proportional to the difference between the slopes of the curves in two adjacent elements prior to an increment. The difference between these slopes may be regarded as a measure for the second order derivative. Hence from this point of view there is a slight relation to the description of real (physical) diffusion.
When the number of elements is increased, the difference between the slopes of two adjacent elements is decreasing. Therefore the amount of numerical diffusion per increment is decreasing as observed from fig. 4.8.

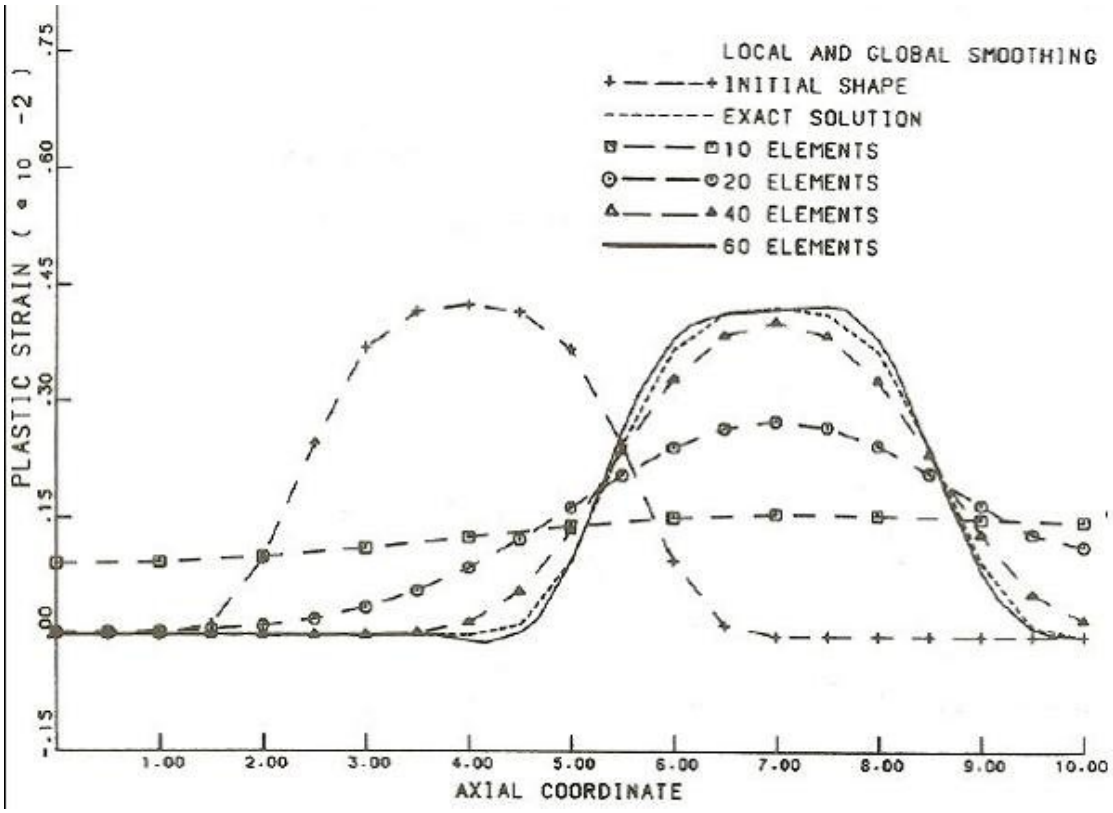

Fig. 4.8 Predicted strain propagation based on both local and global smoothing with increasing mesh refinement.

On the other hand, the total amount of diffusion is proportional to the number of increments, independent of the material flow. Hence if many steps are required to carry out a simulation of a forming process (due to highly nonlinear constitutive equations), numerical diffusion will smooth the results too much. This undesired effect must be avoided.
If we regard the limiting case that the relative displacements vanish (updated Lagrange), no smoothing is required to avoid either oscillations or overshoot. On the other hand, if the relative displacement increment is large (experiments were carried out with increments up to the element length), global smoothing is necessary to suppress oscillations. Therefore a weight factor was introduced depending on the relative displacement increment, which accounts for the amount of global smoothing that has to be taken into account. This weight factor w_s has a value between one and zero. If $w_s = 1$, integration point values are calculated by using equation (4.3.19), which means no global smoothing. When w_s decreases the contribution of equation (4.3.19) decreases whereas the contribution of equation (4.3.20) increases accordingly with a weight factor $(1-w_s)$• Consequently pure global smoothing occurs when $w_s = o$•
The value of w_s depends on the displacement Δu of the material, relatively to the (displacement of the) element (i.e. the difference between material and nodal displacement increment) and the dimension of the element represented by a length ℓ. We require that no smoothing occurs in the limiting case when the relative displacement vanishes. Hence if $\Delta u = o$ then $w_s = 1$• Firstly we will regard an assumed relation between w_s and Δu given by

$$w_s = 1-\beta \frac{\Delta u}{\ell} \qquad \text{if} \qquad \beta \frac{\Delta u}{\ell} \leqslant 1$$

$$w_s = o \qquad \text{if} \qquad \beta \frac{\Delta u}{\ell} > 1 \tag{4.3.24}$$

The amount of diffusion (dif) is roughly proportional to the number of increments n, the square of the length of the elements and to $(1-w_s)$

$$dif = n\, \ell^2\, (1-w_s) = n\, \ell^2\, \beta \frac{\Delta u}{\ell} \tag{4.3.25}$$

If u is the total (relative) displacement then we can write

$$\Delta u = \frac{u}{n} \tag{4.3.26}$$

and hence

$$dif = \beta\ n\ \ell^2\ \frac{u}{n\ell} = \beta\ \ell\ u \qquad (4.3.27)$$

This result implies that the amount of diffusion is independent of the number of increments in which the relative displacement is subdivided. This is of course an improvement with respect to the case of pure global smoothing, but the diffusion will not vanish if the size of the displacement increments is reduced. Only an increasing number of elements will decrease the diffusion.
We shall require that the diffusion also vanishes when the displacement increments are decreasing. This can be accomplished by requiring that

$$\lim_{\Delta u \to o} \frac{\partial w_s}{\partial(\Delta u)} = o \qquad (4.3.28)$$

This condition is satisfied by adopting formula

$$w_s = 1 - (\beta\ \frac{\Delta u}{\ell})^{\gamma} \qquad \gamma > 1 \qquad (4.3.29)$$

The amount of diffusion can now be expressed as

$$dif = n\ \ell^2\ (\beta\ \frac{u}{\ell n})^{\gamma} = n^{1-\gamma}\ \ell^{2-\gamma}\ (\beta\ u)^{\gamma} \qquad (4.3.30)$$

In order to satisfy the condition that the diffusion vanishes for an increasing number of increments and increasing number of elements (decreasing ℓ) independently from each other, γ should satisfy the condition that

$$1 < \gamma < 2 \qquad (4.3.31)$$

A reasonable choice seems to be $\gamma = 1{\bullet}5$

Various numerical tests were carried out to determine a value for $\beta{\bullet}$
Results of these experiments are summarized in fig. 4.9.
From these experiments it has been established that a proper value for $\beta = 4/3$,

$$w_s = 1 - (\frac{4}{3}\ \frac{\Delta u}{\ell})^{1{\bullet}5} \qquad (4.3.32)$$

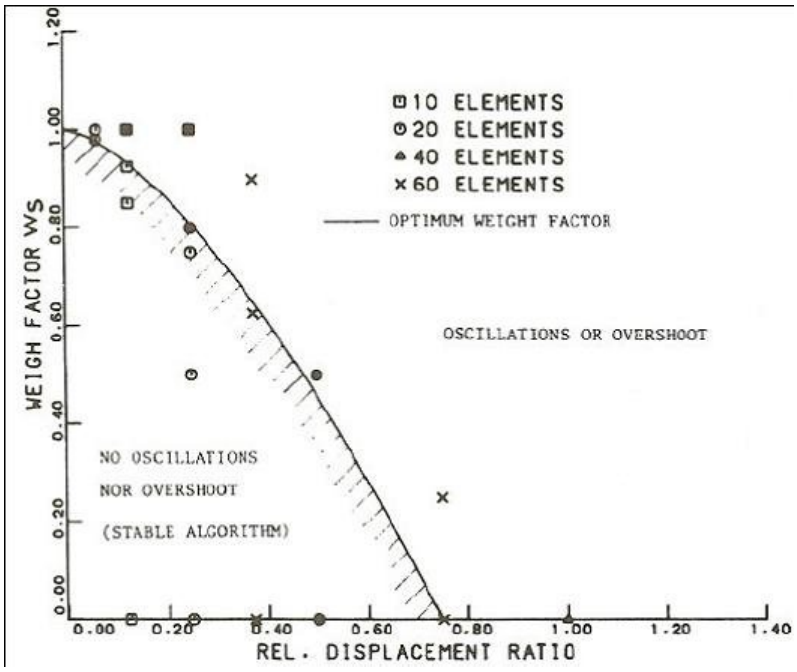

Fig. 4.9 Survey of numerical experiments with various relative displacement increment sizes and weight factors for smoothing.

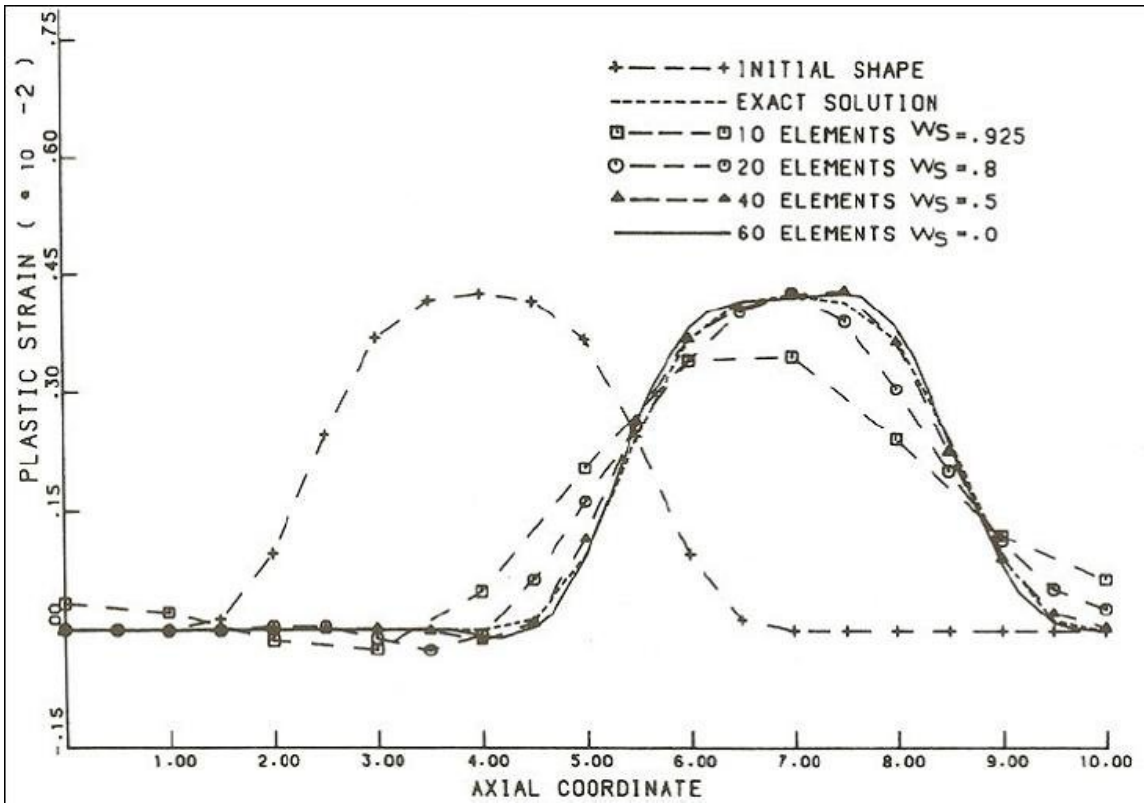

Fig. 4.10 Predicted strain propagation based on weighed global smoothing, 24 equal displacement increments (Δu = 0•125 mm/step) and increasing mesh refinement.

This line is drawn in fig. 4.9. When a value is chosen beyond this line, overshoot and oscillations are observed. When a value below this line is chosen, no oscillations are predicted. Values far below this line resulted in too much numerical diffusion.

The finite element programme has been adapted to calculate the weight factor automatically according to (4.3.32) at element level. Fig. 4.10 and fig. 4.11 show results obtained with this optimum weight factor for various numbers of elements and displacement increments. The results presented by fig. 4.10 are obtained from simulations using equal displacement increments as shown by fig. 4.8 in the case of pure global smoothing.

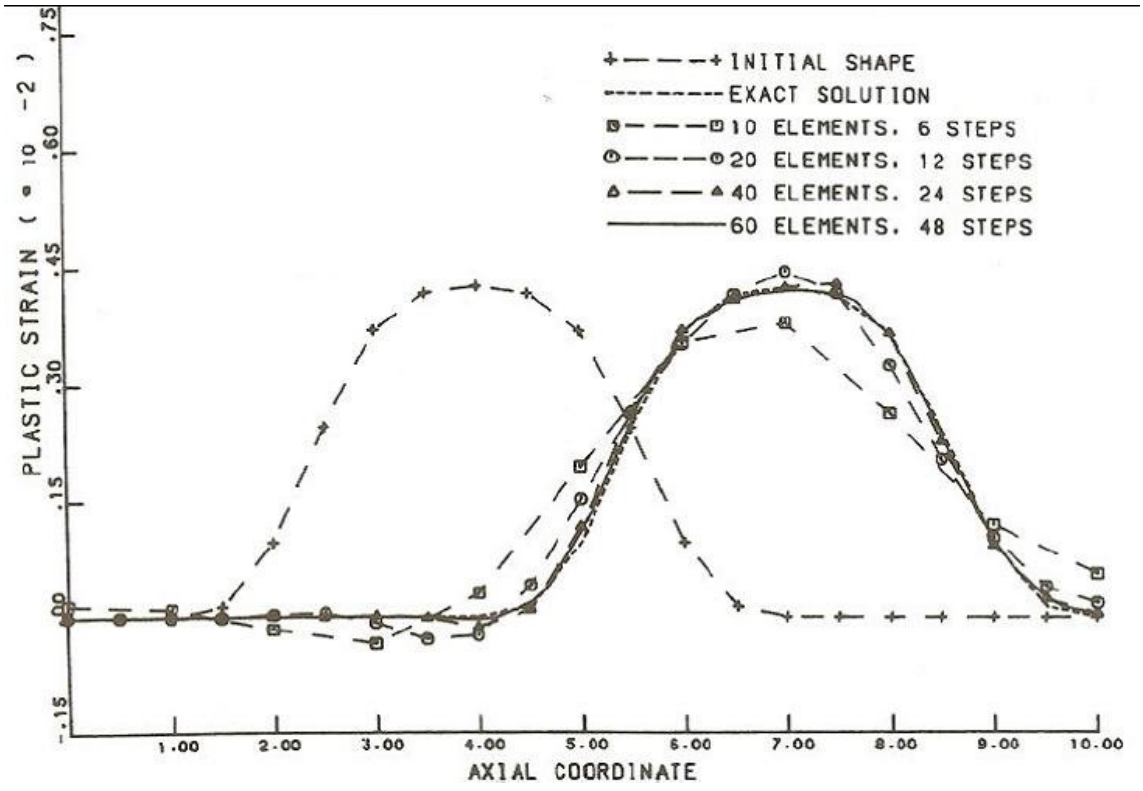

Fig. 4.11 Predicted strain propagation based on weighed global smoothing, increasing mesh refinement and (proportional with the element length) decreasing displacement increments.

The improvement due to weighed smoothing is obvious from these two figures. In the case of 60 elements, both figures show the same curve because the optimum weight factor is zero for the corresponding ratio of

displacement increment and element size (0.75). A ratio larger than 0.75 should be avoided. Fig. 4.11 shows that for a smaller value a better agreement with the 'exact' solution is obtained. The prediction for 60 elements and 48 steps (relative displacement ratio = 0.375) nearly coincides with the 'exact' solution.
In the case of 10 elements the deviations are still rather large, but the initial shape is already poorly approximated by 10 elements because insufficient nodal points are available for prescribing the initial longitudinal displacement field. Hence no accurate prediction can be expected for 10 elements.

Fig. 4.12 shows result for 40 elements and different numbers of displacement increments (decreasing size of displacement increments). It is observed that due to the automatic weighed smoothing procedure the prediction obtained in only 24 steps is much more accurate than the prediction without global smoothing obtained in 96 steps (see fig. 4.12 and fig. 4.6 b respectively).

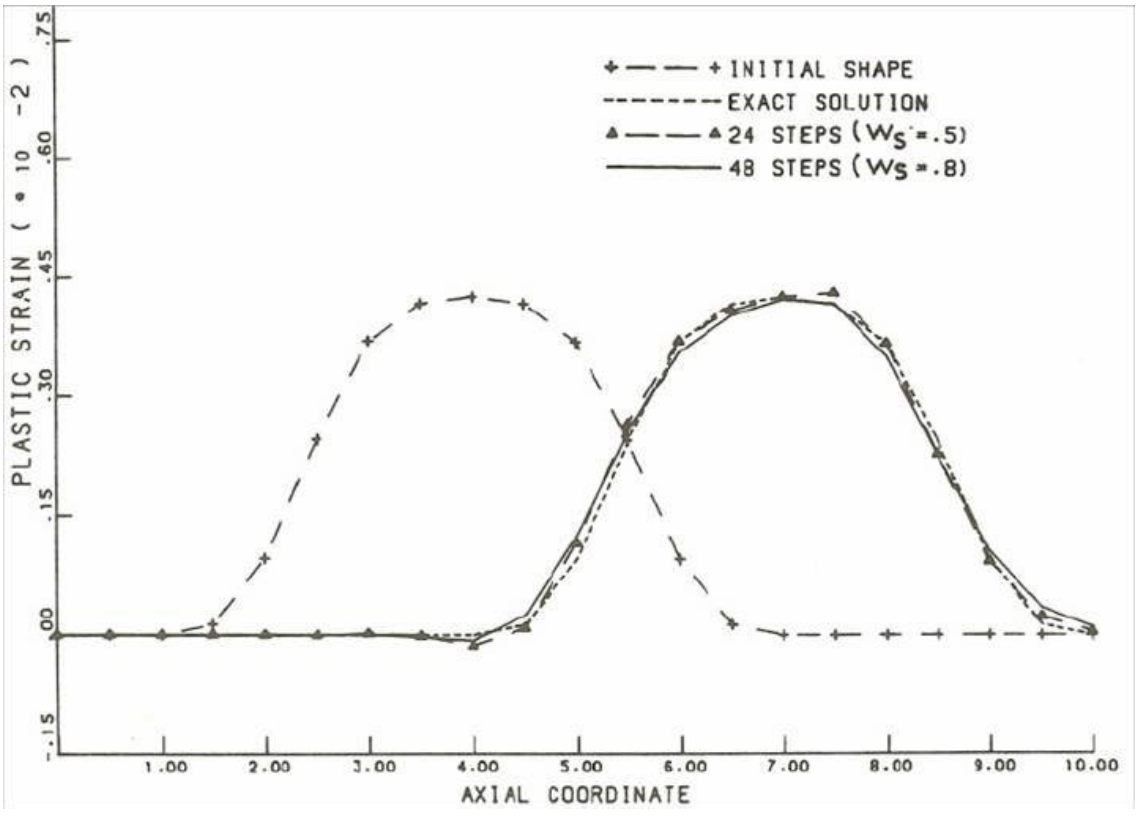

Fig. 4.12 Predicted strain propagation based on weighed global smoothing, 40 elements, various number of increments

As has been noticed before, global smoothing will generally disturb nodal point equilibrium, even if the relative displacement of the material (with respect to the elements) vanishes because integration point values are replaced by those obtained from the continuous fields. By introducing weighed global smoothing, this disadvantage vanishes because no global smoothing occurs if there is no relative displacement of the material.

The preceding discussion has been focussed on (dependent) material associated quantities stored at integration points of elements. But also for (independent) material associated quantities stored at nodal points (displacement, temperature), convection has to be taken into account. This was carried out in the same way as for integration point values, except that the natural coordinates of the integration points were replaced by the natural coordinates of the nodal points at element level.

Note: Within the simulation it is not necessary to calculate the (accumulated) total displacement. However, the total displacement yields an impression as regards the accuracy of the simulation by subtracting the displacement from the current position of the nodal points (see chapter V).

Initially the nodal point associated quantities are continuous at element boundaries, but their gradients are not. Hence if convection is taken into account at element level, discontinuous fields are obtained. These fields are treated in the same way as fields stored at integration points in order to calculate average nodal point values and, by interpolation, new continuous fields. A difference with respect to integration point values is that only these new continuous fields are stored at nodal points. This actually means that pure global smoothing is taken into account. In order to avoid numerical diffusion, a weight factor according to (4.3.32) has been applied with respect to the amount of local smoothing for each component of the displacement.

Results obtained by this procedure from the previously described numerical experiments are shown in fig. 4.13 and fig. 4.14. These results are obtained from the same calculations as those given in fig. 4.11.

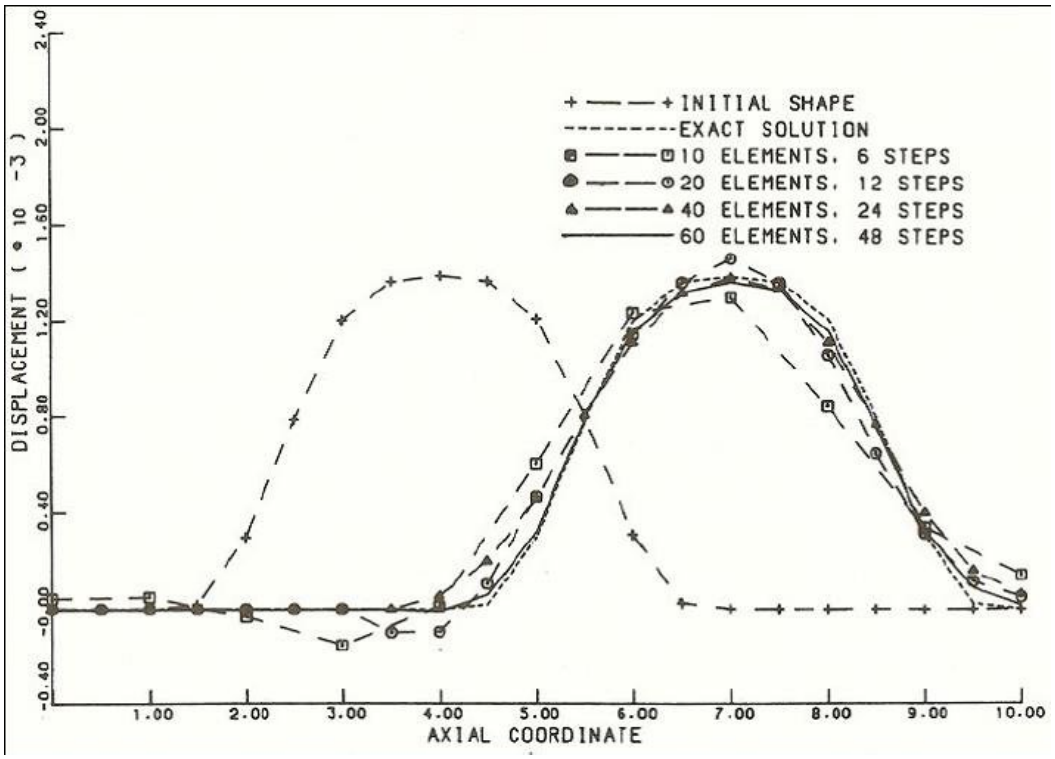

Fig. 4.13 Predicted transverse displacement propagation at the outer surface of the rod.

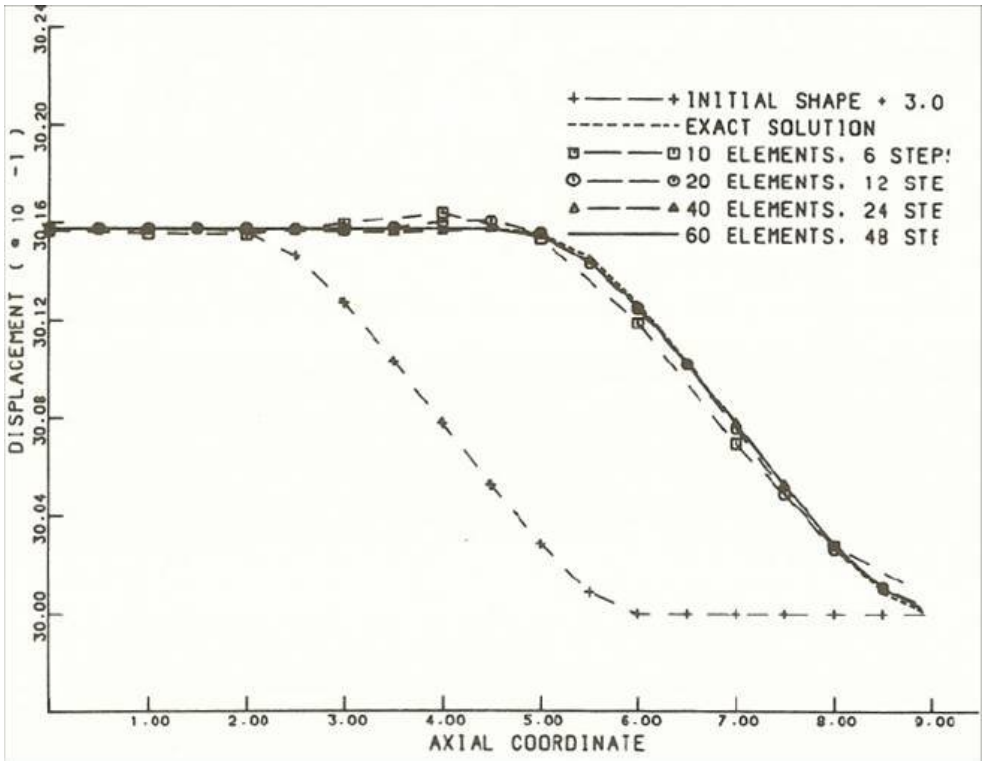

Fig. 4.14 Predicted longitudinal displacement propagation.

It is observed that the prediction of the displacement propagation is not basically different from the strain propagation.

For eight node elements the same kind of procedure was followed in order to take into account convective terms. However, the local smoothing procedure was chosen according to the least square smoothing method proposed by Hinton [22], (also reported by Zienkiewicz [51]).
This least square smoothing method will be explained briefly.
The stress and strain field within an element can be represented by a completely biquadratic interpolation through the nine integration points. Extrapolation to the nodal points may result into unrealistic nodal point values. Hinton proposed a bilinear least square fit of a biquadratic field within each element. He proved that this bilinear fit can be found by calculating values at the position of four Gaussian integration points of a 'reduced integration' scheme. After that nodal point values are calculated by bilinear extrapolation from these four integration points to the eight nodal points.
Nodal point values of stresses and strains calculated by this least square smoothing procedure were found to be much more realistic than values obtained by biquadratic extrapolation or by direct calculation at the nodal points.
Besides local smoothing, also weighed global smoothing has been taken into account for eight node elements.
The same relation between the weight factor and the relative displacement ratio has been adopted as in the case of four node elements. Numerical convection tests similar to the tests for four node elements were carried out. Results of these tests are shown in fig. 4.15. It is observed from this figure that the procedure of local and weighed global smoothing results into satisfactory agreement with the exact solution for eight node elements too.

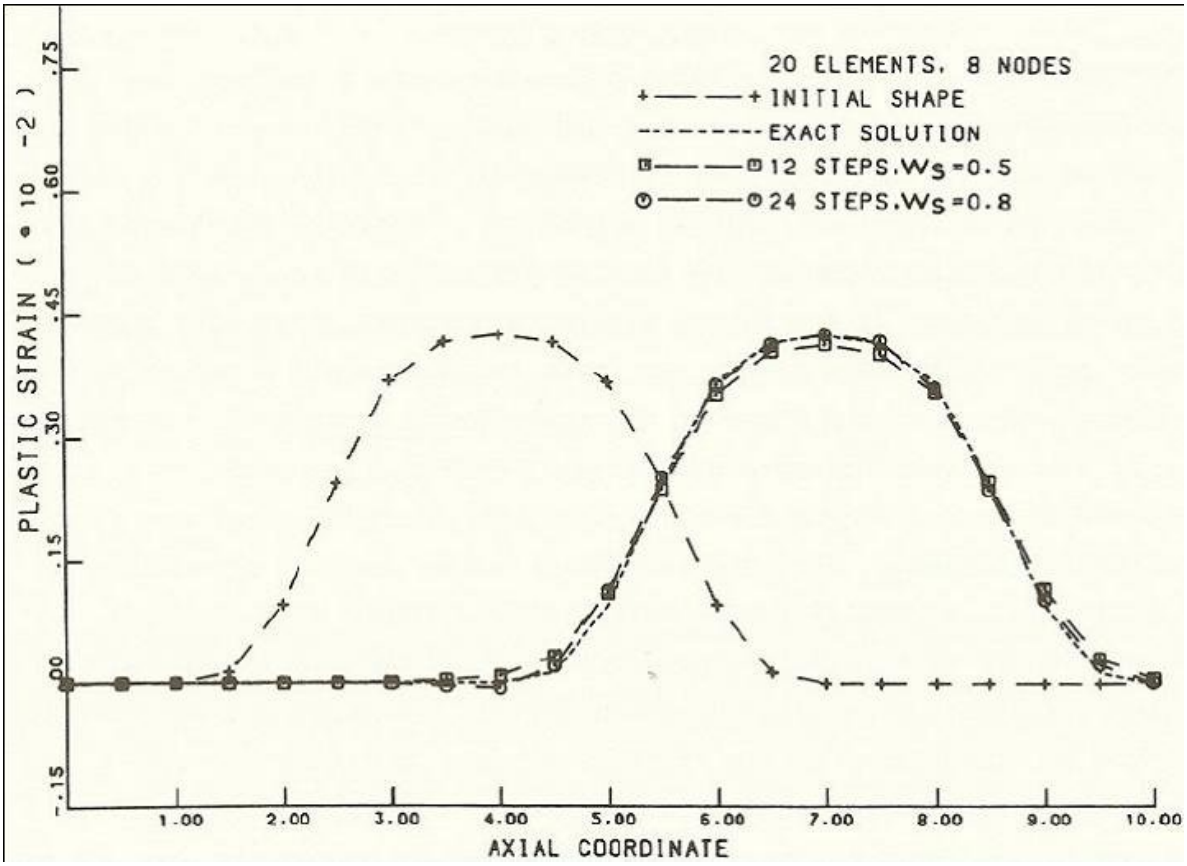

Fig. 4.15 Predicted strain propagation for twenty elements with eight nodes, with local 'least square' smoothing and weighed global smoothing.

4.3.2.2. Adaptation of nodal point coordinates, moving boundary surfaces.

In problems with free outer surfaces or moving contact surfaces between different materials (forming material and tool), coordinates of nodal points that are initially on that surface must be adapted in a way that they remain on the surface. This is a necessary condition for taking into account the changing shape of the forming product with correct local material properties. In the finite element programme, nodal points can be assigned as being surface points. At least two points are required in the two-dimensional case, and three in the three-dimensional case, to define a (part of a) surface. The new coordinates of each surface point are determined by prescribing a direction in which the nodal point moves (not the material movement). The intersection of a line in this direction through the initial position of a nodal surface point, with a spline through a number of material surface points after the increment, is designated as the new position of the nodal surface point considered. This procedure is illustrated in fig. 4.16. It is observed that the new position of nodal surface points is not exactly on the surface found by the element boundaries if the material displacement increments are followed. However, if the new position of the nodal points would have been chosen on these element boundaries, then a piece of material is lost at every increment. In the case of using a spline, the amount of material that is lost is more or less in equilibrium with the added material.

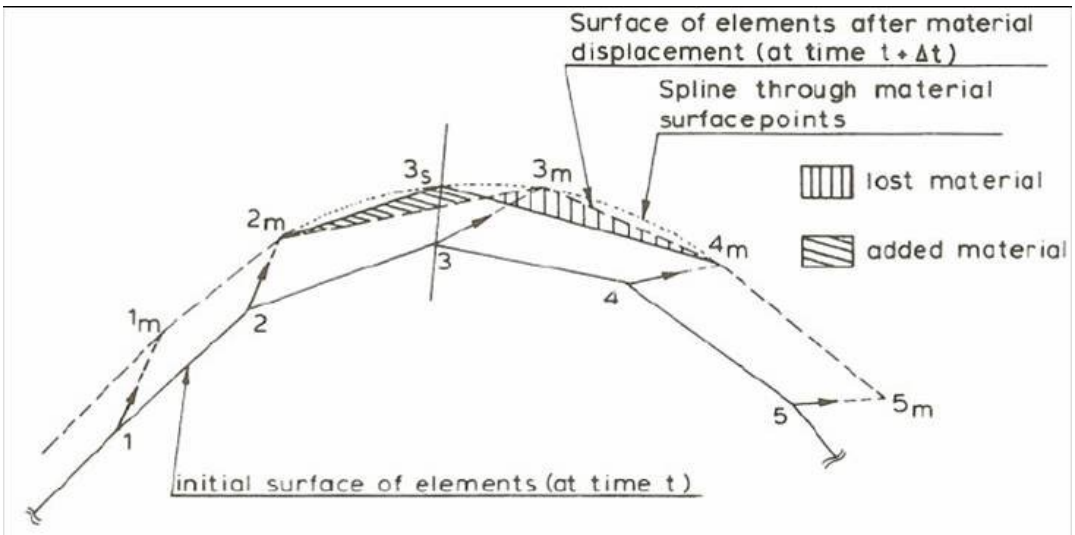

Fig. 4.16 Adaption of nodal surface point location.

The procedure has been verified by a numerical simulation of a longitudinal translation of a rod with a non-uniform cross-section. The initial element mesh is shown in fig. 4.17a. Only one element in radial direction suffices for this test because no material deformations occur. Internal nodal points (at the centerline) are spatially fixed. The locations of surface points are changing with the condition that they are moving in the direction of the (local) normal vector of the surface. The predicted change of the free surface of the mesh due to rigid translation of the material is shown in figs. 4.17b to 4.17d inclusive.
From these results it is observed that the predicted shape of the translating bulge remains unchanged.

Instead of adapting the surface point location in the direction of the local normal vector of the surface, another direction may be chosen. If in the example of fig. 4.17 a direction normal to the centerline was chosen, then the oblique shape of the elements could be prevented.

In an actual simulation of a forming process the size of all elements will generally not be equal. Therefore a one dimensional convection simulation was carried out with a finite element mesh containing 26 element of different size. The initial mesh is shown in fig. 4.18 a. In this test both free surface movements and strain propagation were taken into account. The mesh is prestrained in the same way as in the preceding section. Fig. 4.18 b shows the changed free surface due to rigid translation and fig. 4.19 shows the predicted strain propagation. The deviations from the exact solution are of the same magnitude as for the case of 20 elements of equal size (see fig. 4.11). Note that the automatically determined weight factors are not equal in all elements due to the non-uniform element size.

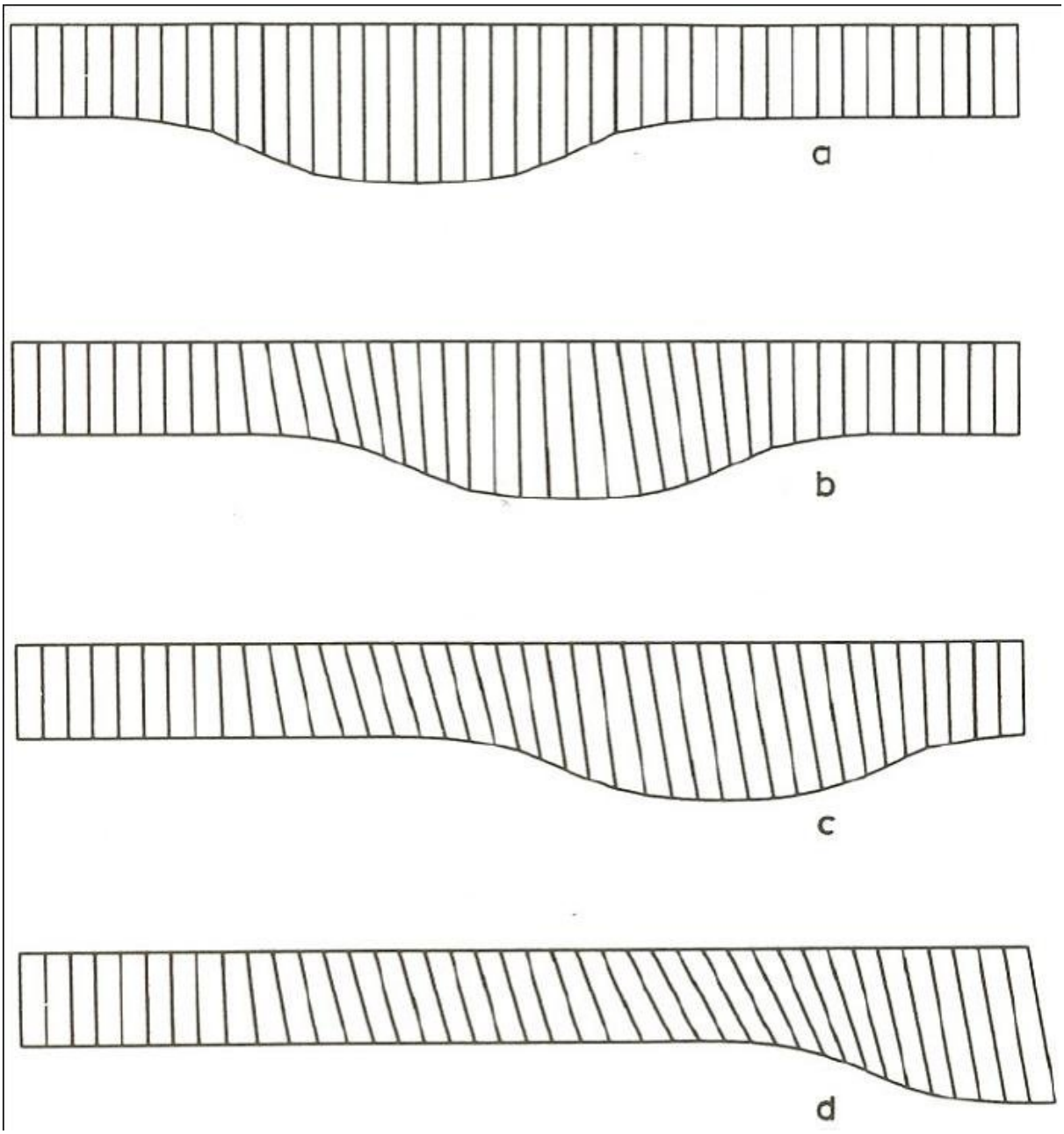

Fig. 4.17 Prediction of free surface movement, test for rigid longitudianal translation, nodal surface point location according to the local normal component of the displacement increments, (a) initial mesh, (b) after 12 steps, (c) after 24 steps, (d) after 48 steps.

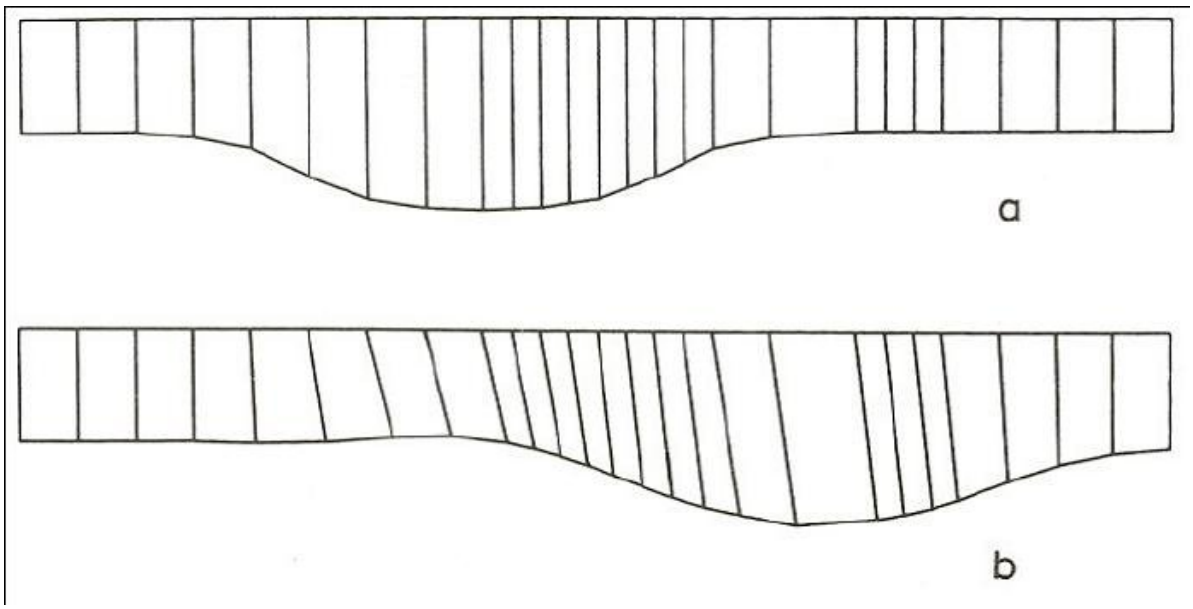

Fig. 4.18 Test problem with varying element size, (a) initial mesh, (b) mesh after 24 steps longitudinal displacement.

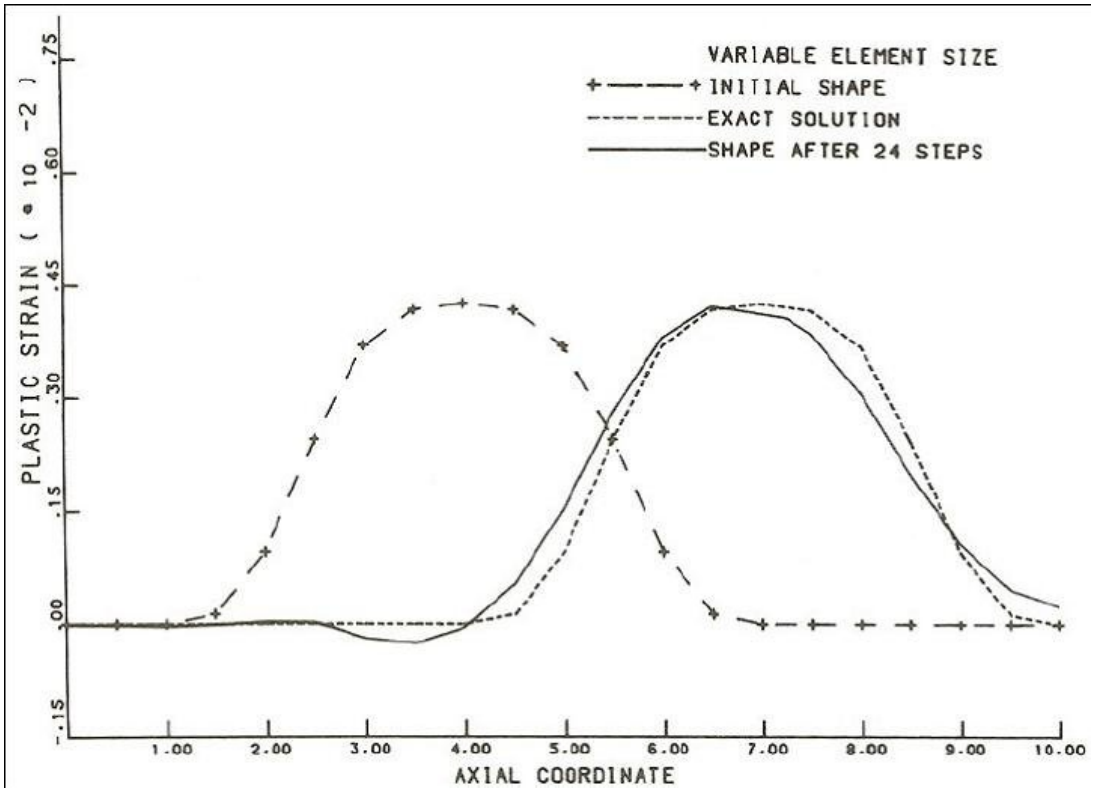

Fig. 4.19 Predicted strain propagation in the case of varying element size (element mesh of fig. 4.18a).

In simulations of forming processes it may be necessary to change not only the surface point coordinates but also those of internal points. These internal point coordinates may be changed independently from the material displacement, provided that the shift within each increment is not too large (say less than half the element size).
A method for determining an optimum finite element mesh after each increment was presented by Schreurs [44]. This optimum mesh is determined from an additional linear elastic problem with the same geometry as the current state of the forming workpiece. A disadvantage of this method is that a linear elastic problem has to be solved simultaneously during (or after) each increment. Schreurs also presented a mixed (or arbitrary) Eulerian - Langrangian method for simulation of forming processes in which convection due to flow of material through elements is taken into account. However, he did not carry out numerical tests on the accuracy by which convection is predicted. From the results that he presented it is not clear whether or not oscillation or overshoot will be predicted in simulations similar to those presented in this and in the previous section.

Another mixed Eulerian - Langrangian method was presented by Haber [21]. This method basically concerns redefining an element mesh in large purely elastic deformation problems. History dependent irreversible problems can not be solved by that method.

A method for adding or removing elements was reported by Bonte [11]. By this method, elements can be added if elements connected to free surfaces are too much elongated. A disadvantage of the method is that a rather large disturbance of mechanical equilibrium occurs in the increment where elements are added or removed, because integration point locations are discontinuously changed.
Besides, in many cases distortion or elongation of elements can be avoided by shifting the location of internal points continuously. This can be carried out by prescribing these shifts or by defining 'internal free surfaces'.

V. Applications

Based on the theory presented in the preceding chapters, a finite element programme called DIEKA has been developed.
Large contributions are supplied by students during the final stage of their study. Result of that work has been published by Henk Huisman [19] and Jaap v.d. Lugt [32]. These students contribute largely to the applications presented in this chapter.

The upsetting process

The first forming process which was simulated is the upsetting process, a process which can be regarded as a benchmark problem in metal forming. The upsetting process is defined as the axial compression of an axisymmetrical body between two rigid plates. The plates are assumed to be sufficiently rough to suppress slip at the interfaces. Besides, these plates are assumed to be perfect insulators. At the free cylindrical outer surface also perfect insulation is considered (natural boundary condition of the heat transfer equations).
The finite element discretization consists of 48 elements with four nodes. Isoparametric elements are used with Gaussian numerical integration [51], and with average dilatation according Nagtegaal et.al. [37]. However, a modification was applied as to the numerical integration of the temperature predictions in the case of fast deformation (small time increments). In that case the contribution of conduction to the temperature rate is very small compared to the contribution due to plastic deformation. The undesired numerical effects that give inaccurate temperature predictions, are illustrated by means of a one dimensional problem without conduction. One of the boundary nodal points is subjected to a prescribed jump in temperature. The predicted temperature distribution is shown in fig. 5.1. All internal nodal temperatures change due to the coupling between nodal point temperatures. This coupling is not a result of physical heat transfer but due to the fact that the interpolation functions are not mutually orthogonal at element level. By shifting the position of the integration points to the location of the nodal points, an apparent orthogonalisation of the interpolation functions is accomplished,

$$\int_{Ve} \Psi^K \Psi^L \, dV \approx \sum_{n=1}^{N} \Psi^K(\underset{\sim}{\chi}_n)\Psi^L(\underset{\sim}{\chi}_n)\, \Delta V_{en} = I^{KL} = 0 \text{ if } K \neq L. \quad (5.1)$$

where Ψ^K and Ψ^L are the interpolation functions, $\underset{\sim}{\chi}_n$ the location of nodal point n, and N the total number of nodes per element.
Applying the modified numerical integration to the same one dimensional problem, yields the temperature distribution shown in fig. 5.2.
Except for the prescribed temperature, the nodal temperature remains unchanged.

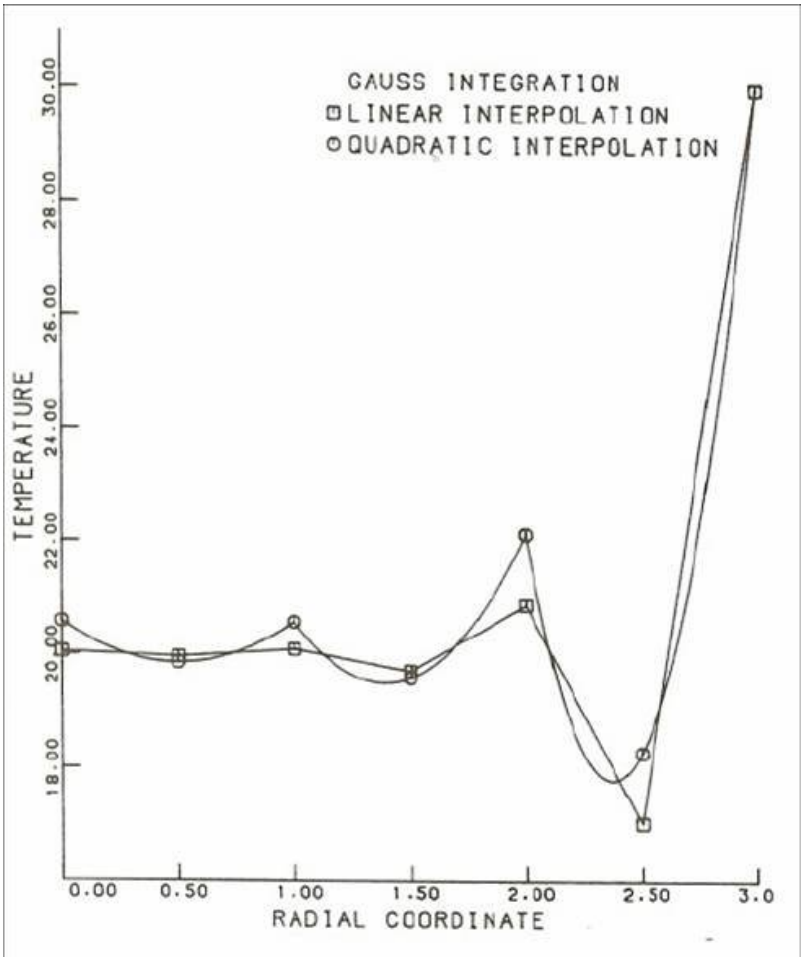

Fig. 5.1 Temperature distribution predicted by isoparametric elements with Gaussian numerical integration, as a response to a prescribed temperature jump at R=3, for 6 elements with linear interpolation and 3 elements with quadratic interpolation respectively.

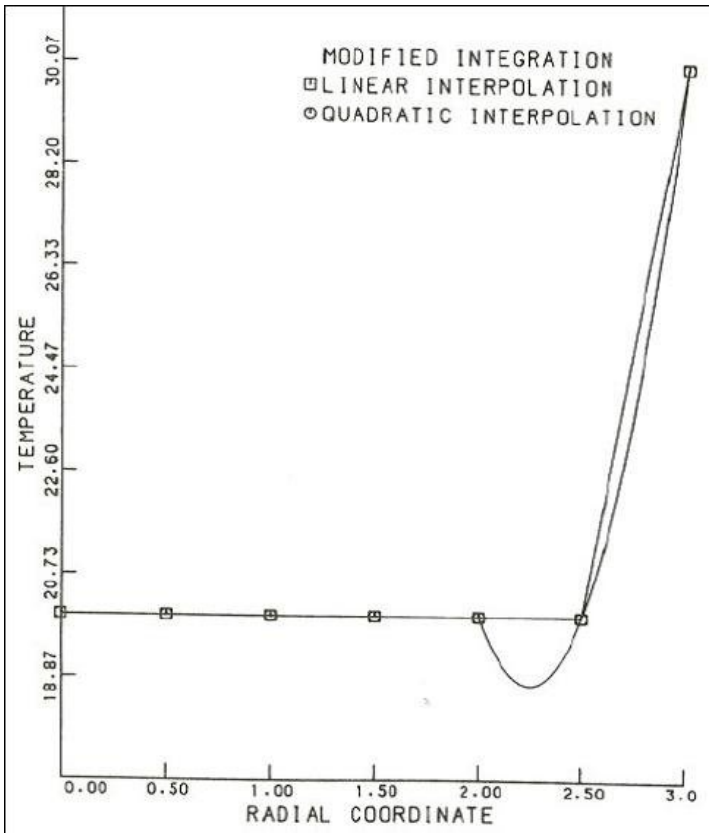

Fig. 5.2 Temperature distribution predicted by isoparametric elements with integration points located at nodal points, as a response to a prescribed temperature jump at R=3, for 6 elements with linear interpolation and 3 elements with quadratic interpolation respectively.

An illustration of inaccurate temperature predictions that may be obtained if no modification of the numerical integration is applied, is found by the numerical analysis of an upsetting problem of T.B. Wertheimer [49]. The undesired numerical effects show up most clearly by the low temperatures in the area where no plastic deformation occurs.
Before the integration was modified we carried out a similar analysis of the upsetting process and found the same kind of unrealistic low temperatures in the 'dead zone', below the initial temperature. With the modified numerical integration, these low temperatures vanished.
Note: The modified numerical integration is restricted to the terms related to the temperature rate. All other terms are integrated using Gaussian points.
We now return to the simulation of the upsetting process. The material

used is low carbon steel with code CK 15.
The mechanical material properties are obtained by tensile tests at several temperatures. The stress-strain curves are shown in fig. 5.3. The material used is assumed to be isotropic.

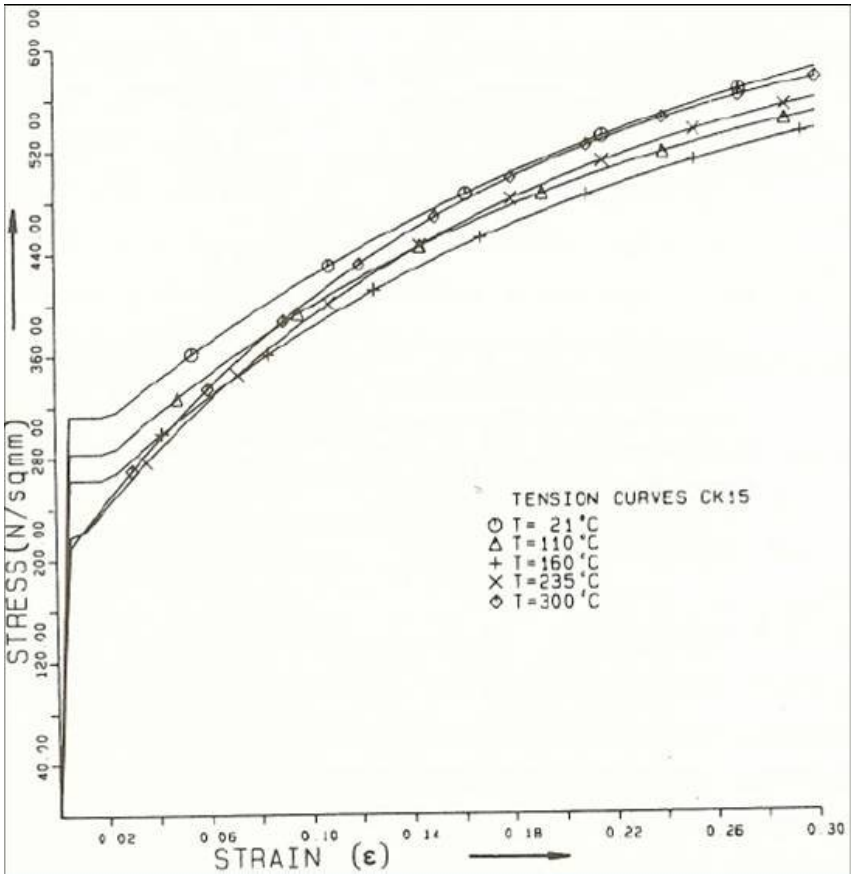

Fig. 5.3 Stress-strain curves of the material used in the upsetting process.

Hardening has been taken into account by a yield stress depending on the plastic strain according to formula

$$\sigma_v = \sigma_{vo} \qquad \text{if } \varepsilon \leqslant \varepsilon_h$$

$$\sigma_v = \sigma_{vo} + \Delta\sigma_v\left(1-\exp\frac{-(\varepsilon-\varepsilon_h)}{\varepsilon_o}\right) \qquad \text{if } \varepsilon > \varepsilon_h \qquad (5.2)$$

where σ_{vo}, $\Delta\sigma_v$, ε_h and ε_o are parameters depending on the temperature; they are determined by interpolation between the values given in table 5.1

	Temperature [C]				
	21	110	160	235	300
initial yield stress σ_{vo} [Mpa]	313	284	263	218	193
hardening stress increment $\Delta\sigma_v$ [Mpa]	400	350	360	415	450
hardening strain parameters					
ε_o	0.25	0.2	0.20	0.17	0.16
ε_h	0.022	0.022	0.021	0.01	0.0
Young's modulus	$E = 210000$ Mpa				
Poisson's ratio	$\nu = 0{\bullet}28$				
coëfficient of thermal expansion	$\alpha = 15 \cdot 10^{-6}$ C^{-1}				
coëfficient of heat conduction	$\lambda = 46$ $W{\bullet}m^{-1}{\bullet}C^{-1}$				
mass density	$\rho = 7830$ $kg{\bullet}m^{-1}$				

Table 5.1 Material data of the upsetting process

The undeformed mesh is shown in fig. 5.4.

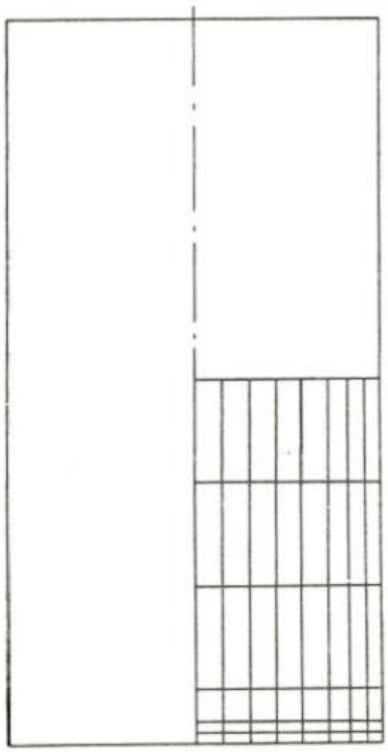

Fig. 5.4 Initial finite element mesh for simulation of the upsetting process.

Only a quarter of the cross section is modelled because of symmetry. There are 126 displacement and 63 temperature degrees of freedom The initial temperature is 20¼C, the initial height is 36 mm and the initial diameter is 18 mm. The total imposed reduction of the height is 16 mm in 1.6 seconds. The analysis was carried out using the mixed Eulerian-Lagrangian method. The element location is adapted in a way that too much distortion of elements is avoided whereas the expansion of the contact surface is continuously taken into account by adapting the surface point location according to the procedure discussed in section 4.3.2.2. The deformed mesh is shown in fig. 5.5.

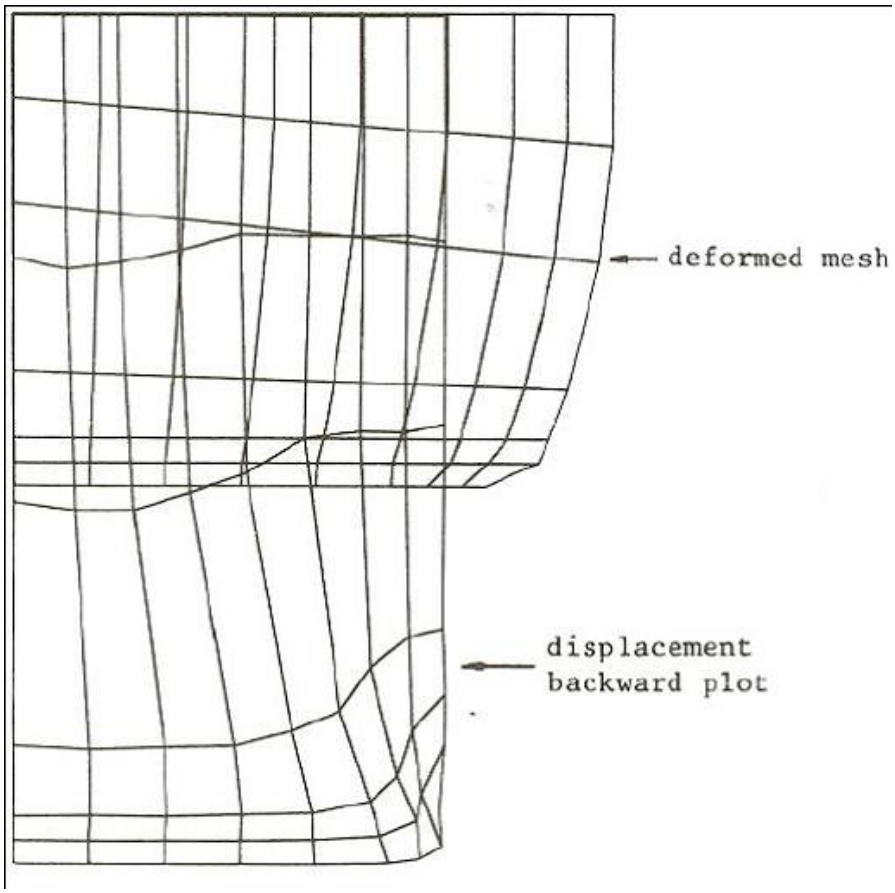

Fig. 5.5 Deformed mesh after upsetting, and displacement backward plot.

In this figure also the 'displacement backward plot' is given, obtained by subtracting the total material displacement of the particles that finally coincide with the nodal points, from the final location of the nodes. The discrepancy between the shape of the billet in the backward plot and the initial shape is a measure for the accuracy of the simulation. It can be observed that in the intersection of the cylindrical free outer surface

and the contact surface a small piece of material is 'lost' due to the incremental expansion of the contact surface.
The predicted temperature and plastic strain distribution are shown by fig. 5.6 and fig. 5.7 respectively.

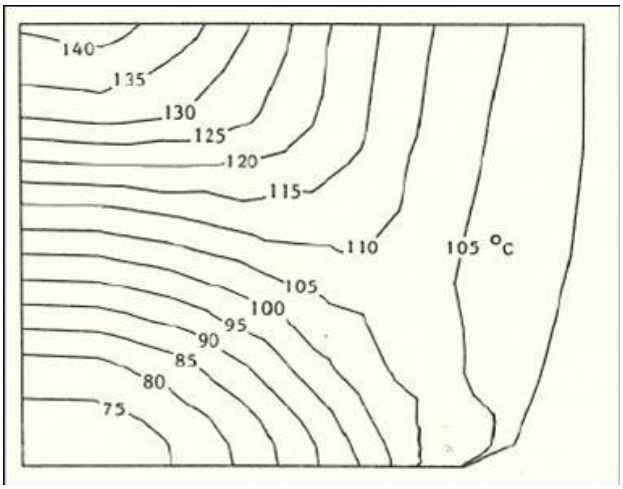

Fig. 5.6 Predicted temperature distribution after upsetting.

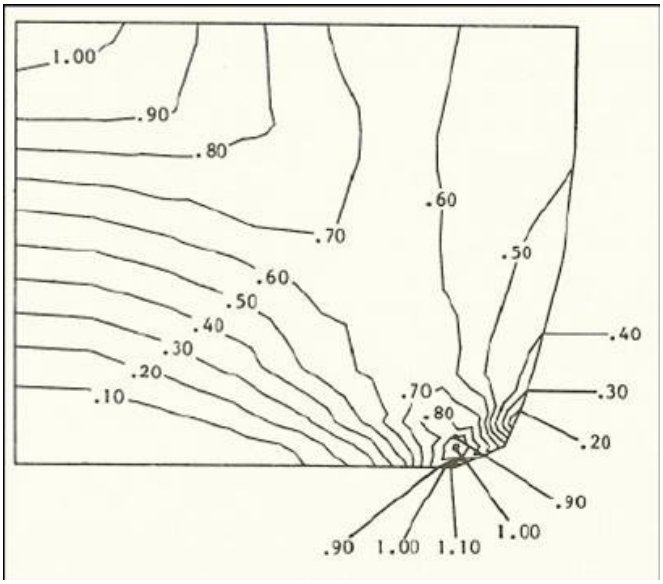

Fig. 5.7 Predicted plastic strain distribution after upsetting.

The simulation was carried out in 95 increments. Within each increment only one or two iterations were necessary.
Verification of the finite element model can be achieved by comparing the

numerical results to the results obtained by experimental methods.
The experiment is performed under the same conditions as mentioned above. The temperature has been measured, at medium height, on the outer surface of the billet. The results are given in figure 5.8.

It can be seen that the boundary condition of perfect insulation is not achieved. Therefore it is necessary to correct the experimental results for heat transfer to the environment.
For the heat transfer to the environment one must know the coefficient of heat transfer between billet and environment (β)• This coefficient follows from the expression of the heat flow (Φ), towards the environment.
When the billet has an almost uniform temperature ($\hat{T}$), the heat flow can be expressed by:

$$\Phi = c\rho V\frac{d\hat{T}}{dt} = \beta(\hat{T}-T_0) \qquad \text{or}$$

$$\beta = \frac{c\rho V\frac{d\hat{T}}{dt}}{\hat{T}-T_0} \tag{5.3}$$

The temperature correction (ΔT_{corr}), at time t and temperature T, can now be written as:

$$\Delta T_{corr} = \frac{1}{c\rho V}\int_0^t \Phi dt \qquad \text{or}$$

$$\Delta T_{corr} = \frac{\hat{\Delta T}}{\Delta t}\frac{1}{(\hat{T}-T_0)}\int_0^t (T-T_0)dt \tag{5.4}$$

The experimental results, with the correction of the temperature for heat loss, are also given in figure 5.8.
The loading time was fast. The heat transfer between billet and thermocouple is a slow process. This has to be taken into account when comparing the corrected experimental results to the numerical results. Therefore it is more reliable to compare the results in the steady state. For this purpose the numerical analysis was continued, with additional time steps and no deformation, to achieve the steady state after the forming process. The results are given in figure 5.8.

Now, the numerical results and the (corrected) experimental results can be compared.

The steady state temperature for the experiment was 100.5 C, and for the numerical analysis 105.0 C. The difference between these temperatures can partly be explained by the difference in the measured, and the calculated work that has been carried out respectively (see figure 5.9).

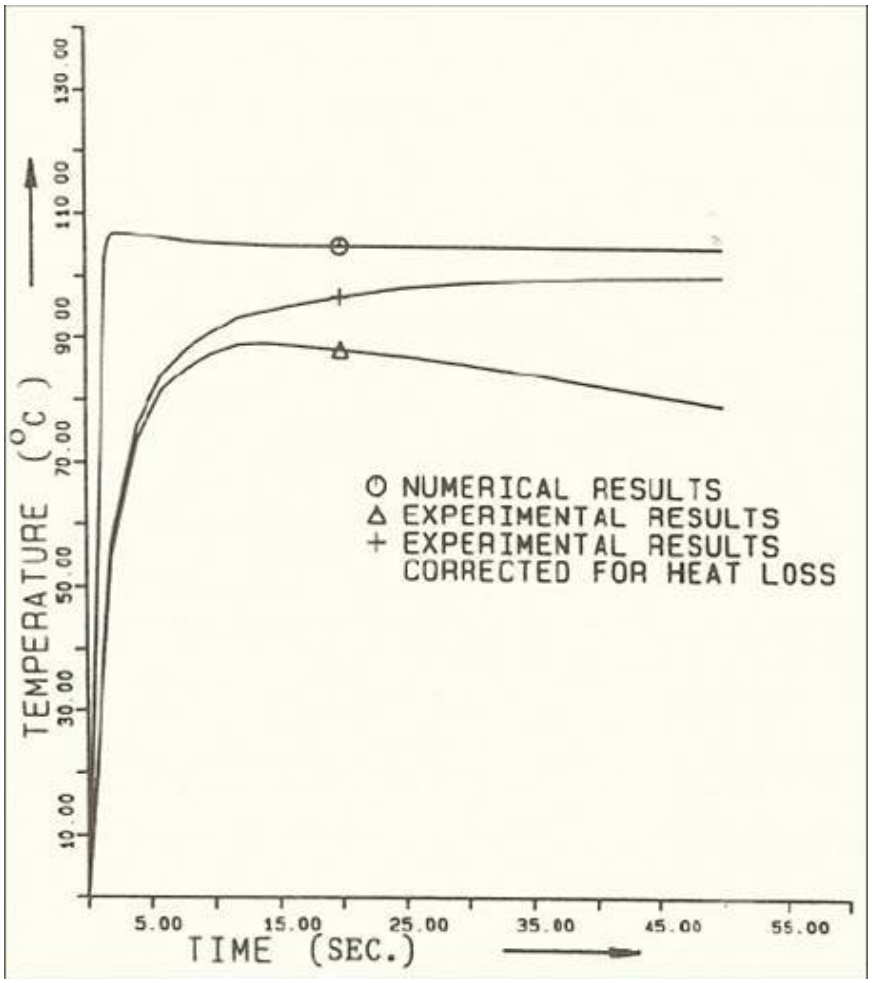

Fig. 5.8 Change of the temperature at medium height on the outer surface of the billet, during and after upsetting.

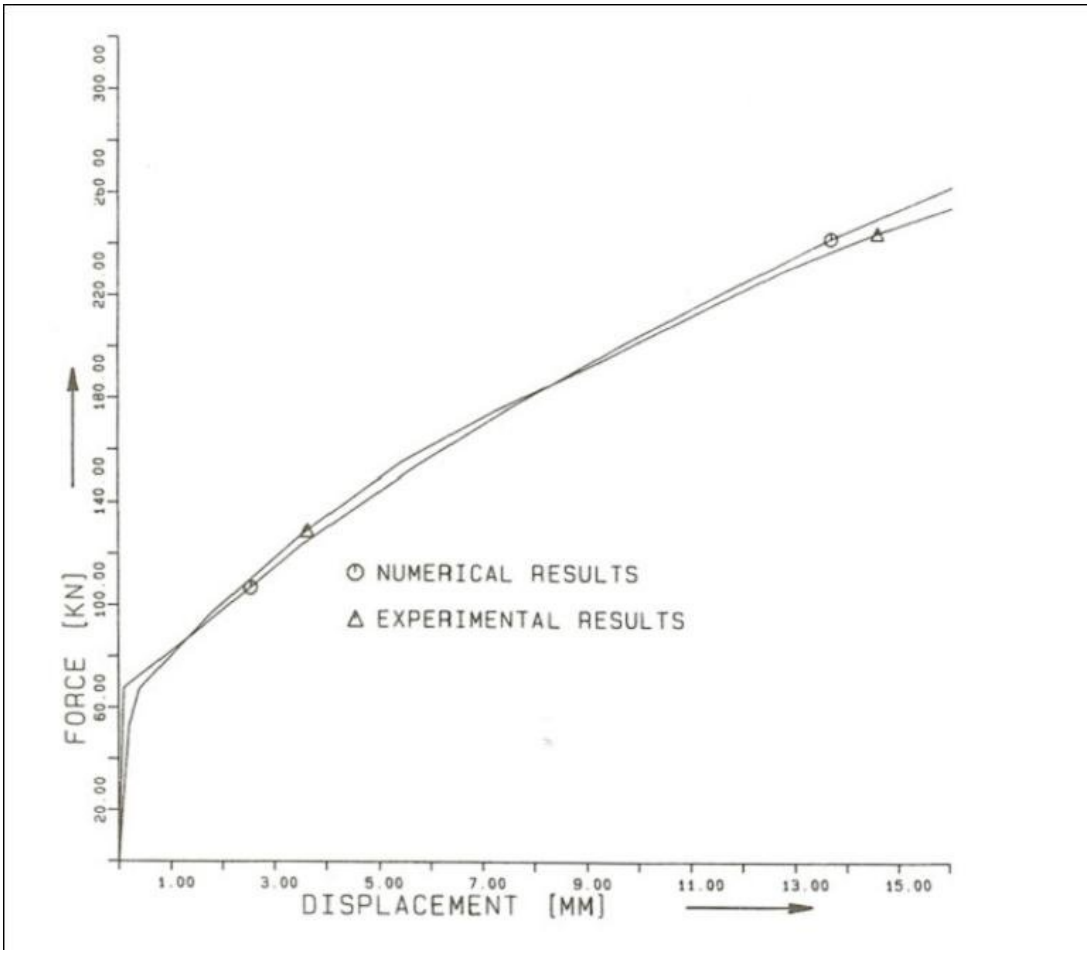

Fig. 5.9 Load-displacement curve of the upsetting process.

Compared with the results shown in [32], a better agreement between experiment and finite element simulation is found for the load-displacement curve. This can mainly be attributed to the improved approximation of the real hardening behaviour of the steel by taking into account a strain range without hardening directly after yielding. Besides, a local refined element mesh has been taken into account near the contact surface between billet and tool, resulting in a better approximation of the deformation process in that part where a large deformation gradient occurs.

The wire drawing process.

The second process simulated is the wire drawing process. First, no thermal effect nor friction have been taken into account. The finite element mesh is shown in fig. 5.10. Isoparametric elements with four nodes are used.

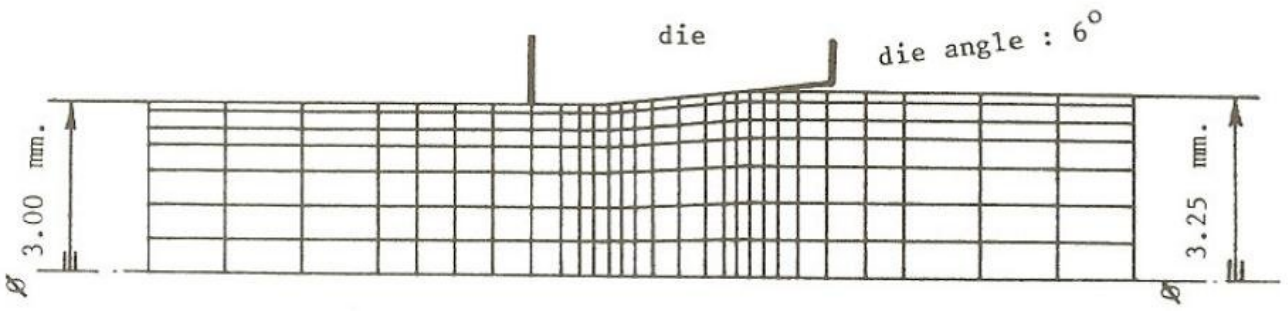

Fig. 5.10 Finite element mesh for simulation of the wire drawing process.

The reduction is accomplished by suppressing the velocity component normal to the contact surface between wire and die. The mixed Eulerian-Lagrangian method was applied. However, the spatial location of the outer surface hardly changes. Hence a purely Eulerian solution results. The simulation is carried out from the start up of the process until a stationary state is achieved. The material used is soft copper. The material properties are given in table 5.2 and fig. 5.11.

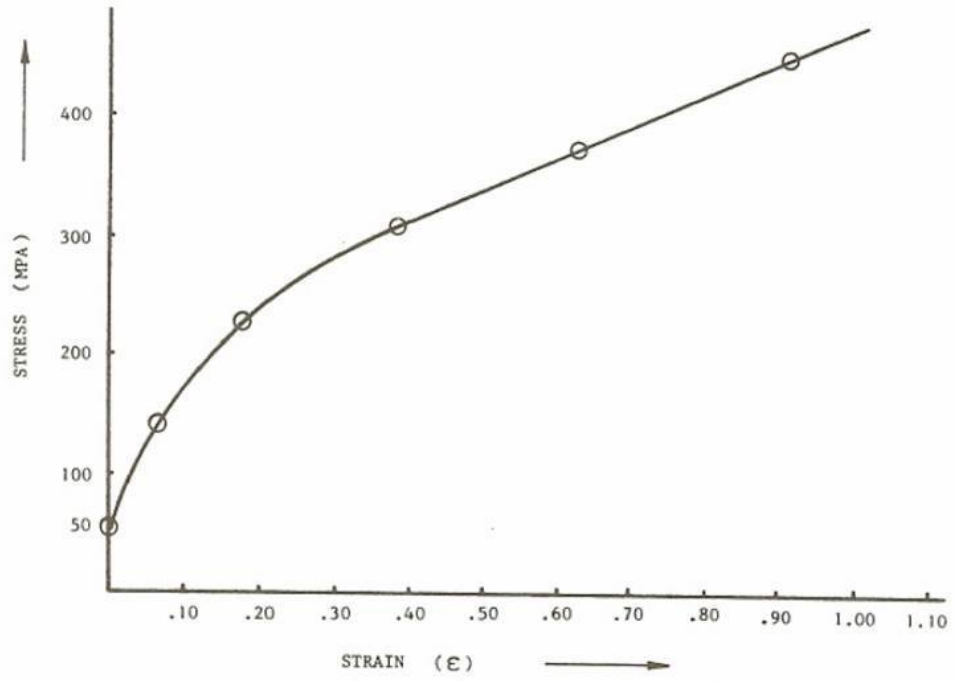

Fig. 5.11 Stress-strain curve of copper, used in the simulation of the wire drawing process.

The material shows a considerable hardening. This has been taken into account by a two fraction model, one elastic - plastic fraction with isotropic hardening according to (5.2) and one purely elastic fraction, resulting in a combined isotropic - kinematic model.
Figure 5.12 shows the predicted equivalent plastic strain distribution for an increasing number of increments. It can be observed that the area in which a stationary state is achieved increases continuously.
The diameter is reduced from 3.25 mm to 3 mm. The corresponding homogeneous strain is then $2\log(\frac{3{\bullet}25}{3}) = 0{\bullet}160{\bullet}$ This is indeed a lower bound of the predicted strain.
Figure 5.13 shows the predicted stress distribution. A highly inhomogeneous axial stress distribution appeared in the wire after reduction. This stress distribution will remain in the wire after unloading (the neutral point is shifted after unloading).

	fraction	
	$\Phi_1 = 0{\bullet}99822$	$\Psi_2 = 0{\bullet}00178$
Young's modulus	120000 [Mpa]	120000 [Mpa]
Poisson's ratio	0.35	0.35
initial yield stress	50 [Mpa]	∞
hardening stress increment $\Delta\sigma_v$ -	160 [Mpa]	-
hardening strain parameters		
ε_o	0.1	-
ε_h	0.	-
coefficient of thermal expansion	$1{\bullet}7\ 10^{-5}$ [C^{-1}]	
coefficient of heat conduction	365 [W $m^{-1}C^{-1}$]	
mass density	8940 [kg m^{-3}]	
specific heat	390 [J kg^{-1}]	

Table 5.2 Material data for the wire drawing process.

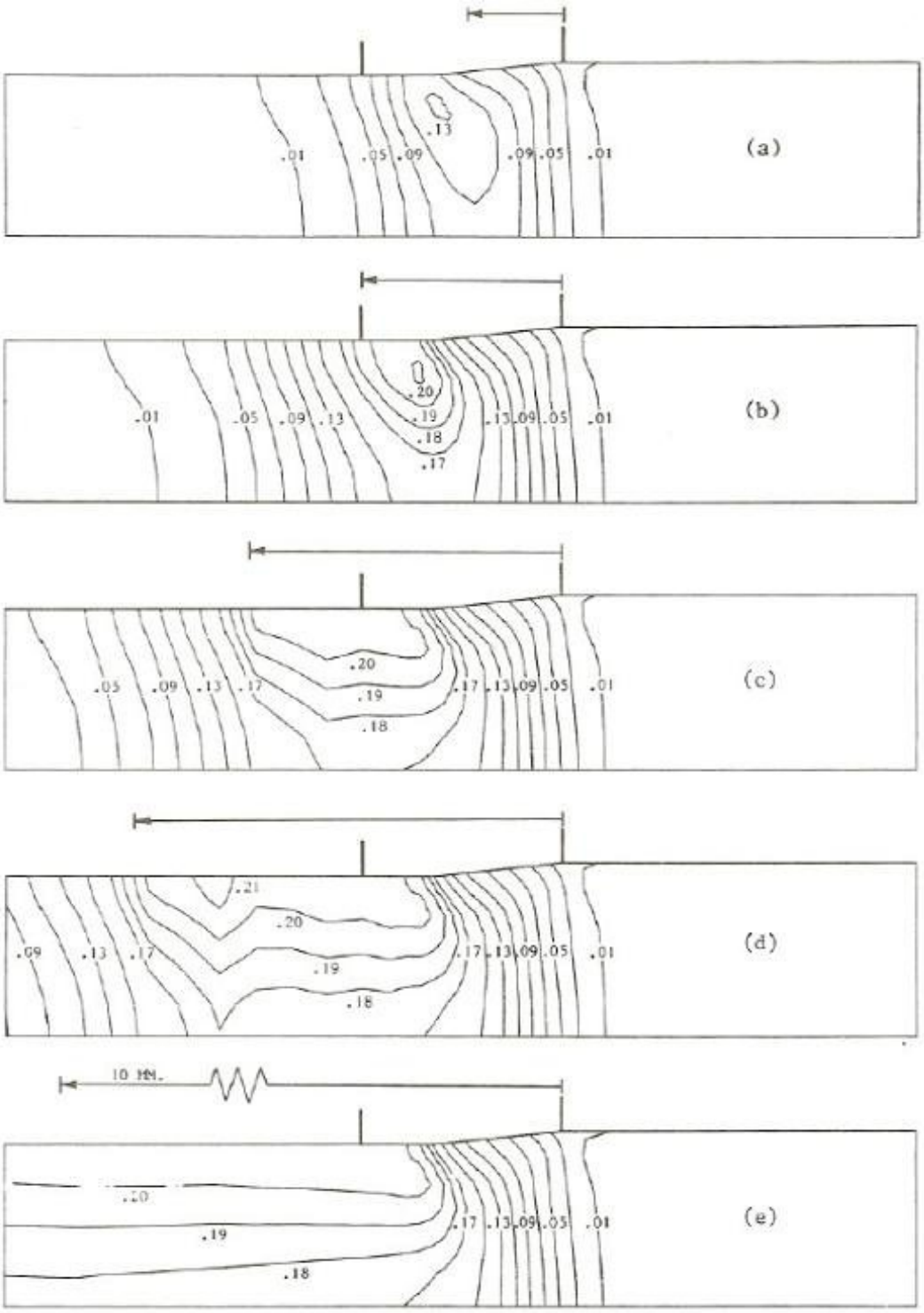

Fig. 5.12 Predicted plastic strain distribution during the start up of the wire drawing process, (a) after 90 increments, (b) after 140 increments, (c) after 175 increments, (d) after 210 increments, (e) after 345 increments. The length of the arrows correspond with the total displacement of the material.

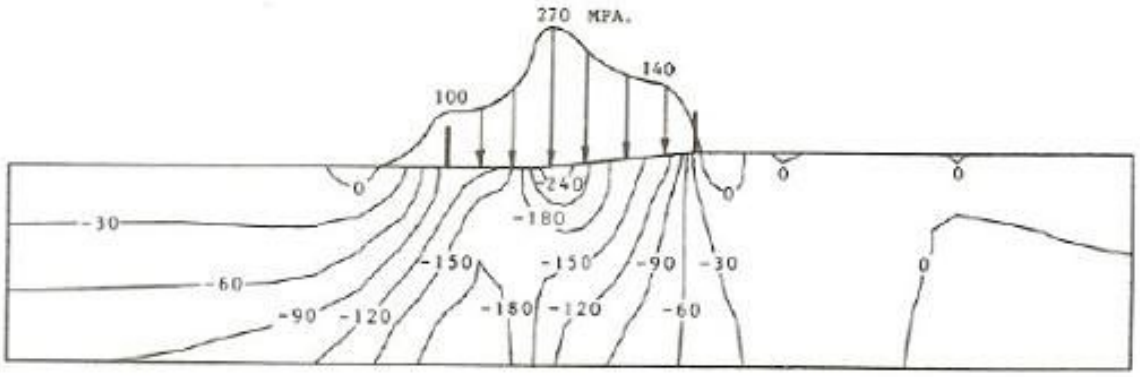

a) radial stress and normal stress at the die interface.

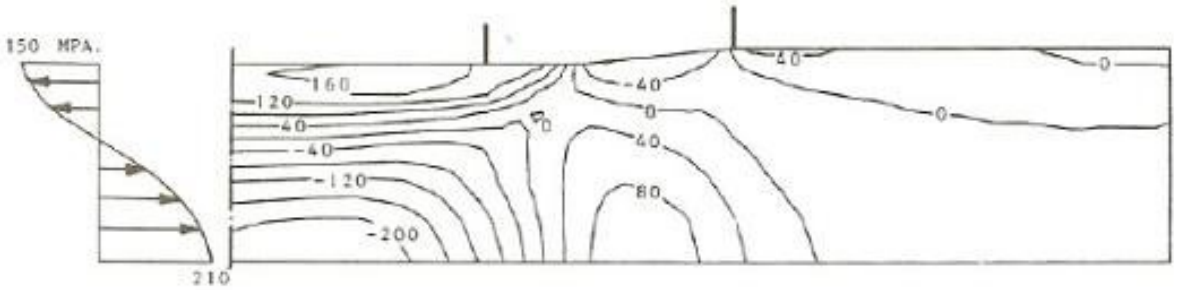

b) axial stress

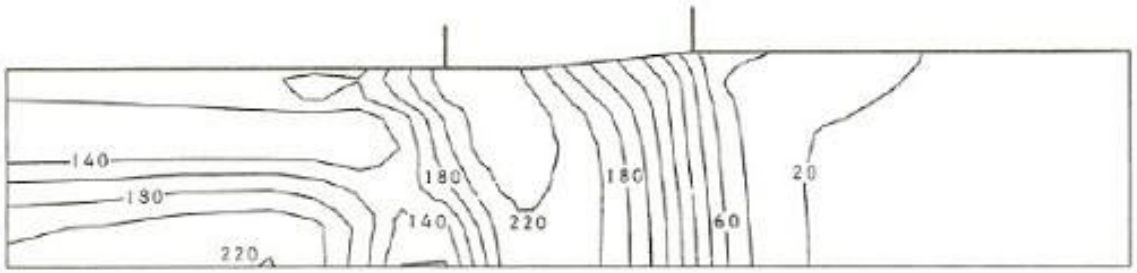

c) equivalent (Von Mises) stress

Fig. 5.13 Predicted stress distribution of the wire drawing process after a stationary state is reached.

The simulation of the wire drawing process was repeated for the case that thermal effects and friction are taken into account. The die is now also part of the finite element mesh as shown in fig. 5.14.

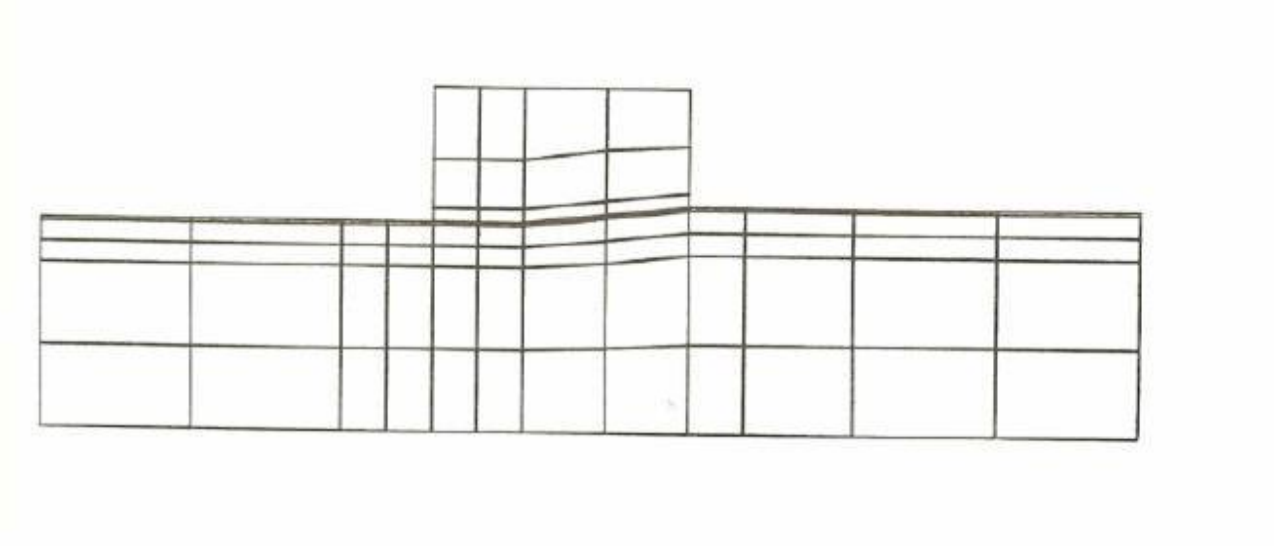

Fig. 5.14 Finite element mesh for the thermo-mechanically coupled simulation of the wire drawing process.

Friction has been taken into account by means of a thin layer of elements at the outer surface of the wire, (special friction elements with temperature degrees of freedom are not yet available in the programme DIEKA). In order to avoid numerical problems in these very thin elements, they are constrained in a way that pure shear occurs in the contact area between wire and die. In this way, 'plastic friction' is obtained.

The properties of the die and the lubrication layer are given in table 5.3 The yield stress of the lubrication layer has been chosen based on the difference between the measured drawing force and the drawing force obtained from the simulation without friction. This difference can be attributed to friction and is simulated by a uniform shear stress in the layer.

	die	lubrication layer (tin)
Young's modulus	600000[Mpa]	45000 [Mpa]
Poisson's ratio	0.28	0.32
yield stress	15 [Mpa]	∞
coefficient of thermal expansion	$5 \cdot 10^{-6}$ [C^{-1}]	$2 \cdot 1\ 10^{-5}$ [C^{-1}]
coefficient of heat conduction	60 [W $m^{-1}C^{-1}$]	65 [W $m^{-1}C^{-1}$]
mass density	14000 [kg m^{-3}]	7300[kg m^{-3}]
specificheat	140 [J kg^{-1}]	220 [J kg^{-1}]

Table 5.3 Material data of the die and lubrication layer.

The resulting temperature distribution after 334 steps is shown in fig. 5.15. In the deformation area and lubrication layer an almost stationary state is achieved. However, in the die the temperature distribution is not yet stationary. This is due to the fact that temperature distribution in the wire is mainly determined by the plastic deformation energy dissipation whereas the temperature distribution in the die is determined by conduction. It will take several hundreds of steps more to achieve a stationary state in the die too. The time steps that are taken correspond to a velocity of 1 m/s. Calculation of the stationary state in the die can be accelerated by the following trick. During relatively long time increments the drawing process is stopped and the coefficient of heat conduction in the wire is set at zero. In the lubrication layer the temperature is kept constant at the level just before the process is stopped. During these long time increments a stationary temperature distribution in the die is approximated. The final temperature distribution is given by fig. 5.16.

Note: Natural boundary conditions with respect to heat transfer were taken into account which means no heat transfer through the boundary of the mesh.

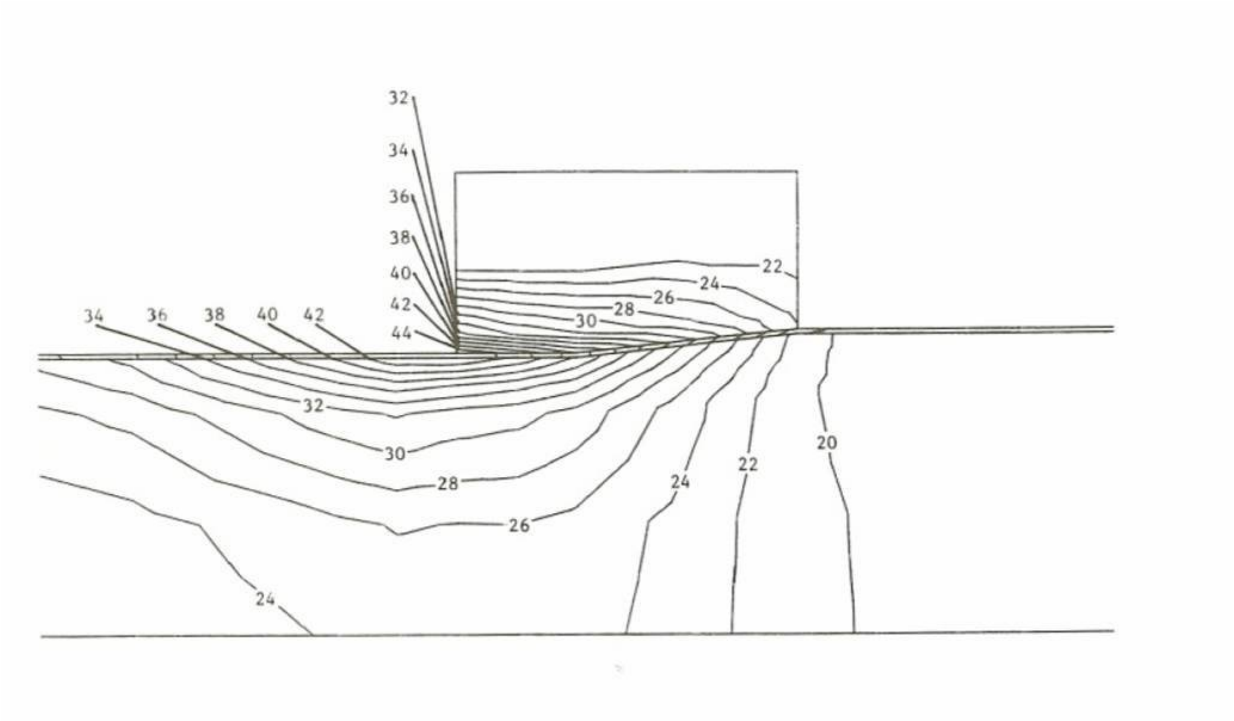

Fig. 5.15 Predicted temperature distribution of the wire drawing process after 334 increments (total axial displacement is 3 mm in 0.003 s).

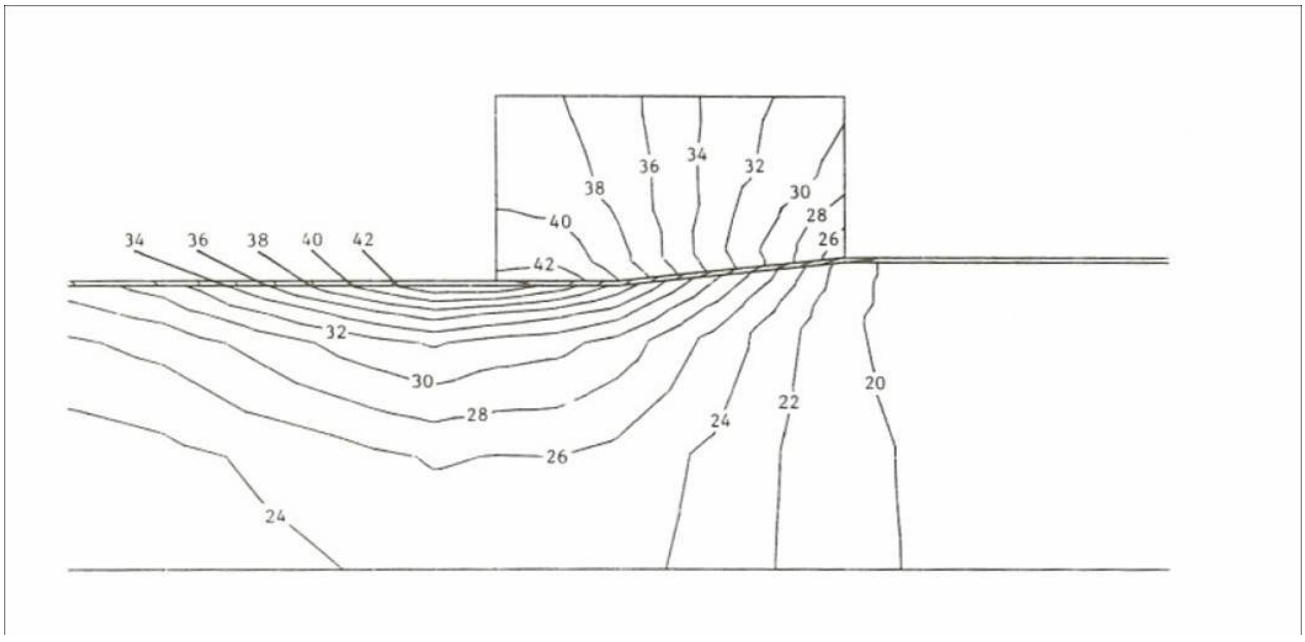

Fig. 5.16 Predicted temperature distribution of the wire drawing process in the stationary state.

A steel quenching process.

A process in which phase changes are strongly affecting the quality of a product is the steel quenching process.
A simulation of a quenching process of a cylindrical bar was carried out. The bar is assumed to be very long relative to the diameter, hence the process can be approximated as a one dimensional problem: the internal state is a function of the radial coordinate only.
The investigation with respect to the phase transformation kinetics were carried out by Nico Verschuren [47]. He also did the programming work and the simulation of the quenching process.
The description of the phase transformation is based on data obtained from a Time-Temperature-Transformation (T.T.T.) diagram of the steel considered. In this diagram the volume fractions of phases are given as a function of the time at constant temperature (after quick cooling to that temperature from a high temperature in the austenite area). The phase transformation at constant temperature can be described by the Avrami-equation,

$$\Psi = \Psi_{Ao} \, (1-\exp(-bt^n)) + \Psi_o \qquad (5.5)$$

where b and n are material parameters depending on the temperature, Ψ is the increasing phase fraction, Ψ_{Ao} is the austenite fraction that is present prior to quenching, and Ψ_o is the fraction of the increasing phase that is present prior to quenching. For the case of transformation from austenite to ferrite whereas no other phases are present, Ψ_o is equal to $1-\Psi_{Ao}$. The rate of change of Ψ is equal to the critical rate of change because the material is quickly cooled below the stable transformation temperature (~ 730°C). This critical rate of change is, according to section 3.6, assumed to be a function of the state variables. Hence the rate of phase change can be written as

$$\dot{\Psi} = bn\left(1 - \frac{\Psi-\Psi_o}{\Psi_{Ao}}\right) \left[\log\left(1 - \frac{\Psi-\Psi_o}{\Psi_{Ao}}\right)^{-\frac{1}{b}}\right]^{\frac{n-1}{n}} \quad (n\neq 1)$$

$$\dot{\Psi} = b\left(1 - \frac{\Psi-\Psi_o}{\Psi_{Ao}}\right) \quad (n=1) \qquad (5.6)$$

The different phases that may be present during the quenching process

are austenite, ferrite, pearlite and martensite. The physical and mechanical properties of ferrite and pearlite are nearly equal and are therefore considered as a single ferritic phase.

At a temperature between 730°C and 330°C no martensite is formed, hence only transformation from austenite to the ferritic phase occurs. The values of the parameters b and n for the austenite-ferrite transformation are presented as a function of the temperature in fig. 5.17.
The T.T.T. diagram has been simulated with equation (5.6). The result is given in fig. 5.18. The curves in this figure correspond to 1% ferrite and 99% ferrite respectively. The simulation started with $\Psi_{Ao}=1$ and $\Psi_{o}=0$.

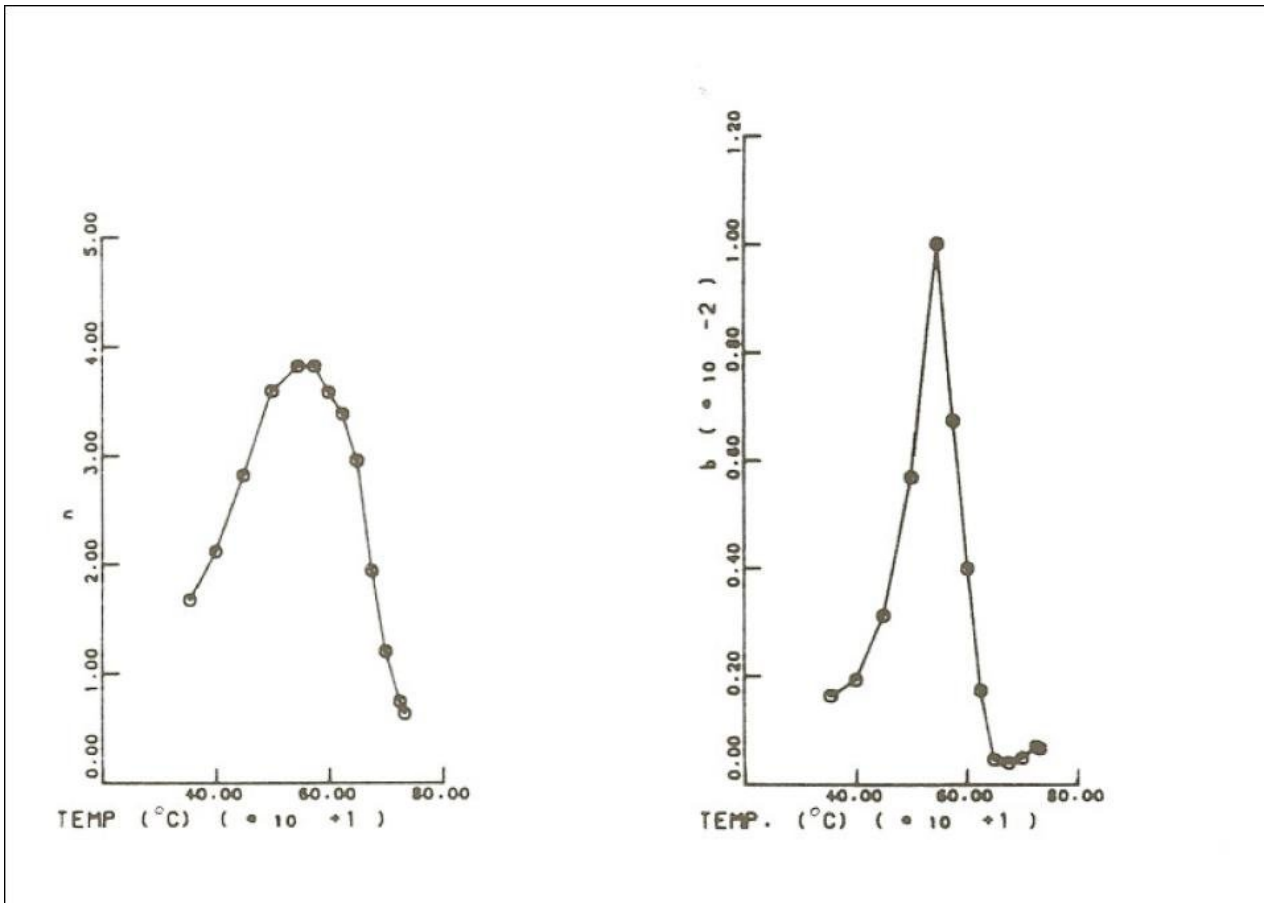

Fig. 5.17 Values of the parameters n and b in the Avrami phase transformation equation (5.5), as a function of the temperature, for steel CK45.

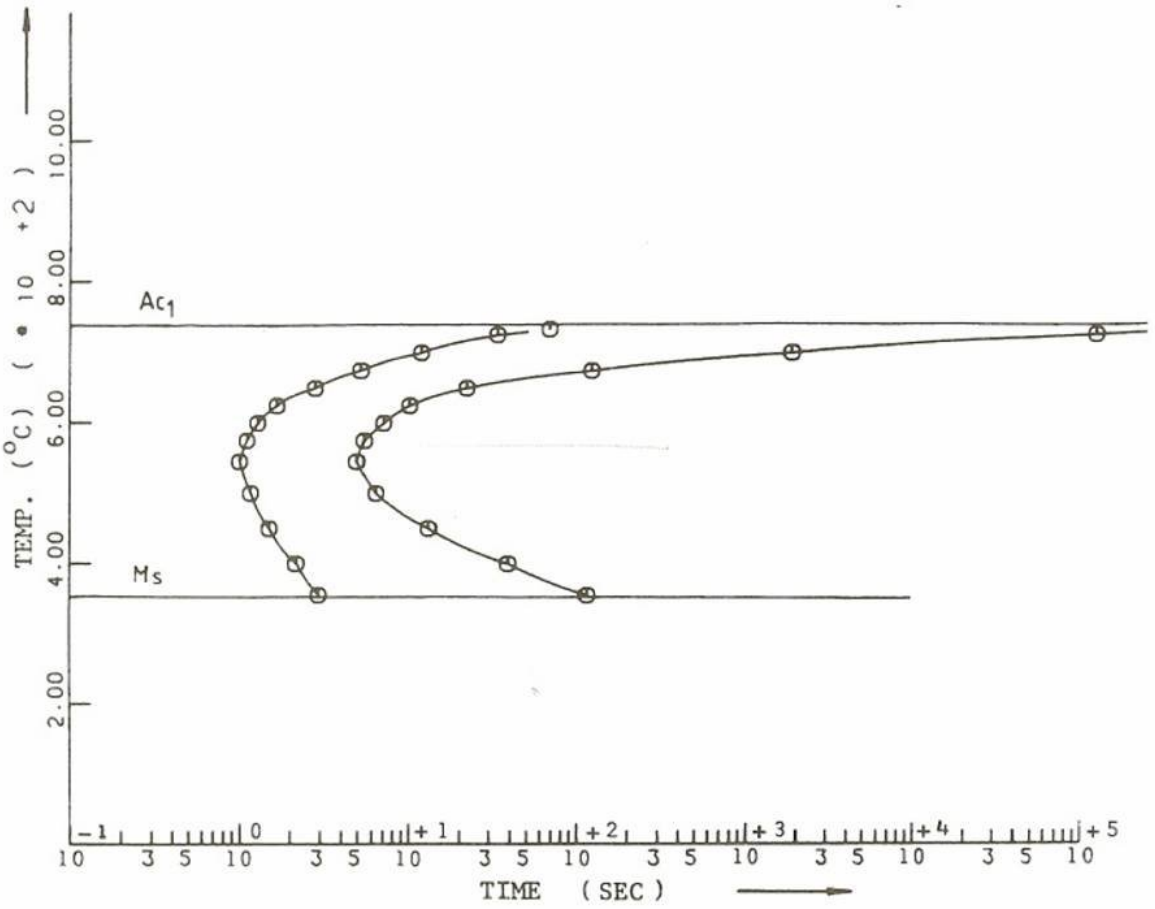

Fig. 5.18 Simplified Time Temperature Transformation (T.T.T.) diagram, simulated with the Avrami equation (5.5).

The transformation from austenite to martensite does not satisfy an equation similar to (5.5). Transformation to martensite occurs for the austenite fraction Ψ_{Ams} that is still present when the m(artensite) s(tart) temperature ($T_{ms} \approx 355^{\circ}C$) is reached. The fraction martensite Ψ_m which is formed, is a function of the temperature to which is cooled quickly [47],

$$\Psi_m = \Psi_{Ams}(1 - \exp(-\gamma(T_{ms} - T)) \quad \text{if } T<T_{ms} \qquad (5.7)$$

The parameter γ is equal to $0{\bullet}011[C^{-1}]$ for most steels. If cooling to a temperature less than T_{ms} is done very quickly, no ferrite is formed and hence $\Psi_{Ams} = \Psi_{Ao}$. In parts of the material where the cooling process is less fast, a part of the austenite has already transformed to ferrite-pearlite and less martensite is formed.

Equation (5.7) describes the transformation after quick cooling followed by a constant temperature. We have also adopted this equation in the case of 'continuous cooling'. The rate of change of the martensite fraction can then be expressed as

$$\dot{\Psi}_m = -\Psi_{Ams} \exp\left(-\gamma(T_m - T)\right) \dot{T}$$

or

$$\dot{\Psi}_m = -\Psi_A \gamma \dot{T} \qquad \dot{T}<0 \qquad (5.8)$$

$$\dot{\Psi}_A = \Psi_A \gamma \dot{T}$$

where Ψ_A is the current austenite fraction.

The yield stresses σ_v^k for each phase were assumed to be linear functions of the hardening parameters H^k (see eqn. 3.6.18 and 3.6.17) for each phase respectively. This is a sufficiently accurate approximation within the plastic strain range of 2 or 3 percent, which will occur in the quenching process.
The steel properties used in the simulation are those of CK45. The chemical analysis is shown in table 5.4.

mass fraction (percent)				
C	Si	Mn	P	S
.42 -.50	.15 - .35	.5 - .8	.035	.035

Table 5.4 Chemical fractions of steel CK45.

The mechanical and thermal properties are shown in table 5.5.

From the transformation heat and specific heat given in this table, the parameters r^k for each phase are calculated at a reference temperature of $20^{\circ}C$, using eqn. (3.61). The results are also given in table 5.5.

	phase	temperature [C]			
		0	300	600	900
Young's modulus	austenite	200000			124000
[Mpa]	ferrite	210000	193000	165000	120000
	martensit	200000		158000	
Poisson's ratio	a/f/m	0.3	0.3	0.3	0.3
yield stress	a	190	110	30	20
[Mpa]	f	360	250	40	20
	m	1600	1480		
hardening rate	a	4000			2480
[Mpa]	f	12600	11580	9900	7200
	m	20000		15800	
heat conduction	a	15.0			25.1
coefficient	f	49.0			27.0
[W $m^{-1}C^{-1}$]	m	43.1		30.1	
specific heat	a	520		607	650
[J $kg^{-1}C^{-1}$]	f	480		667	760
	m	485		670	
mass density	a	8018	7819		7576
[kg m^{-3}]	f	7850	7759	7645	
	m	7760	7670		
transformation heat [J kg^{-1}]					
	austenite → ferrite -50000 at 730°C				
	austenite → martensite -80000 at 350°C				
internal energy parameter (r^k) at a reference temperature of 20 C, determined from specific heat and transformationheat. [J kg^{-1}]					
- austenite	0.				
- ferrite	-64000.				
- martensite	-77700.				

Table 5.5 Mechanical and thermal properties of steel CK45.

As observed before, the quenching process has been approximated as a one-dimensional problem. In the finite element programme DIEKA, no one-dimensional elements are available; hence a layer of two-dimensional axial-symmetric elements has been used. The finite element mesh is shown in fig. 5.19.

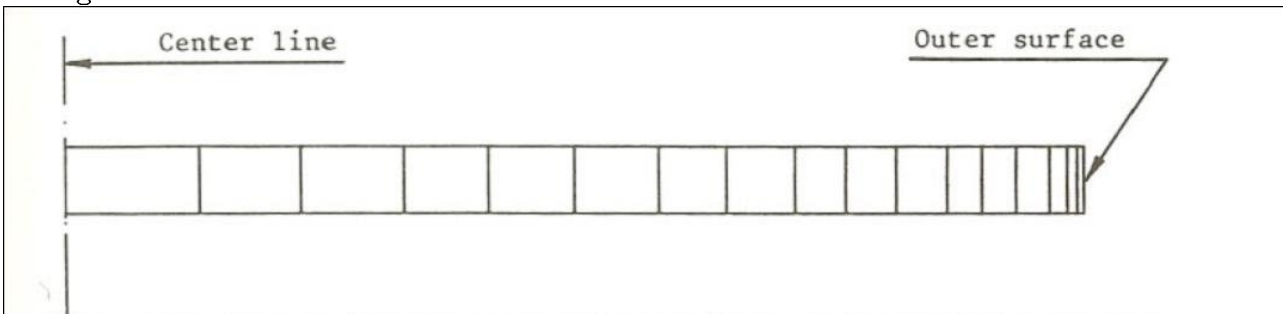

Fig. 5.19 Finite element mesh for simulation of a quenching process of an 'infinitely long' steel bar with a diameter of 60 mm.

The nodal degrees of freedom have been coupled in a way that the condition of an infinite bar is satisfied. A mesh refinement has been applied near the outer surface of the bar because large gradients are to be expected there. The diameter of the bar is 60 mm. The bar is quenched in water with a temperature of 20 C. The heat transition coefficient from the bar to the water has been assumed to be constant at 5860 $Jm^{-2}s^{-1}C^{-1}$.

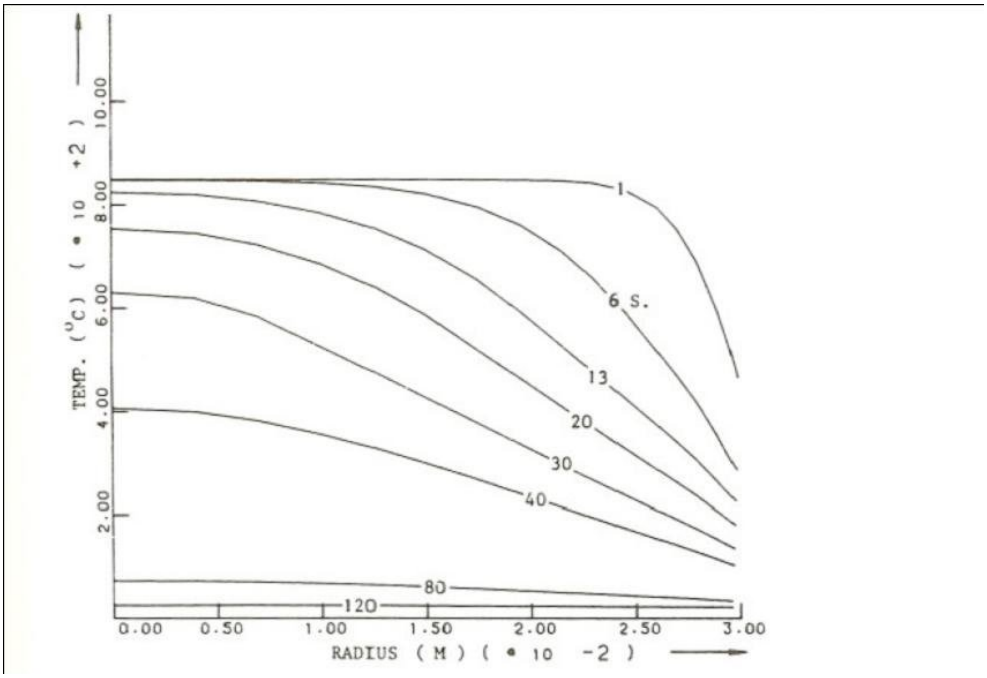

Fig. 5.20 Predicted temperature distribution in the bar, as a function of time.

Fig. 5.20 shows the predicted temperature distribution history. Figs. 5.21

to 5.23 inclusive show the predicted stress distribution history for the radial, axial and circumferential stress components respectively.

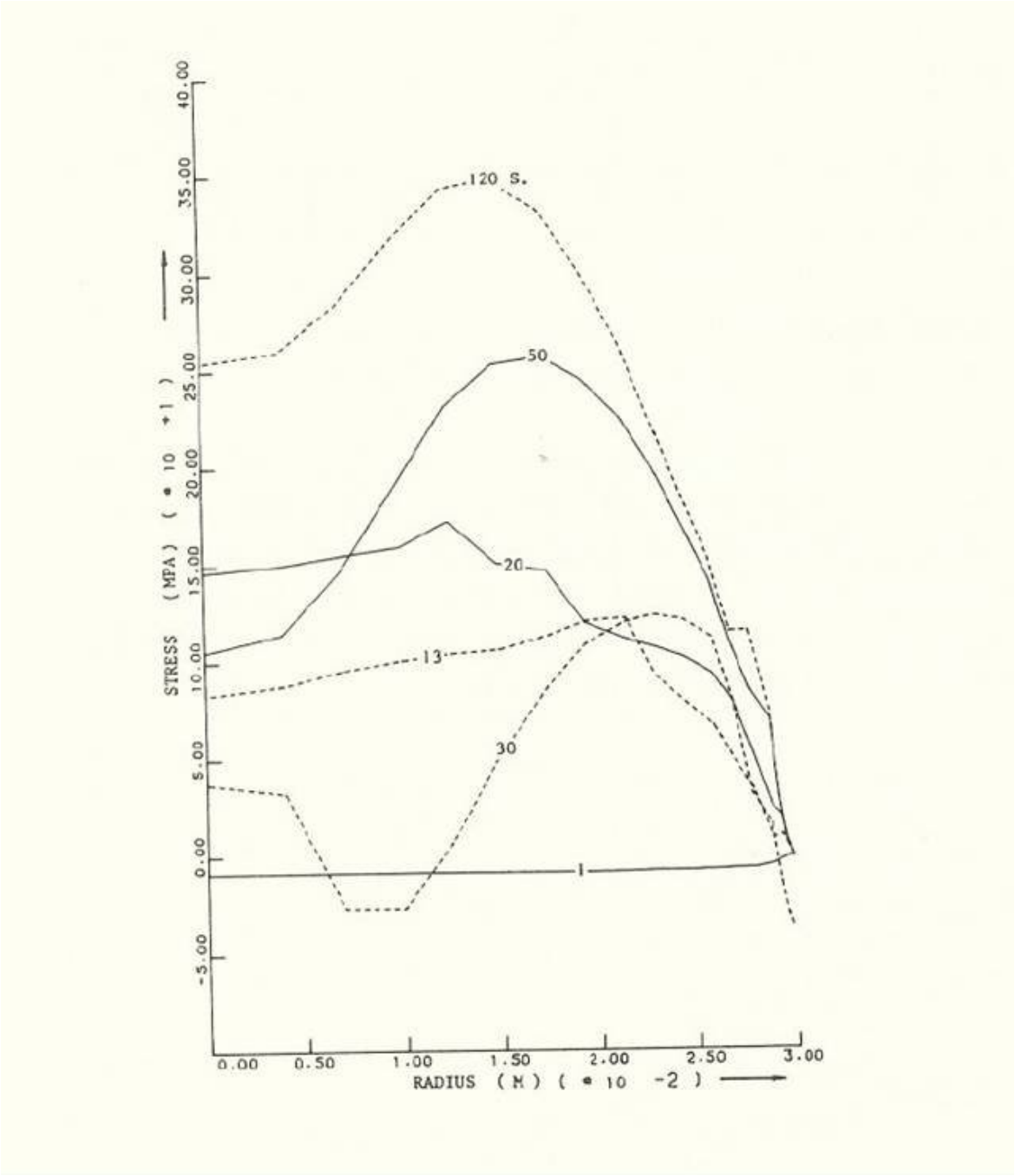

Fig. 5.21 Predicted radial stress distribution in the bar, as a function of time.

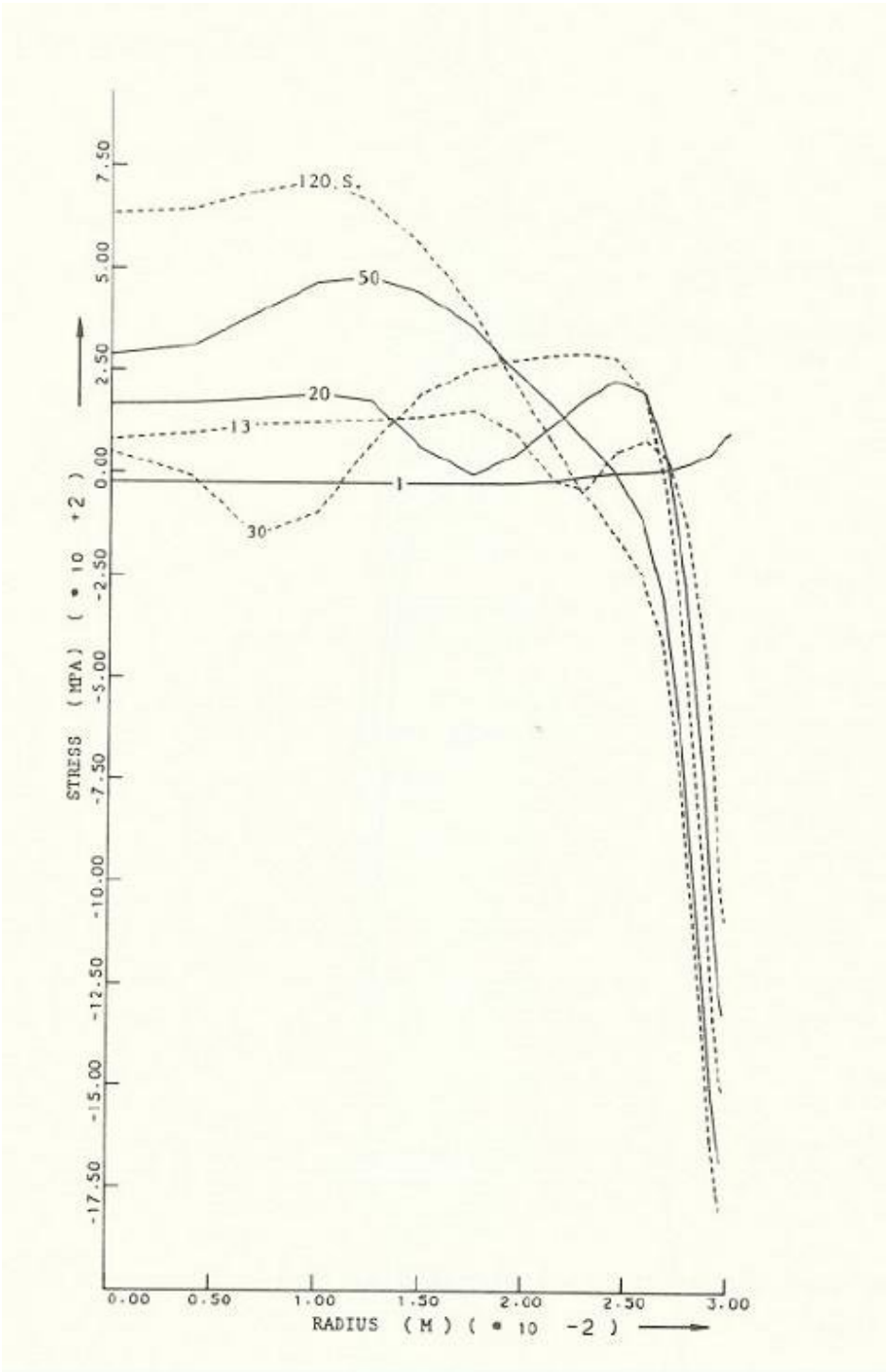

Fig. 5.22 Predicted axial stress distribution in the bar, as a function of time.

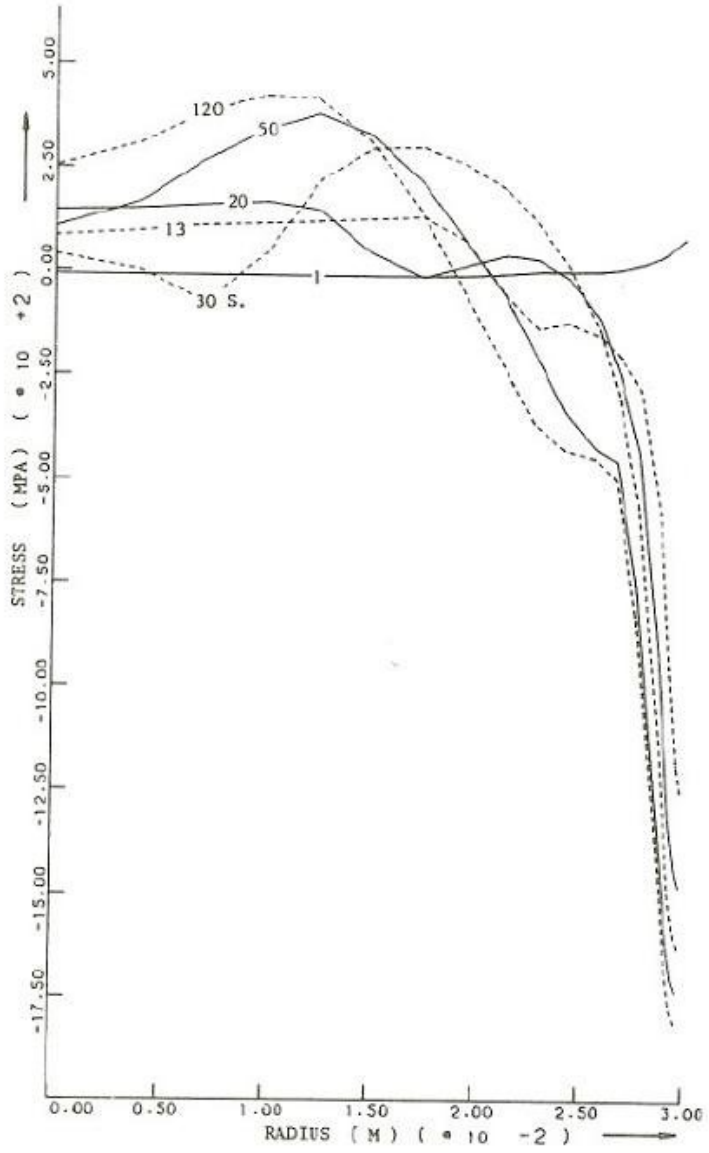

Fig. 5.23 Predicted circumferential stress distribution, as a function of time.

The plastic strain history is shown in fig. 5.24. A little softening due to transformation can be observed near the outer surface. The propagation of the ferritic phase is shown in fig. 5.25. The transformation front coincides with a dip in the stress distribution which can be observed most clearly in fig. 5.22 for the axial stress.
Fig. 5.26 shows a close-up of the martensite phase propagation in a thin layer near the outer surface.

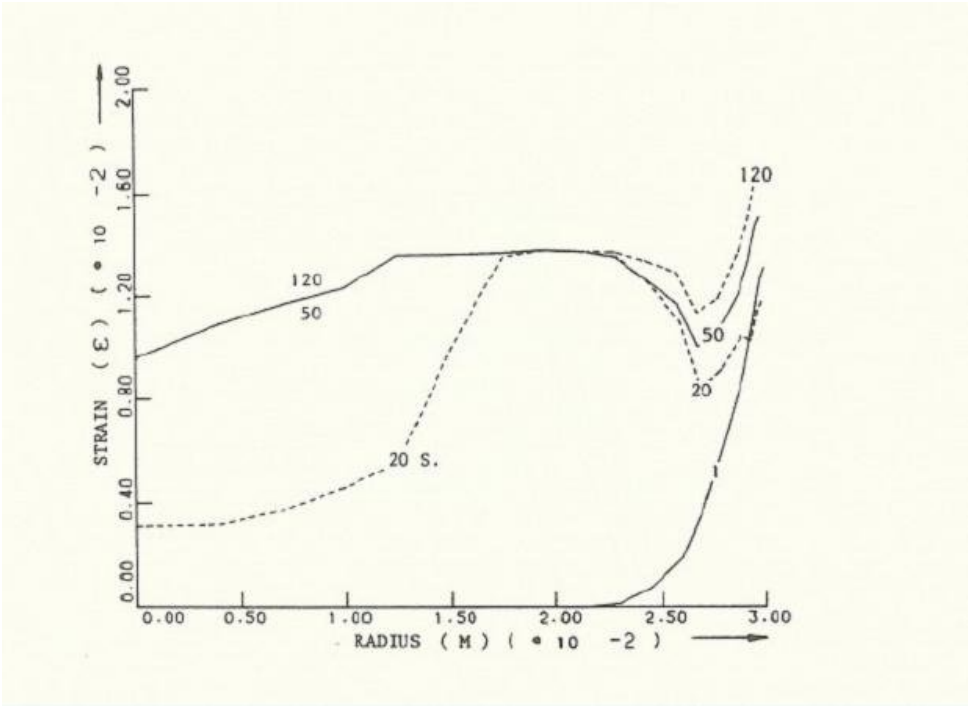

Fig. 5.24 Predicted equivalent plastic strain distribution in the bar, as a function of time.

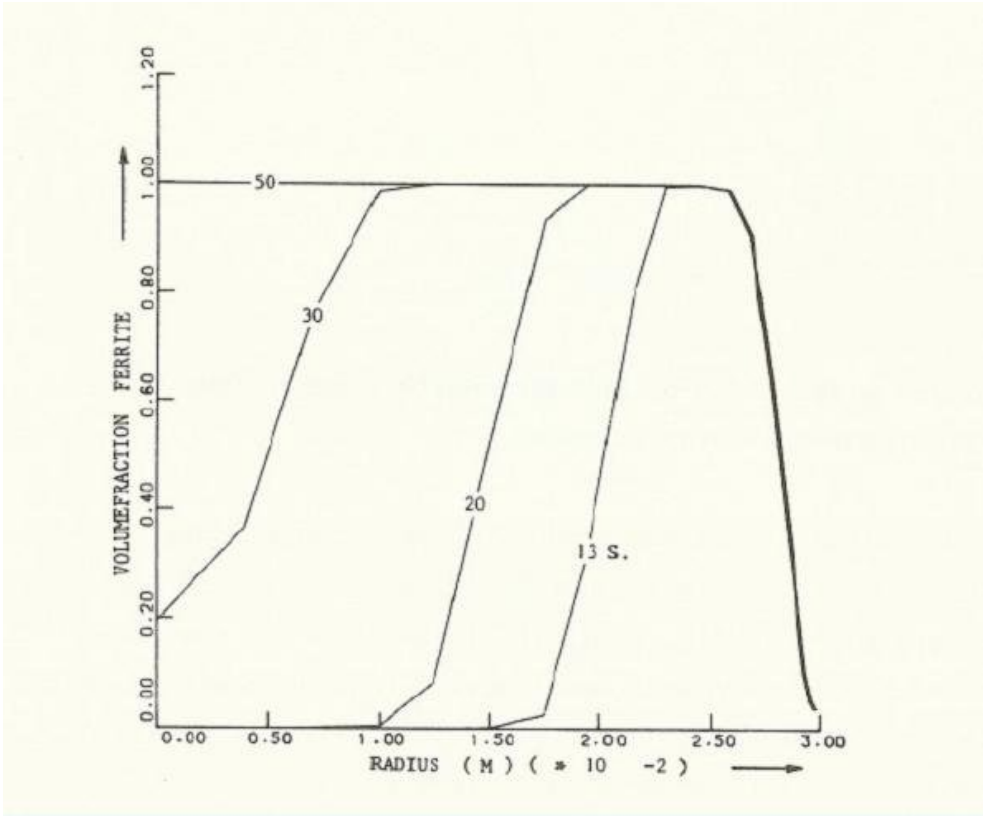

Fig. 5.25 Predicted propagation of the ferrite phase.

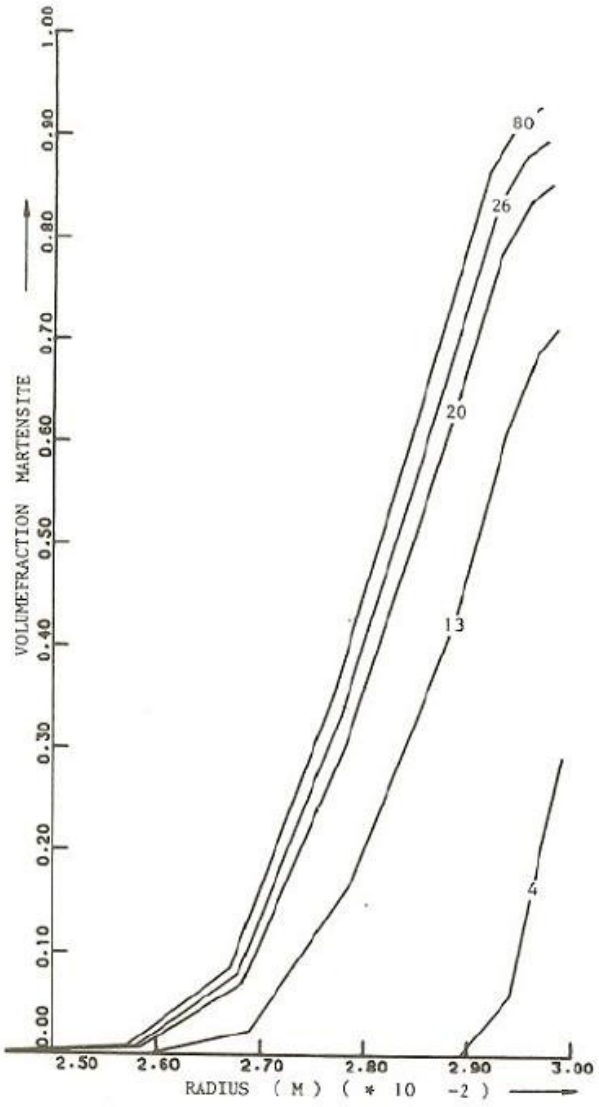

Fig. 5.26 Predicted propagation of the martensite phase (close up of the area near the outer surface).

The final stress distribution was compared with experimental data presented by Inoue [23] and theoretical predictions by Inoue and Sjostrom [45]. The results are given in fig. 5.27. It can be observed that the predictions obtained from the present model show a fair agreement with the experimental data. The agreement is even better than with the models of Inoue and Sjostrom, except for one measured stress point located at the outer surface. However, the calculated axial stress distribution satisfies axial equilibrium, but the measured stress is higher or equal to the calculated

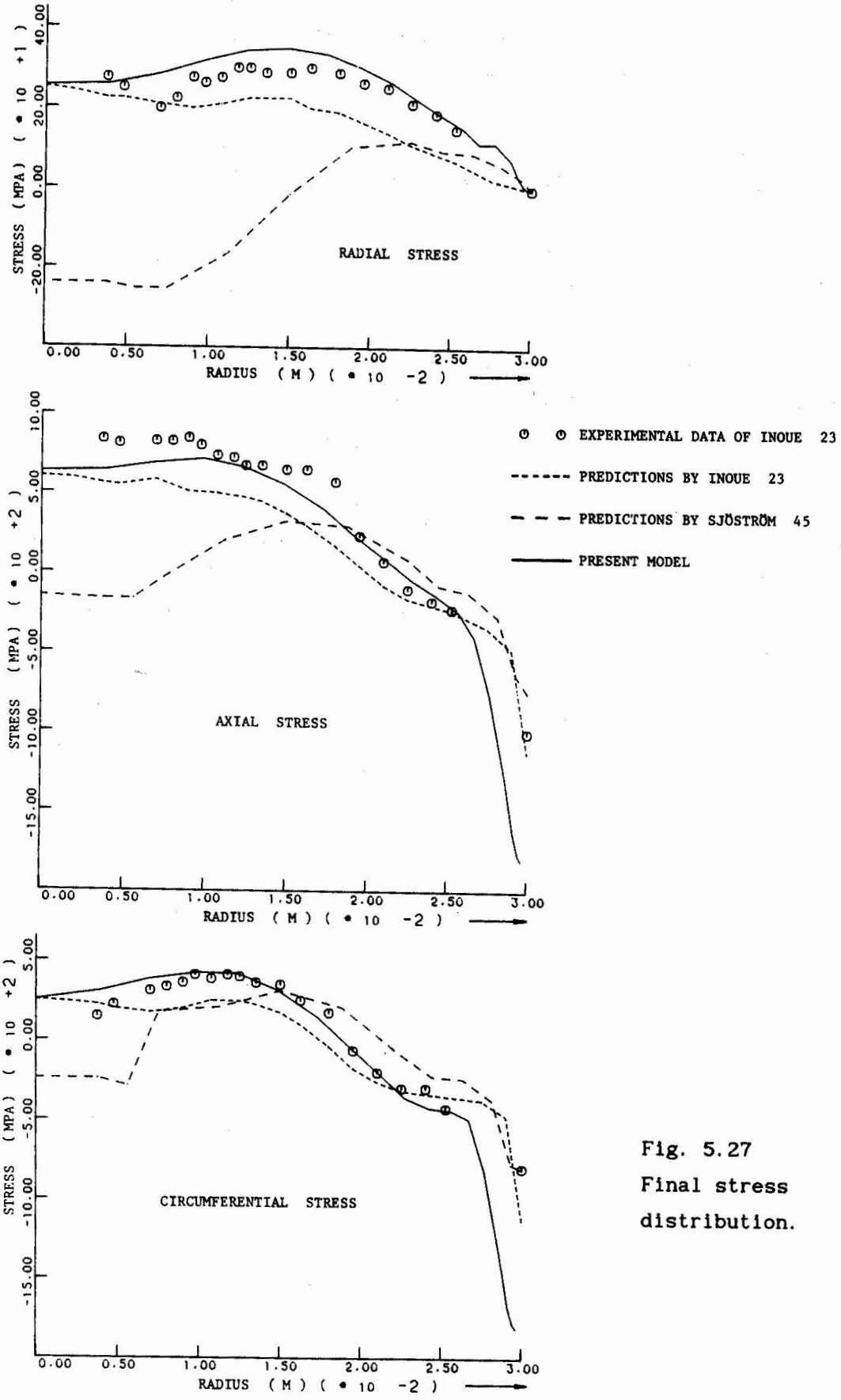

Fig. 5.27
Final stress distribution.

stress and does not satisfy axial equilibrium. So there may be some doubt about the accuracy of the stresses measured by Inoue.

The objective of the presented simulation of a steel quenching process is to show the features of a finite element simulation of phase changes. Not all phenomena that significantly affect the results have been considered, as for instance stress dependency of phase changes and transformation plasticity. Effects of transformation plasticity were taken into account by Nico Verschuren [47].
The resulting stress distributions are only a few percents different from those obtained in a case without transformation plasticity.

The computer programme ”DIEKA” was also applied to a simulation of a cold rolling process [35]. A friction/contact element has been developed in order to predict the deformation of the roll.
The developments as to the simulations of cold rolling are not finished and therefore no results are presented here.

VI. Concluding remarks

The mixed Eulerian-Lagrangian finite element method for simulation of forming process, as presented in this thesis, yields a method to uncouple material displacements from nodal point displacements. Numerical problems due to large element distortions, which may occur in the case of an updated Lagrange approach, can be avoided. Free-surface movements and history-dependent material properties can be taken into account.
The method allows a simultaneous analysis of workpiece and tool including slipping friction more easily. This can be accomplished by keeping nodal points of both parts at the same spatial location, independently from the actual difference of the tangential velocity components at both sides of the contact interface. An appropriate description of the friction requires the development of special friction elements, including convective changes of the frictional condition and energy dissipation. The development of this kind of friction elements is part of the current research programme.

REFERENCES.

1. Argysis, J.H. and Doltsinis, J. St.
On the large strain inelastic analysis in natural formulation.
Comp. Meth. Appl. Mech. Eng. 20, 2 (1979) 213 - 251.

2. Argyris, J.H. and Doltsinis, J. St.
On the natural formulation and analysis of large deformation couple thermomechanical problems.
Comp. Meth. Appl. Mech. Eng. 25, 2 (1981), 195 - 253.

3. Avizur, B.
Handbook of metal-forming processes.
John Wiley and Sons, New York (1983).

4. Besseling, J.F.
A theory of elastic, plastic and creep deformations of an initially isotropic material.
J. Appl. Mech. 25 (1958), 529 - 536.

5. Besseling, J.F.
A thermodynamic approach to rheology.
Proc. IUTAM Symp. on irreversible aspects of continuum mechanics.
Springer-Verlag, Wien (1968) 16 - 53.

6. Besseling, J.F. and Van der Heijden, A.M.A.
Trends in solid mechanics.
Proc. symp. dedicated to the 65th Birthday of W.T. Koiter.
Delft Univ. Press and Sythhoff & Noordhoff publ. (1979), 53 - 78.

7. Besseling, J.F.
Models of metal plasticity; Theory and experiment.
Plasticity Today, edited by A. Sawczuk and G. Bianchi, Elsevier (1985), 97 - 113.

8. Biot, M.A.
Variational Lagrangian - thermodynamics of nonisothermal finite strain mechanics of porous solids and thermomolecular diffusion.
Int. J. Solids Struc. 13 (1977), 579 - 597.

9. Bird, R.B., Armstrong, R.C. and Hassager, O.
Dynamics of polymeric liquids, volume 1 fluid mechanics.
John Wiley and sons (1977).

10. Bathe, K.J. and Wilson, E.L.
Numerical methods in finite element analysis.
Prentice Hall (1976).

11. Bonte, H. de
Omvormprocessen als stromingsprobleem (formingprocesses regarded as a flow problem) (in Dutch).
TH Delft, LTM report 775 (1984).

12. Eringen, A.C.
Mechanics of continua.
John Wiley, New York (1967).

13. Gelten, C.J.M. and Konter, A.W.A.
Application of mesh-rezoning in the updated Lagrange method to metal forming analysis.
Proc. Int. Conf. Numerical methods in Industrial Forming Processes
Pinerige Press, Swansea U.K. (1982), 511 - 521.

14. Gortemaker, P.C.M.
Application of an elastic-plastic finite element program for large deformations, thesis.
TH Twente, Enschede, The Netherlands (1980).

15. Hibitt, H.D., Marcal, P.V. and Rice, J.C.
A finite element formulation for large strain and large displacement.
Int. J. Solids Struc. 6 (1970) 1069 - 1086.

16. Hutchinson, J.W.
Finite strain analysis of elastic plastic solids and structures.
In "Numerical solution of Nonlinear Structural Problems"
R.F. Hartlung (ed), ASME 17 - 29 (1973).

17. Hill, R.
A general theory of uniqueness and stability in elastic plastic solids.
J. Mech. Phys. Sol., 6 (1958) 236 - 249.

18. Heijden, A.M.A. van der and Besseling, J.F.
A large strain plasticity theory and the symmetry properties of its constitutive equations.
TH Delft, LTM report 726 (1982) (to be published in Comp. and Struct).

19. Huisman, H.J. and Huetink, J.
A combined Eulerian-Lagrangian three-dimensional finite element analysis of edge-rolling.
J. Mechanical Working Technology, 11 (1985) 333 - 353.

20. Huetink, J.
Analysis of metal forming processes based on a combined Eulerian-Lagrangian finite element formulation.
Proc. Int. Conf. Num. meth. Industr. Forming Processes, Peneridge Press, Swansea U.K. (1982) 501 - 509.

21. Haber, R.B.
A mixed Eulerian-Lagrangian displacement model for large-deformation analysis in solid mechanics.
Comp. Meth. Appl. Mech. Eng., 43 (1984), 277 - 292.

22. Hinton, E. and Campbell, J.S.
Local and Global smoothing of discontinuous finite element functions using least squares method.
Int. J. Num. Mech. Eng., 8 (1974), 461 - 480.

23. Inoue, T. et. a.
Description of transformation kinetics heat conduction and elastic-plastic stress in the course of quenching and tempering of some steels.
Ingenieur Archiv 50 (1981), 315 - 327.

24. Irons, B.M.
Quadrature rules for brick based elements.
Int. J. Num. Meth. Eng., 3 (1971), 293 - 294.

25. Janssen, G.T.M. and Huetink, J.
Experimental verification of constitutive equations for plasticity under biaxial, cyclic and non-radial loading conditions.
6th SMIRT Conf. Paper L 4/2, Paris, 1981.

26. Jong, E. de
Numerical Analysis of Metalforming processes, thesis.
TH Eindhoven, The Netherlands (1983).

27. Kobayashi, S.
Thermo viscoplastic analysis of metal forming problems by the finite element method.
Proc. Int. Conf. Num. Meth. Industry Forming Processes.
Peneridge Press, Swansea U.K. (1982), 17 - 25.

28. Lee, E.H.
Elastic-plastic deformation at finite strains.
J. Appl. Mech. 36 (1969), 1 - 6.

29. Lee, E.H.
Concerning elastic and plastic components of deformation.
Int. J. Solids Structures, 16 (1980), 715 - 721.

30. Lee, E.H.
Some comments on elastic-plastic analysis.
Int. J. Solids Structures, 17 (1981), 859 - 872.

31. Lee, E.H.
Finite deformation effects in plasticity analysis.
Proc. Int. Conf. Num. meth. Industr. Forming Processes.
Peneridge Press, Swansea U.K. (1982), 39 - 50.

32. Lugt, J. van der and Huetink, J.
Thermal mechanically coupled finite element analysis in metal forming processes.
Comp. Meth. Appl. Mech. Eng., 54 (1986), 145 - 160.

33. Leigh, D.C.
Non-linear continuum mechanics, Mc. Graw-Hill, New York (1968).

34. Mc. Meeking, R.M. and Rice, J.C.
Finite element formulation for problems of large elastic-plastic deformation.
Int. J. Solids Structures, 11 (1975), 611 - 616.

35. Miedema, J.R.
Ontwikkeling en toepassing van een contactelement voor de analyse van plastische vormgevingsprocessen (Development and application of a contact-element for analysis of forming processes) (in Dutch).
TH Twente, The Netherlands, report WT-74 (1985).

36. Mellor, P.B. and Johnson, W.
Engineering Plasticity.
Van Nostrand Reinolds, London (1973).

37. Nagtegaal, J.C., Parks, D.M. and Rice, J.C.
On Numerical accurate finite element solutions in the fully plastic range.
Comp. Meth. Appl. Mech. Eng., 4 (1974), 153 - 177.

38. Nagtegaal, J.C. and Jong, J.E. de
Some computational aspects of elastic plastic large strain analysis.
Int. J. Num. Meth. Eng. 17 (1981) 15 - 41.

39. Nagtegaal, J.C. and Jong, J.E. de
Some aspects of non-isotropic workhardening in finite strain plasticity.
Proc. Workshop Plasticity of metals at finite strain, Stanford (1982), 65 - 102.

40. Prager, W.
Introduction to Mechanics of Continua.
Ginn (1961).

41. Prager, W.
A new Method of Analyzing Stresses and Strains in workhardening solids.
J. Appl. Mech. 23 (1956), 493 - 496.

42. Parkus, H.
Thermo-elasticity.
Second revised and enlarged edition, Springer Verlag, Wien-New York.

43. Rowe, G.W.
Principles of industrial metalworking Processes.
Edward Arnold Ltd., 1977.

44. Schreurs, P.J.G.
Numerical Simulation of Forming Processes, thesis.
TH Eindhoven, The Netherlands (1983).

45. Sjöström. S.
The calculation of quench stresses in steel.
Linkoping Studies in Science and Technology, dissertation 84 (1982).

46. Vermeer, P.A.
Formulation and analysis of sand deformation problems, thesis.
TH Delft (1980).

47. Verschuren, N.W.M.
Spanningsanalyse in thermisch geharde materialen (Stress analysis in quenched materials) (in Dutch).
Report TH Twente, The Netherlands, Dept. Mech. Eng. (1985).

48. Wilkinson, J.H. and Reinch, C.
Solution of Real and Complex Systems of Linear equation.
Handbook for Automatic Computation Vol. II, Linear algebra (1971), 93 - 110.

49. Wertheimer, T.B.
Thermal mechanically coupled analysis in metal forming processes.
Proc. Int. Conf. Num. Meth. Industrial Forming Processes.
Pinerige Press Swansea U.K. (1982), 425 - 434.

50. Ziegler, H.
A modification of Prager's hardening rule.
Quaterly Appl. Math. Provedence, 17 (1959), 55 - 65.

51. Zienkiewicz, F.R.S.
The finite element Method, third edition.
Mc. Graw-Hill, 1977.

52. Zerna, W. and Green, A.E.
Theoretical Elasticity.
Oxford, Claredon Press (1968).

53. Rice, J.R. and Tracy D.M.
'Computational fracture mechanics' in
Proc. Symp. Num. and Comp. meth. struc. Mech., Urbana Illinois, 1971
(Ed. S.J. Fenves), Academic Press, New York (1973), 585 - 623.

Appendix A

Summary of tensor notation.

In this appendix a summary of the applied tensor notation and properties of tensors are given. These properties are frame independent. Components of tensors can be referred to an arbitrary curvilinear coordinate system.
However, no curvilinear coordinates are used in this paper and hence in this appendix only components of tensors referred to a Cartesian frame are given.
The summation convention is adopted with respect to subscript indices. Most rules are given without proof. More detailed information can be found in [9, 12, 40, 52].

A vector will be denoted by a subscript wiggle and can be expressed in components referred to a Cartesian reference frame by

$$\underset{\sim}{a} = a_i \, \underset{\sim}{e}_i \qquad \text{(A 1)}$$

where $\underset{\sim}{e}_i$ are mutually orthogonal unit base vectors.
The scalar product of two vectors $\underset{\sim}{a}$ and $\underset{\sim}{b}$ is denoted by a dot and can be expressed in the components by

$$\underset{\sim}{a} \cdot \underset{\sim}{b} = a_i \, b_i \qquad \text{(A 2)}$$

The result is a scalar and

$$\underset{\sim}{a} \cdot \underset{\sim}{b} = \underset{\sim}{b} \cdot \underset{\sim}{a} \qquad \text{(A 3)}$$

The magnitude of a vector $\underset{\sim}{a}$ is denoted as

$$\| \underset{\sim}{a} \| = (\underset{\sim}{a} \cdot \underset{\sim}{a})^{1/2} \qquad \text{(A 4)}$$

The scalar product is related to the magnitude of the vectors $\underset{\sim}{a}$ and $\underset{\sim}{b}$ and the angle ϕ between the vectors, according to

$$(\underset{\sim}{a} \cdot \underset{\sim}{b}) = \| \underset{\sim}{a} \| \; \| \underset{\sim}{b} \| \; \cos \phi \qquad \text{(A 5)}$$

The vector product (cross product) of two vectors is a vector defined by

$$\underset{\sim}{a} \times \underset{\sim}{b} = \| \underset{\sim}{a} \| \; \| \underset{\sim}{b} \| \; \sin \phi \; \underset{\sim}{n} \qquad \text{(A 6)}$$

where $\underset{\sim}{n}$ is a vector of unit length normal to $\underset{\sim}{a}$ and $\underset{\sim}{b}$ and pointing in the direction that a right hand screw will move if turned from $\underset{\sim}{a}$ to $\underset{\sim}{b}$ through the angle ϕ•

The dyadic product of two vectors is denoted by $\underset{\sim}{a}\ \underset{\sim}{b}$ • The following multiplication operations are defined

$$(\underset{\sim}{a}\ \underset{\sim}{b}) \cdot \underset{\sim}{c} = \underset{\sim}{a}\ (\underset{\sim}{b} \cdot \underset{\sim}{c}) = \underset{\sim}{a}\ \underset{\sim}{b} \cdot \underset{\sim}{c} \qquad \text{(A 7)}$$

$$\underset{\sim}{a} \cdot (\underset{\sim}{b}\ \underset{\sim}{c}) = (\underset{\sim}{a} \cdot \underset{\sim}{b})\ \underset{\sim}{c} = \underset{\sim}{a} \cdot \underset{\sim}{b}\ \underset{\sim}{c} \qquad \text{(A 8)}$$

$$(\underset{\sim}{a}\ \underset{\sim}{b}) \cdot (\underset{\sim}{c}\ \underset{\sim}{d}) = \underset{\sim}{a}(\underset{\sim}{b} \cdot \underset{\sim}{c})\ \underset{\sim}{d} = \underset{\sim}{a}\ \underset{\sim}{b} \cdot \underset{\sim}{c}\ \underset{\sim}{d} \qquad \text{(A 9)}$$

$$(\underset{\sim}{a}\ \underset{\sim}{b}) : (\underset{\sim}{c}\ \underset{\sim}{d}) = (\underset{\sim}{a} \cdot \underset{\sim}{c})\ (\underset{\sim}{b} \cdot \underset{\sim}{d}) = \underset{\sim}{a} \cdot \underset{\sim}{c}\ \ \underset{\sim}{b} \cdot \underset{\sim}{d} \qquad \text{(A 10)}$$

The trace of a dyadic product is the scalar product, denoted as

$$\text{tr}\ (\underset{\sim}{a}\ \underset{\sim}{b}) = \underset{\sim}{a} \cdot \underset{\sim}{b} \qquad \text{(A 11)}$$

A tensor is a linear operator that transfers a vector to another vector. This operation is written as

$$\underset{\sim}{c} = \underline{A} \cdot \underset{\sim}{b} \qquad \text{(A 12)}$$

A tensor is denoted by an underscore. It is a linear operator hence

$$\underline{A} \cdot (\alpha\underset{\sim}{a} + \beta\underset{\sim}{b}) = \alpha\underline{A} \cdot \underset{\sim}{a} + \beta\underline{A} \cdot \underset{\sim}{b} \qquad \text{(A 13)}$$

Similar to vectors, we can define components of a tensor. From (A 12) follows that

$$\underset{\sim}{e}_i \cdot \underset{\sim}{c} = c_i = \underset{\sim}{e}_i \cdot \underline{A} \cdot \underset{\sim}{e}_j\ b_j \qquad \text{(A 14)}$$

The components of $\underline{A}$ are defined by

$$A_{ij} = \underset{\sim}{e}_i \cdot \underline{A} \cdot \underset{\sim}{e}_j \qquad \text{(A 15)}$$

and an operation according to (A 12) can be replaced by a transfer of the components

$$c_i = A_{ij}\ b_j \qquad \text{(A 16)}$$

A tensor can be expressed as a linear combination of dyadic products of the base vectors

$$\underline{\underline{A}} = A_{ij}\, \underset{\sim}{e}_i\, \underset{\sim}{e}_j \qquad \text{(A 17)}$$

Consequently the trace of a tensor can be defined as a linear operator which, according to (A 11), is given by

$$\text{tr}\, \underline{\underline{A}} = A_{ij}\, \underset{\sim}{e}_i \bullet \underset{\sim}{e}_j = A_{ii} \qquad \text{(A 18)}$$

where

$$\underset{\sim}{e}_i \bullet \underset{\sim}{e}_j = \delta_{ij} = \begin{cases} 1 & \text{if } i = j \\ 0 & \text{if } i \neq j \end{cases} \qquad \text{(A 19)}$$

The symbol δ_{ij} is known as the kronecker delta.

As a tensor is a linear combination of dyadic products it is called a second order tensor. A vector is also denoted as a first order tensor. Tensors of higher order can be defined similarly.
A third order tensor is denoted by a subscript wiggle and an underscore

$$\underset{\approx}{\underline{B}} = B_{ijk}\, \underset{\sim}{e}_i\, \underset{\sim}{e}_j\, \underset{\sim}{e}_k$$

A third order tensor is a linear operator that transfers a vector to a second order tensor by

$$\underline{\underline{A}} = \underset{\approx}{\underline{B}} \bullet \underset{\sim}{a} \qquad \text{(A 20)}$$

or transfers a second order tensor to a vector by

$$\underset{\sim}{c} = \underset{\approx}{\underline{B}} : \underline{\underline{A}} \qquad \text{(A 21)}$$

A fourth order tensor is denoted by a double underscore. The following operations can be performed:

$$\underline{\underline{A}} = \underline{\underline{\underline{D}}} : \underline{\underline{C}} \qquad \text{(A 22)}$$

$$\underset{\approx}{\underline{B}} = \underline{\underline{\underline{D}}} \bullet \underset{\sim}{a} \qquad \text{(A 23)}$$

$$\underline{\underline{\underline{E}}} = \underline{\underline{\underline{D}}} \bullet \underline{\underline{C}} \qquad \text{(A 24)}$$

etc.

Of course a dyadic product of two vectors is a second order tensor and a triadic product of three vectors is a third order tensor, etc. The multiplication operations (A 7) through (A 10) also apply to tensors of higher order.

The transpose of a second order tensor is denoted by a superscript capital T and satisfies the following rules

$$\underline{A}^T \cdot \underset{\sim}{a} = \underset{\sim}{a} \cdot \underline{A} \tag{A 25}$$

$$\underline{A}^T = A_{ji}\, \underset{\sim}{e}_i\, \underset{\sim}{e}_j \tag{A 26}$$

The second order identity tensor is denoted by the symbol $\underline{I}$ and satisfies the condition that for any vector $\underset{\sim}{a}$

$$\underset{\sim}{a} = \underline{I} \cdot \underset{\sim}{a}$$

The components of $\underline{I}$ are given by the kronecker delta

$$\underline{I} = \delta_{ij}\, \underset{\sim}{e}_i\, \underset{\sim}{e}_j = \underset{\sim}{e}_i\, \underset{\sim}{e}_i \tag{A 27}$$

and

$$\text{tr } \underline{I} = 3 \tag{A 28}$$

The trace of a product of two second order tensors satisfies relation

$$\text{tr } (\underline{A} \cdot \underline{B}) = \underline{A} : \underline{B}^T \tag{A 29}$$

The determinant of a second order tensor is defined by

$$\begin{aligned} \det \underline{A} &= \frac{1}{6} (\text{tr } (\underline{A}))^3 - \tfrac{1}{2} \text{tr } (\underline{A}) \text{ tr } (\underline{A}\cdot\underline{A}) + \frac{1}{3} \text{tr } (\underline{A}\cdot\underline{A}\cdot\underline{A}) \\ &= \det [A_{ij}] = \sum_{i=1}^{3} A_{i1} \text{ cofactor } A_{i1} \\ &= \sum_{i=1}^{3} A_{i2} \text{ cofactor } [A_{i2}] = \sum_{i=1}^{3} A_{i3} \text{ cofactor } [A_{i3}] \end{aligned} \tag{A 30}$$

The fourth order identity tensor is denoted by the symbol $\underline{\underline{H}}$ and is defined by the condition that for any second order tensor $\underline{A}$

$$\underline{A} = \underline{\underline{H}} : \underline{A} \qquad \text{(A 31)}$$

This fourth order identity tensor can be expressed as

$$\underline{\underline{H}} = H_{ijk\ell}\, \underset{\sim}{e}_i\, \underset{\sim}{e}_j\, \underset{\sim}{e}_k\, \underset{\sim}{e}_\ell \qquad \text{(A 32)}$$

where $H_{ijk\ell} = \delta_{ik}\, \delta_{j\ell}$

The product of $\underline{\underline{H}}$ and $\underline{I}$ satisfies the condition

$$\underline{\underline{H}} \bullet \underline{I} = \underline{\underline{H}} \qquad \text{(A 33)}$$

Multiplication rules of tensor are not commutative. The following rule can be applied for permutation of products of tensors

$$\underline{A} \bullet \underline{B} \bullet \underline{C} = (\underline{A} \bullet \underline{\underline{H}} \bullet \underline{C}^T) : \underline{B} \qquad \text{(A 34)}$$

This rule cannot be found in the references [9, 12, 42, 50] and hence the proof is given below

$(\underline{A} \bullet \underline{\underline{H}} \bullet \underline{C}^T) : \underline{B} =$

$(A_{ij}\, \underset{\sim}{e}_i\, \underset{\sim}{e}_j \bullet \delta_{km}\, \delta_{\ell n}\, \underset{\sim}{e}_k\, \underset{\sim}{e}_\ell\, \underset{\sim}{e}_m\, \underset{\sim}{e}_n \bullet C_{qp}\, \underset{\sim}{e}_p\, \underset{\sim}{e}_q) : B_{rs}\, \underset{\sim}{e}_r\, \underset{\sim}{e}_s =$

$A_{ij}\, \underset{\sim}{e}_i\, (\underset{\sim}{e}_k\, \underset{\sim}{e}_m)\, \delta_{jk}\, \underset{\sim}{e}_n\, (\underset{\sim}{e}_n \bullet \underset{\sim}{e}_p)\, (\underset{\sim}{e}_m \bullet \underset{\sim}{e}_r)\, (\underset{\sim}{e}_q \bullet \underset{\sim}{e}_s)\, C_{qp}\, B_{rs}$

$A_{ik}\, \underset{\sim}{e}_i\, \underset{\sim}{e}_k \bullet B_{ms}\, \underset{\sim}{e}_m\, \underset{\sim}{e}_s \bullet C_{qn}\, \underset{\sim}{e}_q\, \underset{\sim}{e}_n =$

$\underline{A} \bullet \underline{B} \bullet \underline{C}$ q•e•d•

Note that the right hand side of A 34 is <u>not</u> associative.

Similarily the following rule can be proven:

$$\underline{A} \bullet \underline{B} \bullet \underline{C} = \underline{B} : (\underline{A}^T \bullet \underline{\underline{H}} \bullet \underline{C}) \qquad \text{(A 35)}$$

Tensors may be functions of other tensors (scalars, vectors, higher order tensors), and we can define (partial) derivatives. Say that f is a scalar function of a vector $\underset{\sim}{x}$, than de derivative with respect to $\underset{\sim}{x}$ is defined by

$$\overset{>}{\nabla}_{\underset{\sim}{x}} f = \frac{\partial}{\partial \underset{\sim}{x}} (f) = \underset{\sim}{e}_i\, \frac{\partial f}{\partial x_i} \qquad \text{(A 36)}$$

The gradient operator $\overset{\rightarrow}{\nabla}$ is a vector operator that associates a vector with a scalar function.

We can also subject a tensor to the gradient operator

$$\overset{\rightarrow}{\nabla} \underline{A} = \frac{\partial}{\partial \underset{\sim}{x}} (\underline{A}) = \underset{\sim}{e}_i \frac{\partial \underline{A}}{\partial x_i} = \underset{\sim}{e}_i \frac{\partial A_{jk}}{\partial x_i} \underset{\sim}{e}_j \underset{\sim}{e}_k \qquad \text{(A 37)}$$

The result is a tensor of one order higher. All multiplication rules that are defined for vectors (and dyadic products) hold for the gradient operator. Dyadic products are not commutative hence

$$\overset{\rightarrow}{\nabla} \underline{A} \neq \underline{A} \overset{\leftarrow}{\nabla} \qquad \text{(A 38)}$$

The arrow points to the tensor that is subjected to the operation.

The left hand side is called the pre-gradient and the right hand side the post-gradient. The post-gradient is defined by

$$\underline{A} \overset{\leftarrow}{\nabla} = \frac{\partial \underline{A}}{\partial \underset{\sim}{x}} = \frac{\partial \underline{A}}{\partial x_i} \underset{\sim}{e}_i = \frac{\partial A_{jk}}{\partial x_i} \underset{\sim}{e}_j \underset{\sim}{e}_k \underset{\sim}{e}_i \qquad \text{(A 39)}$$

We can also differentiate with respect to higher order tensors

$$\overset{\rightarrow}{\nabla}_{\underline{A}} f = \frac{\partial}{\partial \underline{A}} (f) = \underset{\sim}{e}_i \underset{\sim}{e}_j \frac{\partial f}{\partial A_{ij}} \qquad \text{(A 40)}$$

$$\overset{\rightarrow}{\nabla}_{\underline{A}} \underline{B} = \frac{\partial}{\partial \underline{A}} (\underline{B}) = \underset{\sim}{e}_i \underset{\sim}{e}_j \frac{\partial B_{k\ell}}{\partial A_{ij}} \underset{\sim}{e}_k \underset{\sim}{e}_\ell \qquad \text{(A 41)}$$

$$\underline{B} \overset{\leftarrow}{\nabla}_{\underline{A}} = \frac{\partial \underline{B}}{\partial \underline{A}} = \frac{\partial B_{k\ell}}{\partial A_{ij}} \underset{\sim}{e}_k \underset{\sim}{e}_\ell \underset{\sim}{e}_i \underset{\sim}{e}_j \qquad \text{(A 42)}$$

From (A 42) it follows that

$$\frac{\partial \underline{A}}{\partial \underline{A}} = \delta_{ki} \delta_{\ell j} \underset{\sim}{e}_k \underset{\sim}{e}_\ell \underset{\sim}{e}_i \underset{\sim}{e}_j = \underline{\underline{H}} \qquad \text{(A 43)}$$

We define

$$\underline{\underline{K}} = \frac{\partial \underline{A}^T}{\partial \underline{A}} = \delta_{\ell i} \delta_{kj} \underset{\sim}{e}_k \underset{\sim}{e}_\ell \underset{\sim}{e}_i \underset{\sim}{e}_j \qquad \text{(A 44)}$$

$\underline{\underline{K}}$ is a special tensor with the property that for every second order tensor $\underline{C}$

$$\underline{\underline{K}} : \underline{C} = \underline{C} : \underline{\underline{K}} = \underline{C}^T \qquad \text{(A 45)}$$

When $\underline{A}$ is a function of B and B is a function of $\underline{C}$ then

$$\frac{\partial \underline{A}}{\partial \underline{C}} = \frac{\partial \underline{A}}{\partial \underline{B}} : \frac{\partial \underline{B}}{\partial \underline{C}} \qquad \text{(A 46)}$$

The gradient of a scalar product of two vectors satisfies a product rule similar to scalar derivatives

$$(\underset{\sim}{a} \bullet \underset{\sim}{b}) \overset{\leftarrow}{\nabla}_{\sim} = \frac{\partial (\underset{\sim}{a} \bullet \underset{\sim}{b})}{\partial \underset{\sim}{x}} = \overset{\rightarrow}{\nabla}_{\sim} \underset{\sim}{a} \bullet \underset{\sim}{b} + \underset{\sim}{a} \bullet \underset{\sim}{b} \overset{\leftarrow}{\nabla}_{\sim} \qquad \text{(A 47)}$$

This rule cannot be extended to higher order tensors

$$\frac{\partial (\underline{A} \bullet \underline{B})}{\partial \underline{C}} \neq \frac{\partial \underline{A}}{\partial \underline{C}} \bullet \underline{B} + \underline{A} \bullet \frac{\partial \underline{B}}{\partial \underline{C}} \qquad \text{(A 48)}$$

The correct rule can be derived from (A 42)

$$\frac{\partial (\underline{A} \bullet \underline{B})}{\partial \underline{C}} = \frac{\partial (\underline{A} \bullet \underline{B})}{\partial C_{ij}} \underset{\sim}{e}_i \underset{\sim}{e}_j$$

or (A 49)

$$\frac{\partial (\underline{A} \bullet \underline{B})}{\partial \underline{C}} = \frac{\partial \underline{A}}{\partial C_{ij}} \bullet \underline{B} \; \underset{\sim}{e}_i \; \underset{\sim}{e}_j + \underline{A} \bullet \frac{\partial \underline{B}}{\partial C_{ij}} \underset{\sim}{e}_i \; \underset{\sim}{e}_j$$

The last term in (A 49) is equal to the last term in (A 48), but the first term of the right hand side of (A 49) is not equal to the corresponding term in (A 48). With (A 34) we can write

$$\frac{\partial \underline{A}}{\partial C_{ij}} \bullet \underline{B} = \underline{I} \bullet \frac{\partial \underline{A}}{\partial C_{ij}} \bullet \underline{B} = (\underline{I} \bullet \underline{\underline{H}} \bullet \underline{B}^T) : \frac{\partial \underline{A}}{\partial C_{ij}} \qquad \text{(A 50)}$$

Substitution in (A 49) yields

$$\frac{\partial (\underline{A} \bullet \underline{B})}{\partial \underline{C}} = (\underline{H} \bullet \underline{B}^T) : \frac{\partial \underline{A}}{\partial \underline{C}} + \underline{A} \bullet \frac{\partial \underline{B}}{\partial \underline{C}} \qquad \text{(A 51)}$$

The scalar product of two second order tensors satisfies the relation

$$\frac{\partial\,(\underline{A} : \underline{B})}{\partial \underline{C}} = \underline{B} : \frac{\partial \underline{A}}{\partial \underline{C}} + \underline{A} : \frac{\partial \underline{B}}{\partial \underline{C}} \qquad \text{(A 52)}$$

The derivative of the determinant of a second order tensor satisfies the relation

$$\frac{\partial \det \underline{A}}{\partial \underline{A}} = (\det \underline{A})\,(\underline{A}^{-1})^{T} \qquad \text{(A 53)}$$

This relation follows from (A 30)

$$\frac{\partial \det \underline{A}}{\partial \underline{A}} = \text{cofactor}\,[A_{ij}]\;\underset{\sim}{e}_i\;\underset{\sim}{e}_j$$

$$= \det[\underline{A}]\;A^{-1}_{ji}\;\underset{\sim}{e}_i\;\underset{\sim}{e}_j$$

$$= \det \underline{A}\;\;(\underline{A}^{-1})^{T}$$

Note that

$$A^{-1}_{ij} = \frac{1}{\det[\underline{A}]}\;\text{cofactor}\,[A_{ji}] \qquad \text{(A 54)}$$

We will write

$$(\underline{A}^{-1})^{T} = \underline{A}^{-T} \qquad \text{(A 55)}$$

The derivative of the inverse of a second order tensor can be written as

$$\frac{\partial \underline{A}^{-1}}{\partial \underline{A}} = -\underline{A}^{-1} \bullet \underline{\underline{H}} \bullet \underline{A}^{-T} \qquad \text{(A 56)}$$

This relation follows from (A 51) with $\underline{B} = \underline{A}^{-1}$

$$\frac{\partial\,(\underline{A} \bullet \underline{A}^{-1})}{\partial \underline{A}} = \frac{\partial \underline{I}}{\partial \underline{A}} = \underline{\underline{0}} = (\underline{\underline{H}} \bullet \underline{A}^{-T}) : \underline{\underline{H}} + \underline{A} \bullet \frac{\partial \underline{A}^{-1}}{\partial \underline{A}}$$

and hence by multiplication with $\underline{A}^{-1}\bullet$

$$\underline{I} \bullet \frac{\partial \underline{A}^{-1}}{\partial \underline{A}} = -\underline{A}^{-1} \bullet \underline{\underline{H}} \bullet \underline{A}^{-T}$$

Appendix B.

Internal energy and free energy.

The internal energy is a function of $\underline{C}$ and the entropy s

$$e = e\ (\underline{C},\ s) \tag{B 1}$$

The free energy F is assumed to be a function of $\underline{C}$ and T and is related to e by

$$F = F\ (\underline{C},\ T) = e - Ts \tag{B 2}$$

Hence with $\underline{C}$ and T as independent state variables

$$\left(\frac{\partial F}{\partial \underline{C}}\right)_T = \left(\frac{\partial e}{\partial \underline{C}}\right)_s + \left(\frac{\partial e}{\partial s}\right)_{\underline{C}} \left(\frac{\partial s}{\partial \underline{C}}\right)_T - T\left(\frac{\partial s}{\partial \underline{C}}\right)_T \tag{B 3}$$

where according (3.3.18)

$$T = \frac{\partial e}{\partial s}$$

Hence

$$\left(\frac{\partial F}{\partial \underline{C}}\right)_T = \left(\frac{\partial e}{\partial \underline{C}}\right)_s \tag{B 4}$$

With (B 2) we can write

$$\left(\frac{\partial F}{\partial T}\right)_{\underline{C}} = \left(\frac{\partial e}{\partial s}\right)_{\underline{C}} \left(\frac{\partial s}{\partial T}\right)_{\underline{C}} - s - T\left(\frac{\partial s}{\partial T}\right)_{\underline{C}} \tag{B 5}$$

or

$$\left(\frac{\partial F}{\partial T}\right)_{\underline{C}} = T\left(\frac{\partial s}{\partial T}\right)_{\underline{C}} - s - T\left(\frac{\partial s}{\partial T}\right)_{\underline{C}} = -s \tag{B 6}$$

Appendix C.

Elaborations referred to isotropic material.

With (A 34) and (A 35) we find that

$$(\underline{B}^T \bullet \underline{\underline{H}} \bullet \underline{B}^T) : \underline{C}^{-1} \ \underline{C}^{-1} : (\underline{B} \bullet \underline{\underline{H}} \bullet \underline{B}) =$$

$$\underline{B}^T \bullet \underline{C}^{-1} \bullet \underline{B} \ \ \underline{B}^T \bullet \underline{C}^{-1} \bullet \underline{B} =$$

$$\underline{B}^T \bullet \underline{B}^{-T} \bullet \underline{B}^{-1} \bullet \underline{B} \ \ \underline{B}^T \bullet \underline{B}^{-T} \bullet \underline{B}^{-1} \bullet \underline{B} = \underline{I} \ \underline{I}$$

and

$$(\underline{B}^T \bullet \underline{\underline{H}} \bullet \underline{B}^T) : (\underline{C}^{-1} \bullet \underline{\underline{H}} \bullet \underline{C}^{-1}) : (\underline{B} \bullet \underline{\underline{H}} \bullet \underline{B}) =$$

$$(\underline{B}^T \bullet \underline{\underline{H}} \bullet \underline{B}^T) : (\underline{C}^{-1} \bullet \underset{\sim}{e}_i \ \underset{\sim}{e}_j \ \underset{\sim}{e}_i \ \underset{\sim}{e}_j \bullet \underline{C}^{-1}) : (\underline{B} \bullet \underline{\underline{H}} \bullet \underline{B}) =$$

$$\underline{B}^T \bullet \underline{C}^{-1} \bullet \underset{\sim}{e}_i \ \underset{\sim}{e}_j \bullet \underline{B} \ \ \underline{B}^T \bullet \underset{\sim}{e}_i \ \underset{\sim}{e}_j \bullet \underline{C}^{-1} \bullet \underline{B} =$$

$$\underline{B}^{-1} \bullet \underset{\sim}{e}_i \ \underset{\sim}{e}_j \bullet \underline{B} \ \ \underline{B}^T \bullet \underset{\sim}{e}_i \ \underset{\sim}{e}_j \bullet \underline{B}^{-T} =$$

$$B^{-1}_{kl} \ \underset{\sim}{e}_k \ \underset{\sim}{e}_l \bullet \underset{\sim}{e}_i \ \underset{\sim}{e}_j \bullet B_{mn} \ \underset{\sim}{e}_m \ \underset{\sim}{e}_n \ \ B_{sr} \ \underset{\sim}{e}_r \ \underset{\sim}{e}_s \bullet \underset{\sim}{e}_i \ \underset{\sim}{e}_j \ \ B^{-1}_{tu} \bullet \underset{\sim}{e}_u \ \underset{\sim}{e}_t =$$

$$B^{-1}_{ki} \ \underset{\sim}{e}_k \ \underset{\sim}{e}_n \ \ B_{jn} \ \ \ B_{ir} \ \underset{\sim}{e}_r \ \underset{\sim}{e}_t \ \ B^{-1}_{tj} =$$

$$B^{-1}_{ki} \ B_{ir} \ \ \underset{\sim}{e}_k \ \underset{\sim}{e}_n \ \underset{\sim}{e}_r \ \underset{\sim}{e}_t \ \ B_{jn} \ B^{-1}_{tj} =$$

$$\delta_{kr} \ \underset{\sim}{e}_k \ \underset{\sim}{e}_n \ \underset{\sim}{e}_r \ \underset{\sim}{e}_t \ \ \delta_{tn} = \ \underset{\sim}{e}_k \ \underset{\sim}{e}_n \ \underset{\sim}{e}_k \ \underset{\sim}{e}_n = \underline{\underline{H}}$$

Dankwoord

Het in dit proefschrift gepresenteerde onderzoek is tot stand gekomen dankzij de bijdragen, inspanning en steun van velen; verschillende studenten (die inmiddels zijn afgestudeerd) hebben belangrijke delen van het eindige-elementen-programma ontwikkeld. Bij de gepresenteerde simulaties heb ik met name gebruik gemaakt van de programmadelen die zijn ontwikkeld door Jaap van der Lugt (thermo-mechanische koppeling) en door Nico Verschuren (fasetransformaties).

Aan de uitvoering van simulaties en de presentatie van de resultaten heeft Joop Brinkman een waardevolle bijdrage geleverd. Bij de grafische verwerking van de resultaten is dankbaar gebruik gemaakt van de door Ruud Spiering ontwikkelde programmatuur.

De experimenten zijn op accurate wijze uitgevoerd door Henk van der Veen.

De aanzet tot het schrijven van dit proefschrift is gegeven door prof. Rijken. Zijn enthousiasme en fysisch inzicht hebben inspirerend gewerkt.

Van de theorieën van prof. Besseling is dankbaar gebruik gemaakt, zijn inzichten liggen ten grondslag aan een belangrijk deel van dit proefschrift.

De samenwerking met het Researchlaboratorium van Hoogovens is als zeer stimulerend ervaren, vooral doordat de ontwikkelde simulatiemethode toepasbaar blijkt te zijn bij o.a. het onderzoek aan walsprocessen.

Het afdelingsbureau van WB heeft een zeer gewaardeerde bijdrage geleverd aan de afwerking en de uitgave van het proefschrift. Harry Slaghuis heeft het een en ander 'soepel geregeld'. Het typewerk is verzorgd door Wil Keuter en Carola Bouwens, de vele ingewikkelde formules hebben zij op zeer kundige wijze verwerkt.

Joop Jasperse heeft enige figuren getekend.

Het manuscript is door mevr. Jalloh gekorrigeerd op spellingsfouten en andere inbreuken op de Engelse taal.

Allen die op enigerlei wijze hebben bijgedragen aan de realisatie van dit proefschrift wil ik hierbij hartelijk danken. In het bijzonder wil ik mijn echtgenote Marijke bedanken voor haar ondersteuning en begrip tijdens de vele avond- en nachturen die ik aan het schrijfwerk heb besteed.

STELLINGEN

behorende bij het proefschrift

ON THE SIMULATION OF THERMO-MECHANICAL FORMING PROCESSES

1. Bij vervanging van een materiële afgeleide van een objectieve tensor door de Jaumann afgeleide in een continuumtheorie gebaseerd op infinitesimale verplaatsingen, wordt hooguit een uitbreiding naar grote rotaties verkregen terwijl aan de vervormingen nog steeds de eis moet worden gesteld dat deze infinitesimaal zijn.

2. Kinematische versteviging kan, ook bij grote vervormingen, goed beschreven worden met een fractiemodel bestaande uit een elastisch - ideaal plastische fractie en een zuiver elastische fractie, mits de elastische fractie grote elastische vervormingen goed kan beschrijven.

   Dit proefschrift, hoofdstuk III.

3. Bij een Eulerse of een gemengd Eulerse-Lagrangiaanse eindige-elementensimulatie van vormgevingsprocessen moeten, ten opzichte van een 'updated' Lagrangiaanse methode, extra convectieve termen worden meegenomen waardoor afgeleiden van een orde hoger geïntroduceerd worden. Het is echter niet noodzakelijk ook een hogere orde-continuïteit van de interpolatiefuncties te eisen.

   Dit proefschrift, hoofdstuk IV.

4. Numerieke instabiliteiten die kunnen optreden bij een eidige-elementen-simulatie van grote vervormingsprocessen volgens een gemengde Eulerse-Lagrangiaanse methode, kunnen worden voorkomen door invoering van 'local smoothing' en gewogen 'global smoothing'.

   Dit proefschrift, hoofdstuk IV.

5. Bij simulatie met de eindige-elementenmethode van thermische processen

waarbij snelle lokale temperatuursveranderingen optreden, kunnen onrealistische oscillaties in de berekende temperatuurverdeling worden voorkomen door de integratiepunten in de knooppunten te kiezen. Bij rechthoekige vier-knoops elementen is de methode dan gelijkwaardig aan de eindige-differentiemethode.

6. In de Verenigde Staten vindt de bewering dat door invoering van sociale voorzieningen de sociale problemen zijn toegenomen, veel steun in conservatieve kringen. Deze bewering zou nader onderzocht moeten worden door na te gaan of in landen met een hoger niveau van sociale voorzieningen dan in de V.S. de sociale problemen meer zijn toegenomen en in landen met een veel lager niveau van sociale voorzieningen de sociale problemen minder zijn toegenomen.

   F. Verhagen, Kruistocht tegen de verzorgingsstaat, Intermediair 21e jaargang nr. 49, 6 december 1985, n.a.v. Charles Murray's boek "Losing Ground, American social policy 1950-1980".

7. Uit een onderzoek van de universiteit van Maastricht naar ski-ongevallen is gebleken, dat de kans op ernstig letsel voor skiërs die alcohol hebben gebruikt kleiner is, dan voor skiërs die geen alcohol hebben gebruikt. Niet de kans op letsel voor de alcoholgebruiker maar de kans op het veroorzaken van een ongeval zou voorop moeten staan bij het bepalen van risico's van alcoholgebruik.

8. Voor het onderwijspersoneel is een extra salariskorting van kracht teneinde het tekort op de begroting van het Ministerie van Onderwijs en Wetenschappen te beperken. Op grond van soortgelijke overwegingen zouden de ambtenaren van Rijkswaterstaat een deel van hun salaris moeten afstaan vanwege de tekorten op de begroting voor de Oosterscheldedam, zou het marinepersoneel moeten inleveren teneinde de kosten van de te duur uitgevallen Walrusonderzeërs te compenseren en zouden de ambtenaren van Economische Zaken het R.S.V.-debâcle moeten betalen.

9. Veel CAD-systemen zijn niet veel meer dan electronische tekenmachines.

Een voordeel ten opzichte van een mechanische tekenmachine is dat zowel potlood als vlakgum minder snel slijten.

10. Het beleid van het Ministerie van Economische Zaken met betrekking tot de prijs van het aardgas vertoont grote gelijkenis met de handel in drugs; eerst wordt het produkt tegen een lage prijs aangeboden. Nadat men er aan verslaafd is, wordt de prijs sterk verhoogd.

Enschede, 20 juni 1986 Han Huetink